Gustatory mechanisms for the detection of fat

Timothy A Gilbertson

Recent evidence suggests that free fatty acids may be one of the important stimuli used by taste receptor cells for the detection of fat. Consistent with this interpretation, the proteins necessary for the release and transport of lipophilic fatty acids are found in the oral cavity, and taste cells have recently been shown to contain fatty-acid-sensitive ion channels and transport molecules for the uptake of fatty acids.

Addresses
Pennington Biomedical Research Center, Louisiana State University, 6400 Perkins Road, Baton Rouge, Louisiana 70808-4124, USA; e-mail: tim.gilbertson@tasteful.com

Current Opinion in Neurobiology 1998, 8:447–452

http://biomednet.com/elecref/0959438800800447

 ISSN 0959-4388

Abbreviations

DRK channel	delayed rectifying K^+ channel
PCR	polymerase chain reaction
PUFA	*cis*-polyunsaturated fatty acid
VEG-P	von Ebner's gland protein

Introduction

It is of particular importance to understand the mechanisms that regulate the intake of dietary fat because of the association between high dietary fat intake and the incidence of obesity and related disorders [1•]. While there has been a significant amount of research aimed at exploring the physiological consequences of fat ingestion, there have been relatively few studies aimed at identifying the gustatory mechanisms by which dietary fat is recognized. Clearly, identifying the transduction mechanisms for fat and its site of action will be critical to our understanding of the processes that contribute to the consumption of dietary fat.

One of the obvious sites that plays a role in shaping ingestive behavior is the peripheral gustatory system. Sensory preferences have been linked to the overconsumption of specific macronutrients (e.g. carbohydrates and fats) and may, in turn, be directly related to the development of obesity [2]. Thus, in recent years, the sensory properties of fats have begun to receive increasing attention. Because of the lipophilic and volatile nature of most molecules contained in fats, the 'flavor' of these compounds has been suggested to result from the cues associated with their texture, taste and smell. Studies of the sensory properties of fats have focused almost exclusively on triglycerides, which represent roughly 98% of ingested fat. From these studies, the generally accepted notion is that the texture of fats may be its most salient feature [3••,4]. However, recent evidence suggests that the free fatty acids contained in fat, or generated during fat ingestion, may affect taste receptor cells directly via interactions with delayed rectifying K^+ (DRK) channels [5••], or they may be taken up in taste cells via fatty-acid transporter proteins [6••], where they may exert intracellular effects.

This review will focus on the role of free fatty acids as potential gustatory stimuli, the associated molecules involved in the release and transport of fatty acids in the oral cavity, and the implications of these gustatory cues for the consumption of dietary fat.

Fatty acids as primary signaling molecules

Recent evidence suggests that free fatty acids may be potent primary messengers in a variety of tissues, such as skeletal, smooth and cardiac muscle (for reviews, see [7,8]). Fatty-acid effects may be either indirect (involving arachidonic acid as the substrate for the well-known lipoxygenase, cyclooxygenase and cytochrome P450 pathways) or direct (whereby free fatty acids interact with a variety of voltage-activated ion channels).

In taste cells, voltage-activated ion channels serve a number of roles. Taste cells contain both voltage-activated Na^+ and K^+ channels, which underlie the action potentials produced during chemostimulation, and voltage-activated Ca^{2+} channels, which enable the rise in intracellular Ca^{2+} necessary for the release of neurotransmitter from the taste cells. Moreover, taste cells contain a variety of voltage-activated, Ca^{2+}-activated and leak ion channels that serve as the targets for different taste stimuli, either directly or indirectly [9]. Thus, when free fatty acids are present in the oral cavity (see below the section entitled Involvement of lingual lipase and von Ebner's gland proteins), it is possible that these channels, similar to those found in other tissues, are responsive to them.

Fatty acids as gustatory stimuli

As mentioned above, most efforts that have focused on identifying the orosensory cues for fat have concentrated on the textural cues for fats. There have been few, if any, studies that have tested directly whether fats affect the taste system and, in particular, taste receptor cells. The results of two recent studies are consistent with the view that free fatty acids are important cues for the detection of fat: my colleagues and I [5••] found that the essential (*cis*-polyunsaturated) fatty acids (PUFAs) inhibit DRK channels is rat taste cells, and Fukuwatari *et al.* [6••] have recently identified fatty-acid transporters in lingual tissue.

Figure 1

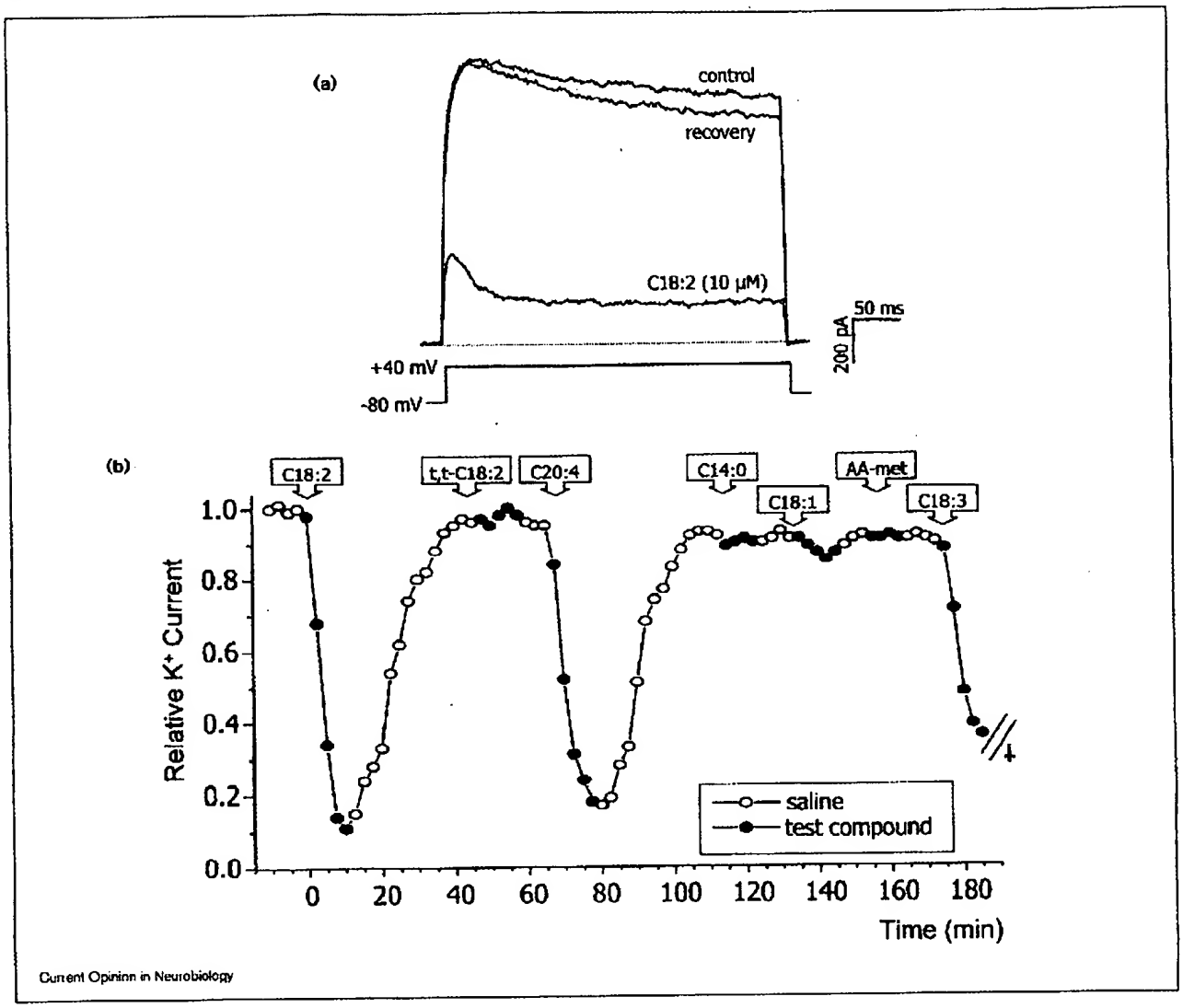

Fatty-acid inhibition of DRK channels in a vallate taste receptor cell. **(a)** The DRK current elicited in response to a potential of +40 mV from a holding potential of −80 mV in a whole-cell variation of the patch-clamp technique is sensitive to linoleic acid (C18:2, 10 µM, 10 min). Note the change in peak current and increased inactivation. Recovery is shown 15 min after washing with saline. **(b)** Specificity and time course of the fatty-acid response. Of the fatty acids tested, only the PUFAs (i.e. C18:2, C20:4 and C18:3) inhibited DRK channels [5••]. The nomenclature refers to the ratio between the number of carbon atoms and the number of double bonds. t,t-C18:2, linolelaidic acid (*trans*, *trans*-linoleic acid); C20:4, arachidonic acid; C14:0, lauric acid; C18:1, oleic acid; AA-met, arachidonic acid methyl ester; C18:3, linolenic acid. All compounds were tested at 10 µM.

Patch-clamp recordings of taste buds isolated from rat tongue show that fatty acids inhibit DRK channels in more than 95% of cells examined [5••]. The effects include inhibition of the peak current and an increase in the inactivation rate, giving a pronounced reduction in the steady-state K^+ current compared to control conditions (Figure 1a). These effects are consistent with fatty acids acting as open-channel blockers of DRK channels [10]. Interestingly, only PUFAs, which are the essential fatty acids [11], inhibit DRK channels in taste cells [5••] (Figure 1b). Thus, the peripheral gustatory system is sensitive to the fatty acids that are required in the diet for survival. It appears that fatty acids act directly on the DRK channel because inhibitors of the lipoxygenase, cyclooxygenase and cytochrome P450 pathways do not inhibit the PUFA response [5••]. Moreover, PUFAs are effective in inhibiting K^+ currents only when applied extracellularly, effectively ruling out changes in membrane fluidity as a major contributor to the effects reported. Preliminary results have identified the fatty-acid-sensitive DRK channel in taste cells as a Shaker Kv1.5-like channel (L Liu *et al.*, abstract 206, 20th Annual Meeting of the Association for Chemoreception Sciences, Sarasota, April 1997). Shaker Kv1.5 channels, which are the major DRK

channels in the heart, show a similar profile of inhibition by PUFAs [10]. It is clear, therefore, that fatty acids can have potent, direct effects at the level of the taste receptor cell.

Consistent with the notion that fatty acids are gustatory cues for dietary fat, Fukuwatari *et al.* [6••] identified a fatty-acid transporter in rat lingual epithelia, using immunocytochemistry and polymerase chain reaction (PCR). Fatty-acid transporters, in general, facilitate the transport of free fatty acids across biological membranes [12••]. These transporters — subtypes of which can transport short-, medium- and/or long-chain fatty acids — are present in a variety of fat-sensitive tissues, including the liver, adipose tissue and heart [13]. Immunocytochemical staining of lingual tissue has revealed that there is a significant amount of the fatty-acid transporter protein in the apical membrane of taste cells [6••] (Figure 2).

Figure 2

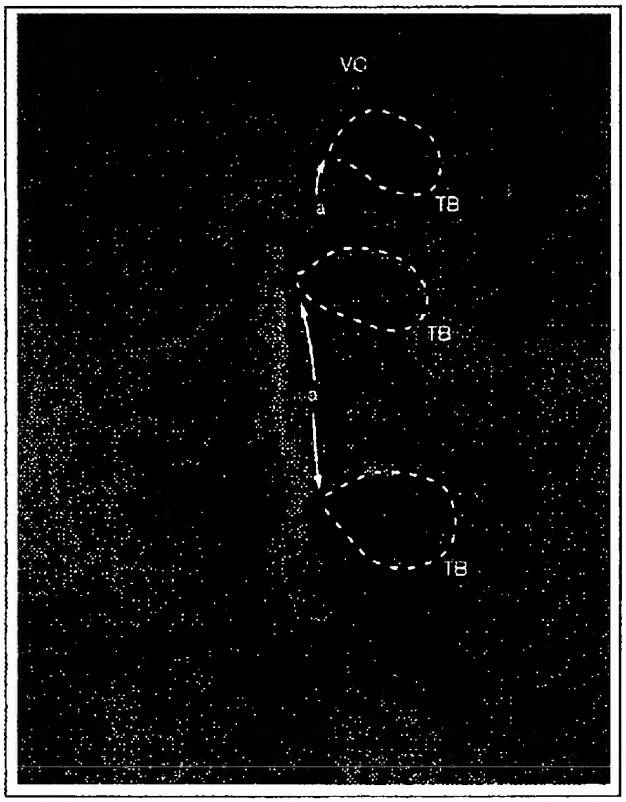

Immunohistochemical staining of rat circumvallate papillae with anti-rat fatty-acid transporter antibody. Significant staining is evident in a number of cells within each taste bud (TB), and the labeling appears concentrated in the apical part (a) of the taste cells. VC, vallate crypt. Reproduced, with permission, from Fukuwatari *et al.* [6••].

One of the apparent roles of fatty-acid transporters in taste tissue is to increase intracellular Ca^{2+} concentrations (T Fushiki, T Kawada, T Fukuwatari, abstract in *Chem Senses* 1997, 22:332). Presumably, this increase in intracellular Ca^{2+} would lead to increased release of neurotransmitter onto gustatory afferent nerve fibers. Because of the widespread effects fatty acids may have on cells [14], the uptake of specific fatty acids into taste receptor cells may lead to additional, as yet undefined, intracellular effects. These effects are probably independent of the effects on DRK channels in taste cells, however, as intracellular application of PUFAs has no effect in patch-clamp experiments [5••]. An alternative hypothesis is that fatty acid transporters play a role in taste cell responses to non-essential (i.e. mono-unsaturated and saturated) fatty acids. Finally, because lingual epithelial cells may also express fatty-acid transporters, it is possible that they transport fatty acids across the lingual epithelium, where they may reach DRK channels on the basolateral membranes of taste cells or may have access to the lingual trigeminal fibers believed to be important for mechanosensitive (e.g. textural) properties in the oral cavity [15].

Involvement of lingual lipase and von Ebner's gland proteins

Free fatty acids are present in a number of foods, often up to 0.5% or more of the weight per volume (w/v) [16]; therefore, it is plausible that they affect the taste cells via the mechanisms outlined above. However, other molecules may play important roles in the generation and transport of free fatty acids in the oral cavity. These include lingual lipase, which is capable of hydrolyzing triglycerides, and von Ebner's gland proteins (VEG-Ps), which are structurally related to the lipocalins and may function in the transport of lipophilic molecules.

Lingual lipase has been identified in both humans and rats [17,18]. Like other members of the acid lipase family (e.g. gastric lipase and lysosomal acid lipase), lingual lipase can hydrolyze triglycerides into free fatty acids and monoglycerides [19•], and it may help pre-digest dietary fat [20]. The release of lingual lipase from the von Ebner's gland into the cleft of the vallate and foliate papillae would bring it directly into the taste-bud-containing regions of the lingual tissue. As DRK channels in foliate and vallate taste cells are inhibited by fatty acids (I Kim, L Liu, T Gilbertson, abstract 205, 20th Annual Meeting of the Association for Chemoreception Sciences, Sarasota, April 1997) and fatty-acid transporters are present in these areas [6••], the generation of free fatty acids by lingual lipase in these clefts would activate both these cellular mechanisms. Thus, lingual lipases may play a critical role in the generation of free fatty acids that, in turn, directly affect the peripheral gustatory system.

The hydrophobicity of fatty acids may necessitate the involvement of another molecule in these fat detection pathways. Another group of proteins released from the von Ebner's glands, VEG-Ps, may facilitate the transport of fatty acids in the aqueous environment of the oral cavity.

Figure 3

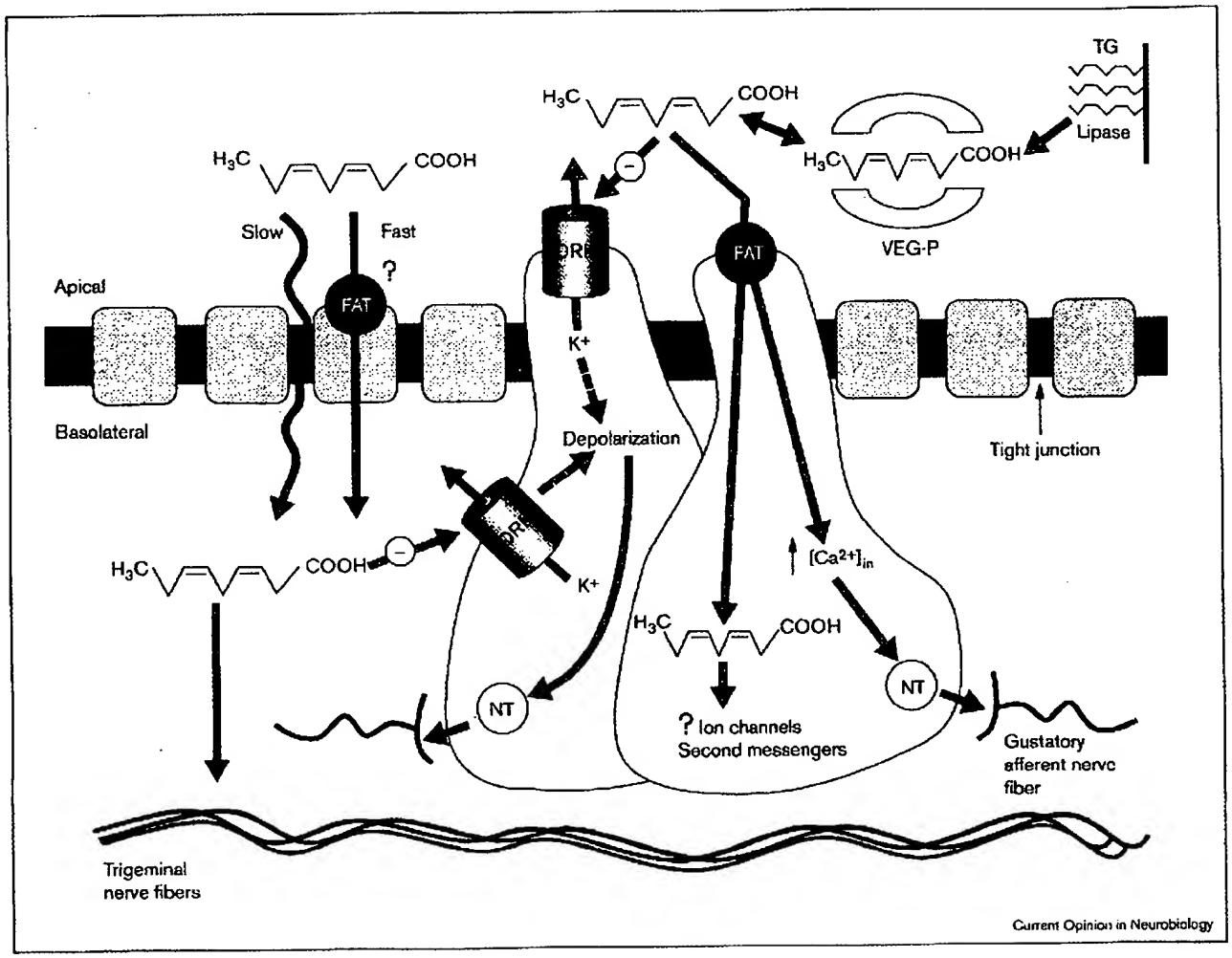

Putative mechanisms in the gustatory response to fatty acids. Free fatty acids, which are present in food or generated from triglycerides (TGs) via lingual lipase, are carried in the aqueous environment of the oral cavity by VEG-Ps. The free fatty acids, existing in equilibrium between the bound and unbound state, may directly inhibit apical DRK channels to depolarize the taste receptor cell, eventually leading to neurotransmitter (NT) release onto afferent nerve fibers. Fatty acids may also be transported by facilitated diffusion via fatty-acid transporters (FATs), where they are accompanied by a rise in intracellular Ca^{2+} and, presumably, an increase in NT release onto gustatory afferents. In addition, the fatty acids taken up into taste cells may have undefined intracellular effects. The fatty acids may also diffuse or be transported through the lingual epithelium, where they may directly affect basolateral DRK channels, trigeminal nerve fibers or other potential targets.

VEG-Ps are structurally related to the lipocalins [21,22], which function primarily in the transport of lipophilic molecules in physiological solutions [23]. It has been hypothesized that VEG-Ps transport bitter stimuli [24], many of which are lipophilic [9,25], to the taste receptor cells. However, binding studies have demonstrated that VEG-Ps do not bind any known bitter compounds; rather, they have been reported to only bind free fatty acids [26]. VEG-Ps have also recently been shown to function as cysteine proteinase inhibitors, suggesting they may play additional roles unrelated to taste [27•]. Nonetheless, there appears to be all the necessary machinery in the oral cavity to implicate free fatty acids as important taste cues for fat. That is, fatty acids may be released in the vicinity of taste cells by lingual lipase, transported to the taste receptor cell by VEG-Ps, and act on specific taste cell proteins (e.g. DRK channels and fatty-acid transporters) to alter the activity of the taste receptor cell. This proposed scheme for the involvement of fatty acids in the gustatory response to fat is illustrated in Figure 3.

Implications of the 'taste of fat'

The identification of specific transduction pathways for the detection of dietary fat may have numerous important implications for the performance of the gustatory system in general. A number of recent reports have postulated the presence of an undefined taste mechanism for the detection of fat. Recently, Mattes [28] demonstrated that oral exposure to fat leads to changes in postprandial

lipid metabolism, consistent with there being a sensory mechanism for the detection of fat.

The involvement of fatty acids as potential gustatory cues in the generation of a response for fat-containing stimuli may have other implications. While it is presently unclear what is the downstream effect of fatty acid transporter mediated uptake of fatty acids in taste cells, the inhibition of DRK channels by PUFAs has predictable consequences. K^+ channels in taste cells have been implicated in the transduction pathway of a variety of taste stimuli [9,25]. Inhibition of outward DRK currents either directly or indirectly via second messengers has been shown to play a role in the response to bitter [29,30], sweet [31•–33•] and acidic [34] stimuli. As PUFAs inhibit DRK currents in more than 95% of taste cells examined, this implies that the response to these and other tastants may be directly affected by fatty acids in food. This potential interaction between the 'taste' of fat and other stimuli might, for example, help explain the reports suggesting that the presence of fat may alter the response (hedonics) to other tastes [35–37].

Interestingly, individuals with the ability to taste the bitter substance 6-n-propylthiouracil (PROP), the so-called 'super-tasters' [38], have the ability to discriminate the fat content of salad dressings (10% versus 40%), whereas PROP-insensitive 'non-tasters' do not [39••]. The super-tasters have a significantly greater density of fungiform taste buds than non-tasters [40], and it has been assumed that this is related not to taste, but to the trigeminal innervation surrounding the taste buds [39••]. Yet, no link have been shown to exist between taste bud number and the degree of trigeminal nerve innervation. An alternative explanation, in addition to these trigeminally mediated (textural) cues, is that greater fat sensitivity may be related to a greater number of taste buds and, hence, a larger number of fatty-acid-sensitive taste cells or fatty-acid transporters in the tongues of the super-tasters.

Conclusions

The recent identification of transduction mechanisms for fatty acids has challenged the notion that fats provide solely textural cues in the oral cavity. The effects of fatty acids in the gustatory system may be important for understanding the ways in which the body recognizes and responds to the presence dietary fat. Indeed, the gustatory mechanisms may represent universal mechanisms for the detection of fat, as cells from the pancreas and duodenum, which are sensitive to dietary fat, contain fatty-acid-sensitive DRK channels (I Kim, L Liu, T Gilbertson abstract 205, 20th Annual Meeting of the Association for Chemoreception Sciences, Sarasota, April 1997); in addition, fatty-acid transporters are found in intestinal epithelial cells [41,42]. Though both PUFA inhibition of DRK channels and fatty-acid transport clearly exist at the cellular level, there is currently little known about the behavioral responses to specific free fatty acids.

Acknowledgements

The author's laboratory is supported by National Institutes of Health grants DC02507 and DC00353 and a grant from Novartis Pharmaceutical Corporation. I thank Tohru Fushiki for permission to use the photograph shown in Figure 2.

References and recommended reading

Papers of particular interest, published within the annual period of review, have been highlighted as:

- • of special interest
- •• of outstanding interest

1. • Drewnowski A: **Why do we like fat?** *J Am Dent Assoc* 1997, **97**:S58-S62.
The author reviews current viewpoints on dietary fat intake, its associated physiological consequences, and the factors that lead to its overconsumption.

2. Drewnowski A, Kurth C, Holden-Wilste J, Saari J: **Food preferences in human obesity: carbohydrates versus fats.** *Appetite* 1992, **18**:207-221.

3. •• Drewnowski A: **Taste preferences and food intake.** *Annu Rev Nutr* 1997, **17**:237-253.
An in-depth review on the link between food intake and its sensory properties (e.g. taste, texture and smell). The author discusses the various factors that contribute to food choice and preference.

4. Mela DJ, Marshall RJ: **Sensory properties and perceptions of fats.** In *Dietary Fats: Determinants of Preference, Selection and Consumption.* Edited by Mela DJ. New York: Elsevier Applied Science; 1991:43-57.

5. •• Gilbertson TA, Fontenot DT, Liu L, Zhang H, Monroe WT: **Fatty acid modulation of K^+ channels in taste receptor cells: gustatory cues for dietary fat.** *Am J Physiol* 1997, **272**:C1203-C1210.
Patch-clamp recordings of isolated rat taste receptor cells reveal that essential (*cis*-polyunsaturated) fatty acids inhibit delayed rectifying K^+ (DRK) channels. This finding is the first direct physiological evidence for a gustatory cue for fat.

6. •• Fukuwatari T, Kawada T, Tsuruta M, Hiraoka T, Iwanaga T, Sugimoto E, Fushiki T: **Expression of the putative membrane fatty acid transporter (FAT) in taste buds of the circumvallate papillae in rats.** *FEBS Lett* 1997, **414**:461-464.
Using immunohistochemistry and polymerase chain reaction (PCR), the authors identify a fatty-acid transporter in circumvallate taste tissue, consistent with there being a gustatory cue for fatty acids in the oral cavity. The largest amount of labeling was in the apical membranes of taste cells, where the potential interaction with fatty acids is likely to occur.

7. Ordway RW, Singer JJ, Walsh JV Jr: **Direct regulation of ion channels by fatty acids.** *Trends Neurosci* 1991, **14**:96-100.

8. Petrou S, Ordway RW, Kirber MT, Dopico AM, Hamilton JA, Walsh JV Jr, Singer JJ: **Direct effects of fatty acids and other charged lipids on ion channel activity in smooth muscle cells.** *Prostaglandins Leukot Essent Fatty Acids* 1995, **52**:173-178.

9. Gilbertson TA, Kinnamon SC: **Making sense of chemicals.** *Chem Biol* 1996, **3**:233-237.

10. Honoré E, Barhanin J, Attali B, Lesage F, Lazdunski M: **External blockade of the major delayed-rectifier K^+ channel (Kv1.5) by polyunsaturated fatty acids.** *Proc Natl Acad Sci USA* 1994, **91**:1937-1944.

11. Horrobin DF: **Nutritional and medical importance of gamma-linoleic acid.** *Prog Lipid Res* 1992, **31**:163-194.

12. •• Glatz JF, Luiken JJ, van Nieuwenhoven FA, Van der Vusse GJ: **Molecular mechanism of cellular uptake and intracellular translocation of fatty acids.** *Prostaglandins Leukot Essent Fatty Acids* 1997, **57**:3-9.
This review summarizes the roles of the various soluble and membrane-associated proteins involved in the uptake of long-chain fatty acids into cells. Both passive and carrier-mediated transport of fatty acids are discussed, as well as the subsequent involvement of cytoplasmic fatty-acid-binding proteins in the cellular response to fatty acids.

13. Berk PD, Zhou SL, Kiang CL, Stump D, Bradbury M, Isola LM: **Uptake of long chain free fatty acids is selectively up-regulated in adipocytes of Zucker rats with genetic obesity and non-insulin-dependent diabetes mellitus.** *J Biol Chem* 1997, 272:8830-8835.

14. Sumida C, Graber R, Nunez E: **Role of fatty acids in signal transduction: modulators and messengers.** *Prostaglandins Leukot Essent Fatty Acids* 1993, 48:117-122.

15. Silver WL, Finger TE: **The trigeminal system.** In *Smell and Taste in Health and Disease.* Edited by Getchell TV, Doty RL, Bartoshuk LM, Snow JB Jr. New York: Raven Press; 1991:97-108.

16. Weiss TJ: *Food Oils and Their Uses.* Westport, Connecticut: Avi Publishing Co.; 1983.

17. Hamosh M, Burns WA: **Lipolytic activity of human lingual glands (Ebner).** *Lab Invest* 1977, 37:603-608.

18. Field RB, Spielman AI, Hand AR: **Purification of lingual amylase from serous glands of rat tongue and characterization of rat lingual amylase and lingual lipase.** *J Dent Res* 1989, 68:139-145.

19. • Lohse P, Lohse P, Chahrokh-Zadeh S, Seidel D: **The acid lipase family: three enzymes, one highly conserved gene structure.** *J Lipid Res* 1997, 38:880-891.
On the basis of gene structure and PCR-based intron amplification, the authors demonstrate that the genes encoding rat lingual lipase and its translation products are highly homologous to other acid lipases, including human lysosomal acid lipase and human gastric lipase. The results are consistent with the interpretation that lingual lipase, like the other acid lipases, shares a common function in the generation of free fatty acids from triglycerides.

20. Hamosh M, Scow RO: **Lingual lipase and its role in the digestion of dietary lipid.** *J Clin Invest* 1973, 52:88-95.

21. Kock K, Bläker M, Schmale H: **Postnatal development of von Ebner's glands: accumulation of a protein of the lipocalin superfamily in taste papillae of rat tongue.** *Cell Tissue Res* 1992, 267:313-320.

22. Kock K, Ahlers C, Schmale H: **Structural organization of the genes for rat von Ebner's gland proteins 1 and 2 reveals their close relationship to lipocalins.** *Eur J Biochem* 1994, 221:905-916.

23. Pervaiz S, Brew K: **Homology of β-lactoglobulin, serum retinol-binding protein and protein HC.** *Science* 1985, 228:335-337.

24. Schmale H, Holtgreve-Grez H, Christiansen H: **Possible role for salivary gland protein in taste reception indicated by homology to lipophilic-ligand carrier proteins.** *Nature* 1990, 343:366-369.

25. Lindemann B: **Taste perception.** *Physiol Rev* 1996, 76:719-766.

26. Schmale H, Ahlers C, Blaker M, Kock K, Spielman AI: **Perireceptor events in taste.** *Ciba Found Symp* 1993, 179:167-185.

27. • van't Hof W, Blankenvoorde MJF, Veerman ECI, Amerongen AVN: **The salivary lipocalin von Ebner's gland protein is a cysteine proteinase inhibitor.** *J Biol Chem* 1997, 272:1837-1841.
The authors present evidence that the lipocalin-like VEG-Ps, in addition to their reported role in the transport of lipophilic molecules, may function as cysteine proteinase inhibitors. They speculate that these molecules may also play a role in the control of inflammatory oral processes.

28. Mattes RD: **Oral fat exposure alters postprandial lipid metabolism in humans.** *Am J Clin Nutr* 1996, 63:911-917.

29. Spielman AI, Huque T, Whitney G, Brand JG: **The diversity of bitter taste signal transduction mechanisms.** In *Sensory Transduction.* Edited by Corey DP, Roper SD. New York: Rockefeller University Press; 1992:307-324.

30. Tsunenari T, Hayashi Y, Orita M, Kurahashi T, Kaneko A, Mori T: **A quinine-activated cationic conductance in vertebrate taste cells.** *J Gen Physiol* 1996, 108:515-523.

31. • Cummings TA, Daniels C, Kinnamon SC: **Sweet taste transduction in hamster: sweeteners and cyclic nucleotides depolarize taste cells by reducing a K^+ current.** *J Neurophysiol* 1997, 75:1256-1263.
Using whole-cell recording of hamster taste cells, the authors provide direct evidence for the involvement of K^+ channels in the response to sweeteners. This response is mimicked by cAMP and cGMP, suggesting that one or both of these cyclic nucleotides is involved in the sweet-responsive pathways in taste cells, culminating in the inhibition of K^+ channels.

32. • Herness MS, Sun XD, Chen Y: **cAMP and forskolin inhibit potassium currents in rat taste receptor cells by different mechanisms.** *Am J Physiol* 1997, 272:C2005-C2018.
Using electrophysiological recording from rat taste cells, the authors show that cAMP and the adenylyl cyclase activator, forskolin, both inhibit K^+ channels in taste cells. However, at higher concentrations, forskolin and its analog (1,9-dideoxyforskolin), which does not stimulate cAMP production, have an additional inhibitory effect on K^+ channels unrelated to cAMP.

33. • Uchida Y, Sato T: **Changes in outward K^+ currents in response to two types of sweeteners in sweet taste transduction of gerbil taste cells.** *Chem Senses* 1997, 22:163-169.
Dual regulation of K^+ channels by different classes of sweeteners is shown in this patch-clamp study of gerbil taste cells. Saccharin and cAMP inhibit K^+ channels, whereas amino-acid sweeteners, such as D-tryptophan, enhance outward K^+ currents, apparently via the second messenger inositol trisphosphate.

34. Kinnamon SC: **Role of apical ion channels in sour taste transduction.** *Ciba Found Symp* 1993, 179:201-210.

35. Bacon AW, Miles JS, Schiffman SS: **Effects of race on perception of fat alone and in combination with sugar.** *Physiol Behav* 1994, 55:603-606.

36. Drewnowski A, Krahn DD, Demitrack MA, Nairn K, Gosnell BA: **Taste responses and preferences for sweet high-fat foods: evidence for opioid involvement.** *Physiol Behav* 1992, 51:371-379.

37. Johnson SL, McPhee L, Birch LL: **Conditioned preferences: young children prefer flavors associated with high dietary fat.** *Physiol Behav* 1991, 50:1245-1251.

38. Bartoshuk LM, Duffy VB, Miller IJ: **PTC/PROP tasting: anatomy, psychophysics and sex effects.** *Physiol Behav* 1994, 56:1155-1171.

39. •• Tepper BJ, Nurse RJ: **Fat perception is related to PROP taster status.** *Physiol Behav* 1997, 61:949-954.
In this psychophysical study, the authors show that the so-called 'super-tasters', who are sensitive to the bitter compound 6-n-propylthiouracil (PROP), can distinguish fat content in salad dressing whereas 'non-tasters', who are insensitive to PROP, cannot. As 'super-tasters' have significantly higher fungiform taste bud densities, this finding suggests a link between the perception of fat and the underlying gustatory anatomy.

40. Miller IJ, Reedy FE: **Variations in human taste bud density and taste intensity perception.** *Physiol Behav* 1990, 47:1213-1219.

41. Shintani T, Takahashi N, Fushiki T, Sugimoto E: **The recognition system of dietary fatty acids by the rat small intestinal cells.** *Biosci Biotech Biochem* 1995, 59:479-481.

42. Shintani T, Takahashi N, Fushiki T, Sugimoto E: **Recognition system for dietary fatty acids in the rat small intestine.** *Biosci Biotech Biochem* 1995, 59:1428-1432.

Proc. Natl. Acad. Sci. USA
Vol. 93, pp. 14146–14151, November 1996
Neurobiology

Coexpression of *Drosophila* TRP and TRP-like proteins in *Xenopus* oocytes reconstitutes capacitative Ca^{2+} entry

(signal transduction/phosphoinositide signaling/*trp* mutant/calcium stores)

B. GILLO*†, I. CHORNA*†, H. COHEN*†, B. COOK*†, I. MANISTERSKY†‡, M. CHOREV§, A. ARNON*†, J. A. POLLOCK¶, Z. SELINGER*‡, AND B. MINKE*†‖

Departments of *Physiology, §Pharmaceutical Chemistry, ‡Biological Chemistry and the †Kühne Minerva Center for Studies of Visual Transduction, The Hebrew University, Jerusalem 91120, Israel; and ¶Department of Biological Sciences, Carnegie Mellon University, Pittsburgh, PA 15213-3890

Communicated by Denis Baylor, Stanford University School of Medicine, Stanford, CA, September 12, 1996 (received for review July 26, 1996)

ABSTRACT **Capacitative Ca^{2+} entry is a component of the inositol-lipid signaling in which depletion of inositol 1,4,5-trisphosphate ($InsP_3$)-sensitive Ca^{2+} stores activates Ca^{2+} influx by a mechanism that is still unknown. This pathway plays a central role in cellular signaling, which is mediated by many hormones, neurotransmitters, and growth factors. Studies of *Drosophila* photoreceptors provided the first putative capacitative Ca^{2+} entry mutant designated transient receptor potential (*trp*) and a *Drosophila* gene encoding TRP-like protein (*trpl*). It is not clear how the Ca^{2+} store depletion signal is relayed to the plasma membrane and whether both TRP and TRPL participate in this process. We report here that coexpressing *Drosophila* TRP and TRPL in *Xenopus* oocytes synergistically enhances the endogenous Ca^{2+}-activated Cl^- current and produces a divalent inward current. Both of these currents are activated by Ca^{2+} store depletion. In the absence of Ca^{2+}, Mg^{2+} is the main charge carrier of the divalent current. This current is characterized by lanthanum sensitivity and a voltage-dependent blocking effect of Mg^{2+}, which is relieved at both hyperpolarizing (inward rectification) and depolarizing (outward rectification) potentials. The store-operated divalent current is neither observed in native oocytes nor in oocytes expressing either TRP or TRPL alone. The production of this current implicates a cooperative action of TRP and TRPL in the depletion-activated current.**

Stimulation of many cell types by hormones, neurotransmitters, and growth-factors activates the inositol-lipid pathway leading to release of Ca^{2+} from intracellular stores. This Ca^{2+} release is followed by an influx of extracellular Ca^{2+} via a capacitative Ca^{2+} entry (CCE) mechanism (1). It has been suggested that activation of the surface membrane Ca^{2+} channels is caused by the depletion of Ca^{2+} in the internal stores and not by the release per se (1–8). Although CCE has been described in a large variety of cells and tissues (summarized in refs. 5 and 9), its mechanism of activation and molecular components is largely unknown. Visual transduction in *Drosophila*, which is triggered by the inositol lipid signaling (reviewed in refs. 10–13) has been suggested by Minke and Selinger (14) as a powerful model system to study CCE. This suggestion was based on the properties of a *Drosophila* mutant designated transient receptor potential *trp* (15, 16). In the *trp* mutant the photoreceptor potential declines to baseline during prolonged intense illumination and renders the photoreceptor cell inactive. The receptor potential recovers within 1 min in the dark (17). Because lanthanum (La^{3+}), a known non-specific blocker of Ca^{2+} channels, mimics many aspects of the *trp* phenotype in wild-type flies (18, 19), it has been suggested that *trp* has defects in Ca^{2+} entry into the photoreceptor cells (14). This prediction has been strongly supported by subsequent experiments demonstrating that the high Ca^{2+} permeability of the light-activated channels (20, 21) is reduced by about 10-fold in the *trp* mutant (22). Furthermore, fluorimetric measurements of cellular Ca^{2+} (23, 24) and measurements of a reduction in extracellular Ca^{2+} (25) have shown that Ca^{2+} influx is reduced by about 3-fold in the *trp* mutant relative to wild-type *Drosophila*, suggesting that TRP takes part in the main route of Ca^{2+} entry into the photoreceptor cells (10, 13, 14).

Molecular cloning of *Drosophila trp* (26, 27) and a related *Drosophila* gene designated transient receptor potential-like, *trpl* (28), revealed that their putative transmembrane domain exhibits weak but significant similarity to the α-subunit of the voltage-gated Ca^{2+} channel (28). Recently, a *trpl* mutant lacking TRPL has been isolated by Zuker and colleagues (29). The *trpl* mutant has a receptor potential similar to wild type and it reveals a strong phenotype only in a *trp* background. Thus, the double mutant *trpl;trp* is almost totally unresponsive to light (29). This study has suggested that TRP and TRPL are capable of responding to light activation independently of each other, but it does not exclude the possibility that TRP and TRPL form a multimeric channel (29). Additional subunit might exist but its function should depend on the presence of TRP and TRPL. Molecular and physiological data on TRP led a number of investigators to express the *Drosophila* TRP or TRPL in insect Sf9 cells (30, 31) or human homologue genes of *trp* (32, 33) in COS, Chinese hamster ovary, and Sf9 cells (9, 34). The heterologously expressed TRPL forms a constitutively active non-selective cation conductance, which could be enhanced by activation of the inositol lipid cascade (31, 35, 36). Heterologous expression of *Drosophila* TRP forms a conductance, which is activated by Ca^{2+} store depletion following treatment with the microsomal Ca^{2+} ATPase inhibitor, thapsigargin (30, 37, 38). Expression of *Drosophila* TRP in *Xenopus* oocytes enhances the endogenous Ca^{2+}-activated Cl^- conductance following depletion of the inositol 1,4,5-trisphosphate ($InsP_3$)-sensitive Ca stores (37). Recently, six *trp*-related genes of the mouse genome were identified in addition to new human homologues of *trp*. The expressed human gene products enhanced Ca^{2+} influx following Ca^{2+} store depletion (9, 34). Furthermore, expression in L cells of small portions of the mouse *trp* genes, in antisense orientation, suppressed the endogenous capacitative Ca^{2+} entry (9).

Here we report that heterologous coexpression of *Drosophila* TRP and TRPL in *Xenopus* oocytes synergistically enhanced the endogenous Ca^{2+}-activated Cl^- current upon Ca^{2+} stores depletion. In addition, the coexpressed TRP and TRPL

The publication costs of this article were defrayed in part by page charge payment. This article must therefore be hereby marked "*advertisement*" in accordance with 18 U.S.C. §1734 solely to indicate this fact.

Abbreviations: CCE, capacitative Ca^{2+} entry; $InsP_3$, inositol 1,4,5-trisphosphate; $InsP_3$-F, inositol 1,4,5-trisphosphate, 3-deoxy-3-fluoro; TRP, transient receptor potential protein; TRPL, TRP-like protein; LIC, light-induced current.

‖To whom reprint requests should be addressed.

produced a novel divalent cation current, which was activated by store depletion but could not be similarly activated when either TRP or TRPL were individually expressed. These findings strongly suggest a cooperative action of TRP and TRPL in the depletion-activated current.

MATERIALS AND METHODS

Analysis of Heterologous Expression of TRP and TRPL. The *trp* (26, 27) and *trpl* (28) cDNAs were subcloned into PGEMHE expression vector, which was constructed for expression in *Xenopus* oocytes (39, 40). Capped cRNA was synthesized *in vitro* and tested by translation in a rabbit reticulocyte lysate system before injection into oocytes. An amount of 0.2 mg/ml *trp*, 0.02 mg/ml *trpl*, and 0.2 mg/ml *trp* in combination with 0.02 mg/ml *trpl* cRNA, all in final volume of 50 nl, were injected into oocytes. The efficiency of translation of the *trp* and *trpl* cRNAs in oocytes was tested by Western blots on days 3–5 after injection. Aliquots equivalent to three oocytes were used for Western blot analyses. Aliquots equivalent to three *Drosophila* heads were used as markers for TRP and TRPL proteins (Fig. 1). Monoclonal anti-TRP antibody (mAb83F6) (41) and affinity-purified rabbit polyclonal anti-TRPL antibodies raised against the C-terminal hexadeca peptide of TRPL and enhanced chemiluminescense (Amersham) were used to visualized the TRP and TRPL proteins (Fig. 1).

Fluorescent Measurements of Ca^{2+} Changes. Fluorescent confocal Ca^{2+} measurements and electrophysiological studies were carried out 3–5 days after injection of cRNAs into oocytes. Oocytes were maintained and examined as described (42). Non-injected (control) oocytes or oocytes injected with cRNA encoding TRP, TRPL, and their combination (TRP+TRPL) were loaded with 50 μM of fluo-3 and 50 μM Fura Red (Molecular Probes). Control oocytes injected with 50 nl of cRNA buffer gave results indistinguishable from those of non-injected oocytes. Fluorescent dyes were injected approximately 20 min before the measurements together with 10 μM inositol 1,4,5,-trisphosphate 3-deoxy-3-fluoro ($InsP_3$-F) (final concentration, Sigma). The oocytes were bathed in Ca^{2+}-free ND96 medium containing: 96 mM NaCl, 2 mM KCl, 5 mM Hepes, 10 mM $MgCl_2$, 0.2 mM EGTA. Intracellular Ca^{2+} changes were measured before and during Ca^{2+} application and after washout of the Ca^{2+}-containing solution. In the Ca^{2+}-containing solution, EGTA was replaced with 2 mM $CaCl_2$ and $MgCl_2$ was reduced to 1 mM. Data acquisition was performed using the Sarastro confocal laser scanning microscope where the excitation light was 488 nm, the dichroic mirror was LP595, and the emission filters were 640DF35 and 530DF30 (Omega Optical, Brattleboro, VT) for the Fura Red and fluo-3 fluorescence, respectively. Scans included 512 × 512 pixels, with a pixel size of 2 μm using the Pl Fl 10/0.30 (Leitz) objective lens and a pinhole of 100 mm. Ratios were calculated as F640/F530 fluorescence. All oocytes were also tested electrophysiologically after the fluorescence measurements and gave results similar to those presented in Fig. 3.

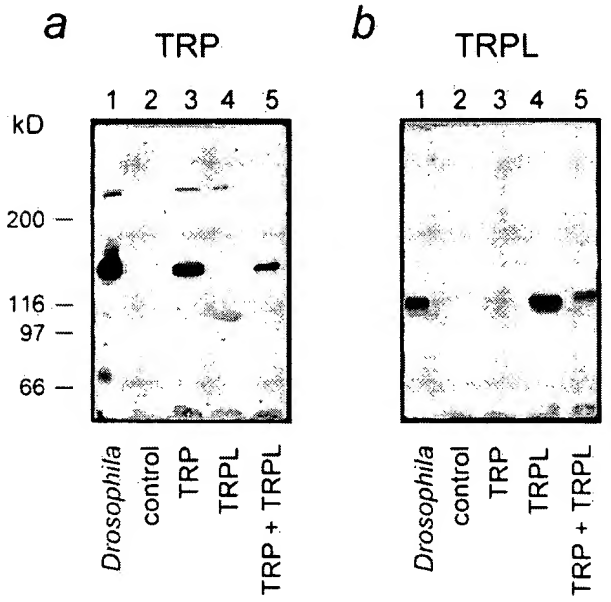

FIG. 1. Heterologous expression of TRP and TRPL gives rise to large amounts of TRP and TRPL proteins. Western blots show the expression of TRP (*a*) and TRPL (*b*) in oocytes injected with cRNA of *trp*, *trpl*, and *trp*+*trpl*, as indicated. Control (uninjected oocytes) and extract of three wild-type *Drosophila* heads (*Drosophila*) show that the equivalent molecular sizes of the *Drosophila* TRP and TRPL were produced in the oocytes, which cannot be confused with endogenous oocyte protein of similar structure and size. The data of this figure were highly reproducible in oocytes from different frogs (n = 8).

Electrophysiological Measurements Using Voltage-Clamped Oocytes. For electrophysiology, oocytes were impaled with two glass microelectrodes, which were filled with 3 M KCl with a resistance of 0.5–2.0 MΩ. The cells were voltage clamped using the standard two electrode-voltage-clamp technique. Drugs were added externally to the perfusate, while $InsP_3$-F (10 mM, final concentration) was injected into the oocyte with a Drummond 10 ml microdispenser. The small differences between the histograms of Fig. 3 *c* and *d* and the summary histogram of Fig. 5 arise from differences in the quality of the oocytes used in the various experiments. The most significant results were obtained in oocyte groups showing no deterioration with age and minimal leak currents.

Whole-Cell Recordings of Light-Induced Current (LIC) in *Drosophila*. Current-voltage relationship of the leak-subtracted peak LIC were plotted from responses to identical 100 ms light flashes of orange light (OG 590, Schott edge filter). The LICs were measured from *Drosophila* isolated ommatidia during whole-cell voltage clamp recordings as described (22, 23). Bath solution contained: 120 mM NaCl, 5 mM KCl, 10 mM TES buffer (pH 7.15), 30 mM sucrose, 8 $MgSO_4$, with no Ca^{2+} added. The whole-cell recording pipette contained: 100 mM CsCl, 15 mM TEA, 2 mM $MgSO_4$, 10 mM TES buffer (pH 7.15), 4 mM MgATP, 0.4 mM Na_2GTP.

RESULTS

Western Blot Analysis Showing Expression of TRP and TRPL. Expression of TRP and TRPL proteins in *Xenopus* oocytes microinjected with cRNA to their respective genes was demonstrated by Western blot analysis using monoclonal anti-TRP antibody (41) (Fig. 1*a*) or affinity-purified anti-TRPL antibody (Fig. 1*b*). We have found that high levels of TRPL expression largely reduced the survival time of the oocytes and, therefore, the level of TRPL expression should be carefully controlled. In contrast, the expression level of TRP had no effect on the survival time of the oocytes. Accordingly, we injected a 10-fold larger amount of cRNA encoding TRP than TRPL. The significant reduction in expression of TRP or TRPL in oocytes coexpressing TRP+TRPL is probably due to competition on the protein synthesis system of the oocyte.

Fluorescent Measurements of Ca^{2+} Changes Reveal Enhanced Ca^{2+} Permeability in TRP+TRPL-Expressing Oocytes. Fluorescent Ca^{2+} indicators were used to detect intracellular Ca^{2+} changes in oocytes expressing TRP, TRPL, or both (TRP+TRPL, Fig. 2). CCE was induced by depletion of the $InsP_3$-sensitive Ca^{2+} stores and measured as a change in intracellular Ca^{2+} following application of Ca^{2+} to the external medium. Confocal images of Fura Red/fluo-3 ratio difference revealed an enhanced rise in cytoplasmic Ca^{2+} in

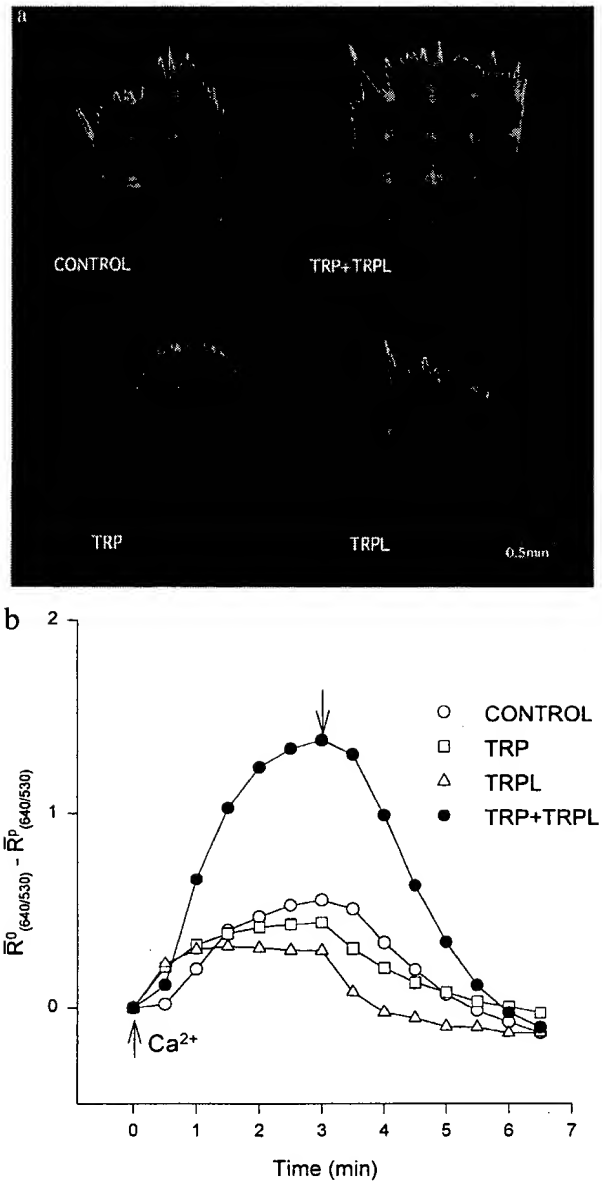

FIG. 2. Coexpression of TRP and TRPL largely enhances Ca^{2+} influx into Ca^{2+} stores-depleted oocytes. (*a*) Confocal images of ratio changes between resting and peak Ca^{2+} levels during application of Ca^{2+} containing solution (2 mM). Changes of ratios were coded as the green-to-red gradient together with the *z*-axis magnitude. One pair of optical sections across the oocyte of about 70 μm deep was analyzed to form each image. The "ring" shape of the image is due to the melanin pigmentation, which interferes with the fluorescence detection from the center of the oocyte. (*b*) A plot of changes in fluorescence ratio as a function of time in the oocytes shown in *a*. The ordinate plots the average ratio difference ($\bar{R}^{o}_{(640/530)} - \bar{R}^{p}_{(640/530)}$) where $\bar{R}$ is the averaged fluorescence ratio of the scan before ($\bar{R}^{o}$) or during and after ($\bar{R}^{p}$) Ca^{2+} application. The ratio of the pixels was averaged for a whole scan after threshold noise reduction. The normalized average ratio difference of TRP+TRPL was 2.08 ± 0.23 (n = 5) times the averaged control (n = 9), as compared with TRPL alone at 0.82 ± 0.10 (n = 5) times the control. The TRP+TRPL group was significantly different from the other oocyte groups ($P < 0.01$), whereas the other oocyte groups were not significantly different ($P > 0.05$). The initial Ca^{2+} level was variable among oocytes; therefore, ratio differences were used to demonstrate consistent results similar to those shown in Fig. 3 *b* and *c*. The magnitude of the ratio differences varied in different experiments; therefore, the summary results were normalized. The time of Ca^{2+} application and removal is indicated by up- and down-pointing arrows, respectively.

TRP+TRPL-expressing oocytes (Fig. 2*a*). Spatial averages of fluorescence ratios at different times are shown in Fig. 2*b*. The oocytes expressing TRP+TRPL showed a 2- to 3-fold larger increase in cytoplasmic Ca^{2+} than did control oocytes or oocytes individually expressing either TRP or TRPL, suggesting a larger Ca^{2+} permeability of the TRP+TRPL-expressing oocytes (Fig. 2*b*). The Western blots (Fig. 1) indicate that the large response of the TRP+TRPL system (Fig. 2) could not be due to excessive expression of either TRP or TRPL.

Functional Coexpression of TRP+TRPL Produced Capacitative Ca^{2+} Entry Currents. To analyze CCE oocytes were bathed in Ca^{2+}-free medium and the $InsP_3$-sensitive Ca^{2+} stores were depleted of Ca^{2+} either by treatment with thapsigargin (1 μM) for ≈2 hr before the measurements, or by intracellular injection of $InsP_3$-F (10 μM). This procedure totally eliminated intracellular calcium as verified by subsequent injection of $InsP_3$-F (10 μM), which failed to induce any response (n = 8) (43, 44). An increase in cellular Ca^{2+} produces a large native Ca^{2+}-activated Cl^- current ($I_{Cl,Ca}$), which interferes with direct Ca^{2+} current measurements (37, 44–46). Therefore, two independent procedures were used to assess divalent cation permeability: (*i*) endogenous $I_{Cl,Ca}$ was used as a sensitive reporter for an increase in cellular Ca^{2+} (Fig. 3*a*), (*ii*) a novel inward current carried mainly by Mg^{2+}, (referred to as *Drosophila* store-operated current, I_{dSOC}) was measured in the absence of external and internal Ca^{2+}. A prior injection of 2 mM EGTA (final concentration, n = 7, see Fig. 3*b*) ensured that the internal Ca^{2+} stores were totally depleted.

$I_{Cl,Ca}$ was activated by a Ca^{2+} pulse, followed by a voltage step from holding voltage of −10 mV to −120 mV in Ca^{2+} store-depleted oocytes. The voltage step increased the driving force for Ca^{2+} influx. An instantaneous leak current followed by a transient inward $I_{Cl,Ca}$ current with well-described characteristics was measured (44, 45). A relatively small $I_{Cl,Ca}$ was observed in non-injected (control) oocytes or in oocytes expressing TRP (Fig. 3*a*, but see Fig. 5*a*). Oocytes expressing TRPL revealed a dependence of $I_{Cl,Ca}$ on the chemical agent used for Ca^{2+} store depletion (see below, Figs. 3 *a* and *c* and 5*a*). Oocytes expressing TRP+TRPL showed the largest $I_{Cl,Ca}$ (Figs. 3 *a* and *c* and 5*a*).

Properties of the Depletion-Activated Divalent Current. To measure I_{dSOC} in Ca^{2+} store-depleted oocytes the holding voltage (−10 mV) was stepped to −120 mV in the presence of 10 mM external Mg^{2+} and Ca^{2+}-free medium. The store-depletion-activated I_{dSOC} was observed only in oocytes expressing TRP+TRPL (Figs. 3 *b* and *d* and 5*b*). Lanthanum, an efficient blocker of the *trp*-dependent conductance in *Drosophila* photoreceptors (19, 22) completely and reversibly blocked $I_{Cl,Ca}$ and I_{dSOC} (Fig. 3 *c* and *d*). I_{dSOC} had a slow rise time of ≈3 min (n = 6); also, it did not decline during the negative voltage step. These properties of I_{dSOC} may arise from a partial voltage-dependent blocking effect of Mg^{2+} (see below) that was slowly removed by the large hyperpolarizing voltage step and from the absence of Ca^{2+}-mediated negative feedback, respectively. Ca^{2+}-mediated negative feedback is typical for $InsP_3$ systems (5, 43).

The current-voltage relationship (I-V curve) of $I_{d_{SOC}}$ (Fig. 4) showed an increased inward current below −80 mV (inward rectification) and outward current above 30 mV (outward rectification). Similarly, the *Drosophila* LIC shows an I-V curve with inward and outward rectification (22, 41) (Fig. 4, *Inset*). When Na^+ was replaced with the impermeable cation *N*-methyl-D-glucamine at 10 mM external Mg^{2+} no significant effect on the I-V curve was observed. This suggests that Mg^{2+} is the main cationic charge carrier of I_{dSOC} (Fig. 4). However, Mg^{2+} had an inhibitory effect on the amplitude of I_{dSOC} showing a decrease in inward current when external Mg^{2+} was increased. Thus, the dependence of I_{dSOC} on external Mg^{2+} concentration is complex and requires further study. There are quantitative differences between the *Drosophila* LIC and

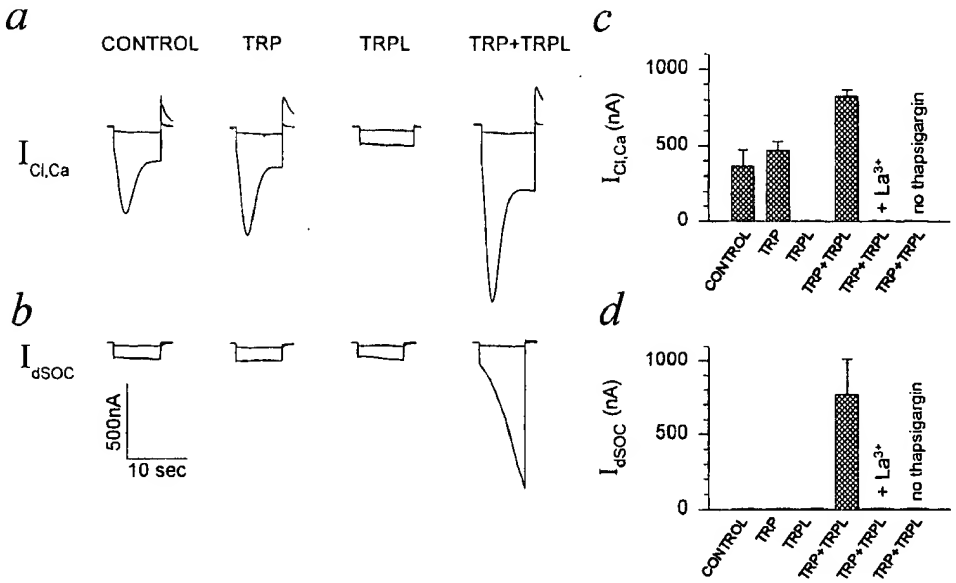

FIG. 3. Functional coexpression of TRP+TRPL in *Xenopus* oocytes produced a capacitative Ca^{2+} entry system revealed by $I_{Cl,Ca}$ and I_{dSOC}. Shown is a single experiment, employing several oocytes from a single frog that were maintained and treated together. (*a*) Measurements of currents ($I_{Cl,Ca}$) in thapsigargin-treated oocytes (1 μM in Ca^{2+}-free solution for 1.5–2 hr). $I_{Cl,Ca}$ was activated by stepping the holding voltage from −10 mV to −30 mV (upper traces) and to −120 mV (bottom traces) to show the relatively small instantaneous leak current in solution containing 1 mM Ca^{2+} (see Fig. 2). Oocytes were injected with cRNA 5 days before the measurements. (*b*) Measurements of I_{dSOC} were carried out as described in *a*. The same oocytes were perfused with Ca^{2+}-free ND96 solution (10 mM Mg^{2+}). In some of the measurements, 2 mM EGTA was injected into the oocytes 1–2 hr before the recordings, but no significant effect on I_{dSOC} was found. I_{dSOC} was totally and reversibly blocked by addition of 1 mM La^{3+} to the perfusate (*c* and *d*). I_{dSOC} was also blocked reversibly by 500 μM, but not by 50 μM, La^{3+} (n = 12). (*c* and *d*) Histograms summarizing the results from all the oocytes of the same experimental run of *a* and *b*. Five to 10 oocytes were used for each of the experimental groups of *a* and *b*. The histograms present the mean and SEM of the peak $I_{Cl,Ca}$ (*c*) and maximal I_{dSOC} (*d*) measured at −120-mV holding potentials after the instantaneous leak currents were subtracted from all current traces. The TRP+TRPL group was significantly different from the other oocyte groups of *c* ($P < 0.01$). The control and TRP groups were not significantly different ($P > 0.05$).

I_{dSOC}. The LIC of *Drosophila* is more sensitive to La^{3+} (ref. 22, and see legend of Fig. 3*b*) and has a larger Na^+ permeability than $I_{d_{SOC}}$ of the oocytes expressing TRP+TRPL (22) (Fig. 4).

Without Ca^{2+} store depletion at non-toxic TRPL expression level (see below), neither $I_{Cl,Ca}$ (44) nor I_{dSOC} could be observed (Fig. 3 *c* and *d*) even with elevated external concentration of Ca^{2+} (10 mM, n = 9) or Mg^{2+} (40 mM, n = 8). Oocytes injected with a 10-fold larger dose of *trpl* cRNA showed a significant $I_{Cl,Ca}$ or inward Mg^{2+} current similar to I_{dSOC}; however, this current was activated by a negative voltage step without depletion of the Ca^{2+} stores (n = 21). The latter effect is reminiscent of a property of the currents that have been described in TRPL-expressing Sf9 cells, which show constitutively active cationic channels (30, 31, 36), but poor ability to conduct Mg^{2+}. However, these conditions were toxic and most of the oocytes died within 4 days depending on the expression level of TRPL.

The summary histogram in Fig. 5*a* shows that oocytes expressing TRP or TRPL exhibited a dependence of $I_{Cl,Ca}$ on the method of Ca^{2+} store depletion. In the TRPL-expressing oocytes, depletion using thapsigargin significantly reduced $I_{Cl,Ca}$ below the control level, whereas depletion using $InsP_3$-F enhanced the $I_{Cl,Ca}$ current above the level of the controls (Fig. 5*a*). In oocytes expressing TRP alone, thapsigargin treatment exhibited a significant increase in $I_{Cl,Ca}$ over control oocytes (37), which was not observed in $InsP_3$-F treated oocytes (Fig. 5*a*). The above differential effects are reminiscent of the results reported for Sf9 cells expressing individually TRP or TRPL (30, 31, 36). At present we do not have sufficient data to explain the effects of either TRP or TRPL on $I_{Cl,Ca}$ or the currents recorded in Sf9 cells. A possible explanation is that the effects shown in Fig. 5*a* are apparently due to individual interactions of TRP or TRPL with the endogenous CCE (8, 9). Such individual interactions may also account for the enhancement of the depletion-activated current described for Sf9 cells or $I_{Cl,Ca}$ recorded in oocytes expressing TRP alone (30, 37, 38). Oocytes expressing TRP+TRPL revealed approximately 3-fold larger $I_{Cl,Ca}$ than the controls regardless of the method used to deplete the Ca^{2+} stores (Fig. 5*a*). The summary histogram in Fig. 5*b* shows that under our experimental conditions the store-depletion activated I_{dSOC} was observed only in oocytes expressing TRP+TRPL.

DISCUSSION

The induction of the I_{dSOC} response to Ca^{2+} store depletion, in oocytes coexpressing *Drosophila* TRP+TRPL, clearly showed that these proteins are efficiently coupled to the endogenous store-depletion signal. Depletion of internal stores in *Drosophila* photoreceptors by thapsigargin fails to induce inward current in the dark (47). However, application of ionomycin together with Ca^{2+} chelators, a procedure that might be expected to deplete intracellular stores, leads to production of inward current in *Drosophila* photoreceptors suggesting that CCE does exist in *Drosophila* photoreceptors (R. C. Hardie, personal communication).

The most significant result of coexpressing TRP+TRPL was revealed by measuring I_{dSOC} and its voltage-dependent Mg^{2+} current showing inward and outward rectification (Fig. 4) in thapsigargin-treated oocytes. Similarly, the LIC of *Drosophila* has a permeability to Mg^{2+} (22), as well as a voltage-dependent blocking effect of Mg^{2+} (48). The creation of La^{3+}-sensitive Mg^{2+} current with inward rectification in the oocyte is thus similar to a unique characteristic of the *Drosophila* photoreceptor cell.

Unlike I_{dSOC}, capacitative Ca^{2+} entry current in various vertebrate cells is carried almost exclusively by Ca^{2+} (3, 4, 49–51; but also see ref. 52). It therefore appears that the

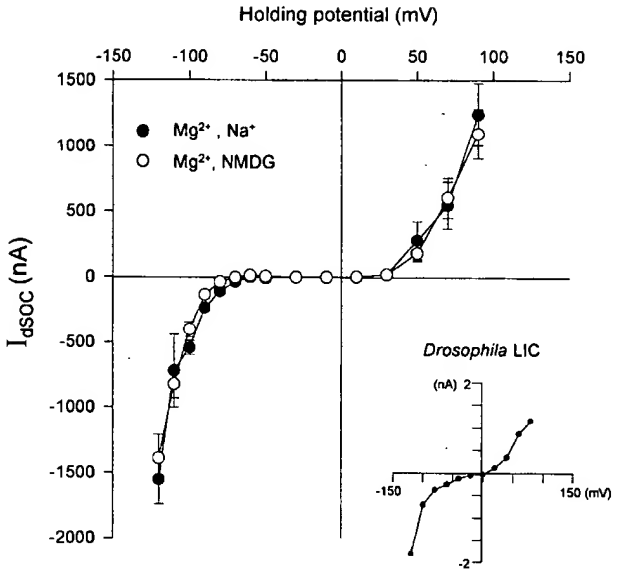

FIG. 4. Current-voltage relationship of I_{dSOC} in oocytes expressing TRP+TRPL. Inward and outward rectification typical of *Drosophila* light-activated current are shown. Current-voltage relationship (I-V curve) plotting the leak-subtracted maximal I_{dSOC} as a function of holding voltage in $InsP_3$-F (10 μM) or thapsigargin-treated oocytes incubated in Ca^{2+}-free medium (see Fig. 3 *a* and *b*). Solutions are as in Fig. 3*b*. The I-V curves were measured before (●) and after (○) Na^+ was replaced by *N*-methyl-D-glucamine (NMDG, 96 mM). Graphs show the average of currents obtained from nine oocytes of a single experiment. Very similar results were obtained in five other experiments. (*Inset*) Current-voltage relationship of the leak-subtracted peak LIC responses to identical 100-ms light flashes of orange light (OG 590, Schott edge filter) recorded from *Drosophila* isolated ommatidia during whole-cell voltage clamp recordings as described (22).

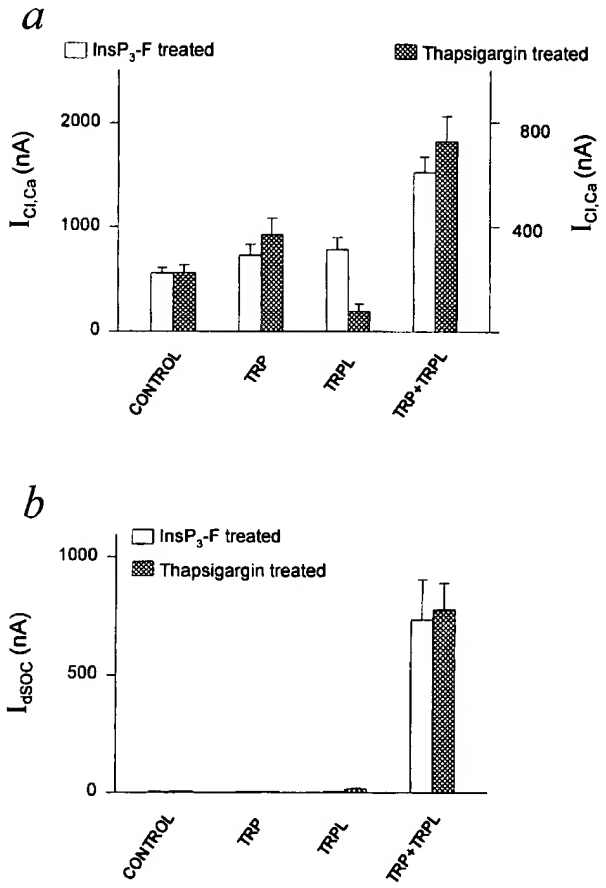

FIG. 5. Histograms summarizing $I_{Cl,Ca}$ and I_{dSOC} in TRP, TRPL, and TRP+TRPL-expressing oocytes in experiments similar to those in Fig. 3. (*a*) $I_{Cl,Ca}$ measured in $InsP_3$-F-treated oocytes (left ordinate) or thapsigargin-treated oocytes (right ordinate). Eleven independent experiments used 16–64 oocytes in each group. The TRP+TRPL groups were significantly different from the other oocyte groups ($P < 0.01$), whereas the other oocyte groups were not significantly different in the $InsP_3$-F-treated oocytes ($P > 0.05$). In the thapsigargin-treated oocytes all groups were significantly different from each other ($P < 0.01$ for a comparison between the control TRPL and TRP+TRPL groups; $P < 0.05$ for a comparison between the control and TRP group). (*b*) I_{dSOC} measured in $InsP_3$-F or thapsigargin-treated oocytes. Seven independent experiments used 8–22 oocytes in each group.

TRP+TRPL-dependent current has some properties different from the capacitative Ca^{2+} entry currents of several vertebrate cells (5, 7). I_{dSOC} is also different from the currents found in the Sf9 cells expressing either TRP or TRPL, which are characterized by a linear I-V curve, absence of a Mg^{2+} block of the TRP-dependent conductance; and a constitutive activity of the TRPL-dependent conductance. The coexpressed TRP+TRPL-dependent current in *Xenopus* oocyte suggests that we have reconstituted a capacitative Ca^{2+} entry mechanism with some similarity to the native *Drosophila* system. Our data suggest that a cooperative action of TRP and TRPL is efficiently coupled to the endogenous Ca^{2+} store-depletion signal. The synergistic activity of TRP and TRPL in the production of the depletion-activated current suggest that these proteins interact with each other (for a review see ref. 13). The simplest interpretation of our results is that TRP and TRPL contribute channel subunits to form a multimeric channel. Nevertheless, our results, as well as the individual expression of *Drosophila* TRP, TRPL, and the human *trp* homologue genes (9, 30, 31, 34–36) have not demonstrated that the various TRP proteins form ionic channels. It is still possible that these expressed proteins exert their function through the endogenous CCE channels (8, 9). Other approaches, such as coimmunoprecipitation of TRP and TRPL should be used in future experiments to demonstrate that the physiological synergism found in this study is based on physical interaction between the two proteins. Also, single-channel recordings should be made to study the identity and properties of the depletion-activated channels. This study has established a useful basis for such future studies.

We thank Dr. Roger C. Hardie for the permission to quote his unpublished results, Drs. Craig Montell and Len Kelly for the cDNA of *trp* and *trpl* in bluescript vector, and Arnd Baumann for the cDNA of the above genes in PGEMHE vector. We thank Drs. U. Benjamin Kaupp, Charles S. Zuker, and Roger C. Hardie for critical comments on an earlier version of the manuscript. We also thank O. Devary, L. Alfonte, M. Eshel, and G. Barkai for technical help. This research was supported by grants from the National Institutes of Health, the Kuhne Minerva Center, the U.S.–Israel Binational Science Foundation (B.M. and Z.S.), the German-Israel Foundation (B.M.), and grants from the National Institutes of Health and National Science Foundation–Center for Light Microscope Imaging and Biotechnology (J.A.P.)

1. Putney, J. W. J. (1990) *Cell Calcium* **11**, 611–624.
2. Hoth, M. & Penner, R. (1992) *Nature (London)* **355**, 353–356.
3. Zweifach, A. & Lewis, R. S. (1995) *J. Biol. Chem.* **270**, 14445–14451.
4. Lewis, R. S. & Cahalan, M. D. (1995) *Annu. Rev. Immunol.* **13**, 623–653.
5. Berridge, M. J. (1995) *Biochem. J.* **312**, 1–11.
6. Clapham, D. E. (1995) *Cell* **80**, 259–268.
7. Clapham, D. E. (1996) *Neuron* **16**, 1069–1072.
8. Friel, D. D. (1996) *Cell* **85**, 617–619.

9. Zhu, X., Jiang, M. S., Peyton, M., Boulay, G., Hurst, R., Stefani, E. & Birnbaumer, L. (1996) *Cell* **85,** 661–671.
10. Hardie, R. C. & Minke, B. (1995) *Cell Calcium* **18,** 256–274.
11. Ranganathan, R., Malicki, D. M. & Zuker, C. S. (1995) *Annu. Rev. Neurosci.* **18,** 283–317.
12. Pak, W. L. (1995) *Invest. Ophthalmol. Visual Sci.* **36,** 2340–2357.
13. Minke, B. & Selinger, Z. (1996) *Curr. Opin. Neurobiol.* **6,** 459–466.
14. Minke, B. & Selinger, Z. (1991) *Prog. Retinal Res.* **11,** 99–124.
15. Minke, B., Wu, C. & Pak, W. L. (1975) *Nature (London)* **258,** 84–87.
16. Cosens, D. J. & Manning, A. (1969) *Nature (London)* **224,** 285–287.
17. Minke, B. (1982) *J. Gen. Physiol.* **79,** 361–385.
18. Hochstrate, P. (1989) *J. Comp. Physiol. A.* **166,** 179–187.
19. Suss-Toby, E., Selinger, Z. & Minke, B. (1991) *J. Gen. Physiol.* **98,** 849–868.
20. Hardie, R. C. (1991) *Proc. R. Soc. London B* **245,** 203–210.
21. Ranganathan, R., Harris, G. L., Stevens, C. F. & Zuker, C. S. (1991) *Nature (London)* **354,** 230–232.
22. Hardie, R. C. & Minke, B. (1992) *Neuron* **8,** 643–651.
23. Peretz, A., Suss-Toby, E., Rom-Glas, A., Arnon, A., Payne, R. & Minke, B. (1994) *Neuron* **12,** 1257–1267.
24. Hardie, R. C. (1996) *J. Neurosci.* **16,** 2924–2933.
25. Peretz, A., Sandler, C., Kirschfeld, K., Hardie, R. C. & Minke, B. (1994) *J. Gen. Physiol.* **104,** 1057–1077.
26. Montell, C. & Rubin, G. M. (1989) *Neuron* **2,** 1313–1323.
27. Wong, F., Schaefer, E. L., Roop, B. C., LaMendola, J. N., Johnson Seaton, D. & Shao, D. (1989) *Neuron* **3,** 81–94.
28. Phillips, A. M., Bull, A. & Kelly, L. E. (1992) *Neuron* **8,** 631–642.
29. Niemeyer, B. A., Suzuki, E., Scott, K., Jalink, K. & Zuker, C. S. (1996) *Cell* **85,** 651–659.
30. Vaca, L., Sinkins, W. G., Hu, Y., Kunze, D. L. & Schilling, W. P. (1994) *Am. J. Physiol.* **267,** C1501–C1505.
31. Harteneck, C., Obukhov, A. G., Zobel, A., Kalkbrenner, F. & Schultz, G. (1995) *FEBS Lett.* **358,** 297–300.
32. Wes, P. D., Chevesich, J., Jeromin, A., Rosenberg, C., Stetten, G. & Montell, C. (1995) *Proc. Natl. Acad. Sci. USA* **92,** 9652–9656.
33. Zhu, X., Chu, P. B., Peyton, M. & Birnbaumer, L. (1995) *FEBS Lett.* **373,** 193–198.
34. Zitt, C., Zobel, A., Obukhov, A. G., Harteneck, C., Kalkbrenner, F., Lückhoff, A. & Schultz, G. (1996) *Neuron* **16,** 1189–1196.
35. Hu, Y., Vaca, L., Zhu, X., Birnbaumer, L., Kunze, D. L. & Schilling, W. P. (1994) *Biochem. Biophys. Res. Commun.* **201,** 1050–1056.
36. Dong, Y., Kunze, D. L., Vaca, L. & Schilling, W. P. (1995) *Am. J. Physiol.* **269,** C1332–C1339.
37. Petersen, C. C. H., Berridge, M. J., Borgese, M. F. & Bennett, D. L. (1995) *Biochem. J.* **311,** 41–44.
38. Sinkins, W. G., Vaca, L., Hu, Y., Kunze, D. L. & Schilling, W. P. (1996) *J. Biol. Chem.* **271,** 2955–2960.
39. Liman, E. R., Tytgat, J. & Hess, P. (1992) *Neuron* **9,** 861–871.
40. Baumann, A., Frings, S., Godde, M., Seifert, R. & Kaupp, U. B. (1994) *EMBO J.* **13,** 5040–5050.
41. Pollock, J. A., Assaf, A., Peretz, A., Nichols, C. D., Mojet, M. H., Hardie, R. C. & Minke, B. (1995) *J. Neurosci.* **15,** 3747–3760.
42. Gillo, B., Lass, Y., Nadler, E. & Oron, Y. (1987) *J. Physiol. (London)* **392,** 349–361.
43. Singer, D., Boton, R., Moran, O. & Dascal, N. (1990) *Pflügers Arch.* **416,** 7–16.
44. Petersen, C. C. & Berridge, M. J. (1994) *J. Biol. Chem.* **269,** 32246–32253.
45. Yao, Y. & Parker, I. (1993) *J. Physiol. (London)* **468,** 275–295.
46. Parekh, A. B., Terlau, H. & Stuhmer, W. (1993) *Nature (London)* **364,** 814–818.
47. Ranganathan, R., Bacskai, B. J., Tsien, R. Y. & Zuker, C. S. (1994) *Neuron* **13,** 837–848.
48. Hardie, R. C. & Mojet, M. H. (1995) *J. Neurophysiol.* **74,** 2590–2599.
49. Lewis, R. S. & Cahalan, M. D. (1989) *Cell Regul.* **1,** 99–112.
50. Zweifach, A. & Lewis, R. S. (1993) *Proc. Natl. Acad. Sci. USA* **90,** 6295–6299.
51. Penner, R., Fasolato, C. & Hoth, M. (1993) *Curr. Opin. Neurobiol.* **3,** 368–374.
52. Lückhoff, A. & Clapham, D. E. (1994) *Biophys. J.* **67,** 177–182.

Vol. 201, No. 2, 1994 BIOCHEMICAL AND BIOPHYSICAL RESEARCH COMMUNICATIONS
June 15, 1994 Pages 1050-1056

APPEARANCE OF A NOVEL Ca^{2+} INFLUX PATHWAY IN Sf9 INSECT CELLS FOLLOWING EXPRESSION OF THE TRANSIENT RECEPTOR POTENTIAL-LIKE (*trpl*) PROTEIN OF *DROSOPHILA*

Yanfang HU, Luis VACA, Xi ZHU*, Lutz BIRNBAUMER*, Diana L. KUNZE, and William P. SCHILLING

Depts. of Molecular Physiology & * Biophysics and Cell Biology
Baylor College of Medicine, Houston, TX 77030

Received May 6, 1994

SUMMARY: Activation of phospholipase C, elevation of free cytosolic Ca^{2+} concentration ($[Ca^{2+}]_i$) and stimulation of Ca^{2+} influx have been implicated in *Drosophila* phototransduction. Electrophysiological studies suggest that *trp* and *trpl* proteins may be important for the light-activated Ca^{2+} current found in *Drosophila* photoreceptor cells. Although these proteins exhibit homologies to voltage-gated Ca^{2+} and Na^+ channels, their actual function in insect cells and their relation to proteins involved in mammalian cell Ca^{2+} signaling remains unknown. In the present study, $[Ca^{2+}]_i$ was examined in fura-2-loaded Sf9 insect cells infected with recombinant baculovirus containing cDNA for the *trpl* protein. Ca^{2+} influx was examined by use of Ba^{2+}, a Ca^{2+} surrogate that is not a substrate for Ca^{2+}-pumps or carriers and by measurement of whole-cell membrane currents. The results suggest that expression of *trpl* is associated with appearance of a Ca^{2+} permeable, non-selective cation channel formed by the *trpl* protein.

Light stimulation of the photoreceptor cells of *Drosophila* initiates a cascade of events involving activation of phospholipase C, an increase in inositol-1,4,5-trisphosphate ($Ins(1,4,5)P_3$), mobilization of intracellular Ca^{2+}, and an opening of cation-selective ion channels in the plasmalemma. This causes an increase in membrane current and a sustained depolarization of the receptor potential (1). In the *transient receptor potential* mutant (*trp*), low level light stimulation of the photoreceptor cell produces a near normal response whereas, stimulation with intense light causes only a transient change in receptor potential; the prolonged depolarization seen in the wild type cell is eliminated as is the sustained inward current (2-4). Although the actual function of the *trp* protein has not been determined, it has recently been proposed that *trp* is a light-activated Ca^{2+} channel (3,5). Another protein initially identified as a calmodulin-binding protein, has been cloned from *Drosophila* and designated as *trp*-like or *trpl* since it shares substantial sequence homology with *trp* (5). The proposed transmembrane segments of both *trp* and *trpl* show homologies to membrane spanning regions of voltage-gated Ca^{2+} and Na^+ channels.

0006-291X/94 $5.00

H COMMUNICATIONS
Pages 1050-1056

IN Sf9 INSECT
T RECEPTOR
HILA

L. KUNZE,

logy

Ca^{2+} concentration
r phototransduction.
ortant for the light-
ese proteins exhibit
insect cells and their
own. In the present
with recombinant
l by use of Ba^{2+}, a
surement of whole-
ed with appearance

cascade of events
ate ($Ins(1,4,5)P_3$),
l channels in the
polarization of the
el light stimulation
with intense light
n seen in the wild
ial function of the
a light-activated
protein, has been
stantial sequence
p and *trpl* show
Na^+ channels.

Interestingly, some light-activated membrane current is observed in the *trp* mutant during intense light stimulation although it is only transiently activated (3). This has led to speculation that *trp* encodes for a Ca^{2+}-selective channel responsible for the sustained current component, whereas *trpl* encodes for a Ca^{2+}-activated, non-selective cation channel responsible for the transient change in membrane current (1,5).

In the present study we infected Sf9 insect cells with recombinant baculovirus containing the *trpl* cDNA under control of the polyhedrin promoter (*trpl* cells). Plasmalemmal permeability to Ca^{2+} was determined using both fura-2 and whole cell patch clamp techniques. As control, the results were compared to Sf9 cells infected with recombinant baculovirus containing the cDNA for the M_5 muscarinic receptor (M_5 cells). The results suggest that expression of *trpl* is associated with an increase in plasmalemmal permeability to Ca^{2+} which reflects the activity of a novel cation channel.

MATERIALS AND METHODS

Solutions and reagents. Unless otherwise indicated, MES-buffered saline (MBS) contained the following: 10 mM NaCl, 60 mM KCl, 17 mM $MgCl_2$, 10 mM $CaCl_2$, 4 mM D-glucose, 110 mM sucrose, 0.1% bovine serum albumin, and 10 mM MES, pH adjusted to 6.2 at room temperature with Trizma-base. The full-length cDNA for *trpl* (pAB3.14/Z9) (5) was generously provided by Dr. Leonard E. Kelly (Department of Genetics, University of Melbourne, Parkville, Victoria, Australia).

Culture of Sf9 cells. Sf9 cells were obtained from Invitrogen (San Diego, CA) and were cultured as previously described (6) using Grace's Insect Medium (Gibco) supplemented with lactalbumin hydrolysate, yeastolate, L-glutamine, 10% heat-inactivated fetal bovine serum, and 1% penicillin-streptomycin solution (Gibco).

Production of recombinant baculoviruses and infection of Sf9 cells. The cDNA encoding the M_5 muscarinic receptor and *trpl* were subcloned into baculovirus tranfer vector, pVL1392 and pVL1393, respectively, using standard techniques (7). Recombinant viruses were produced using the BaculoGold Transfection Kit (PharMingen, San Diego, CA). For routine infection, Sf9 cells in Grace's medium were allowed to attach to the bottom of a 100 mm plastic culture dish (10^7 cells/dish). Following incubation for 15 min to 1 hr, an aliquot of viral stock (multiplicity of infection was 20 and 3 for M_5 and *trpl*, respectively) was added and the cultures were maintained at 27°C in a humidified air atmosphere. Unless otherwise indicated, cells were used at 30-36 hrs. post-infection.

Measurement of free cytosolic Ca^{2+} concentration ($[Ca^{2+}]_i$) in dispersed Sf9 cells. $[Ca^{2+}]_i$ was measured at room temperature using the fluorescent indicator, fura-2, as previously described (8-10). $[Ca^{2+}]_i$ was calculated by the equation of Grynkiewicz et al. (11) using the K_d value for Ca^{2+} binding to fura-2 of 278 nM determined at 22°C (12). The figures show representative traces from experiments performed at least 3 times.

Electrophysiological methods. The patch clamp technique for whole-cell recording was utilized in these studies (13). All electrophysiological experiments were performed at room temperature. Currents were acquired on line and analyzed using the commercially available pClamp programs (Axon Intruments). The pipette (intracellular) solution contained 100 mM Na-Gluconate, 1 mM KCl, 10 mM *HEPES*, pH. 6.5. Osmolarity was adjusted to 320 mosM with mannitol. The bath (extracellular) solution was MBS.

RESULTS AND DISCUSSION

In order to examine endogenous Ca^{2+} signaling mechanisms, Sf9 cells were infected with recombinant baculovirus containing the cDNA for the M_5 receptor. Addition of carbachol to fura-2-loaded M_5 cells produced the typical biphasic $[Ca^{2+}]_i$ profile commonly seen in non-excitable cells of mammalian origin (Fig. 1). The $[Ca^{2+}]_i$ initially increased 6 to 8-fold over the basal value and subsequently declined with time to a steady elevated phase. Addition of the Ca^{2+} influx blockers, Gd^{3+} (Fig.1; 1 μM) or La^{3+} (10 μM; not shown), during the sustained component of the response to carbachol rapidly returned $[Ca^{2+}]_i$ to the basal level suggesting that the sustained component is dependent upon Ca^{2+} influx. Thus, although the Sf9 cells have an endogenous Ca^{2+} influx pathway that can be activated by stimulation a heterologous membrane receptor, this Ca^{2+} influx is blocked by low concentrations of lanthanides. Carbachol had no effect on uninfected Sf9 cells or on cells infected with baculovirus containing an unrelated cDNA.

In contrast to M_5 infected cells in which the resting $[Ca^{2+}]_i$ was 88 ± 5 nM, basal $[Ca^{2+}]_i$ was significantly ($p<0.001$) increased to 293 ± 21 nM in *trpl* cells examined 30 to 36 hrs post-infection (mean ± S.E. of 7 independent infections). Basal $[Ca^{2+}]_i$ in *trpl* cells was unchanged at 6 and 12 hrs post-infection, but increased in a time-dependent fashion from 24 to 48 hrs (Fig. 2). Thus, the increase in basal $[Ca^{2+}]_i$ in the *trpl* cells occurs over a time frame appropriate for expression of a protein under control of the polyhedrin promoter (14).

The change in basal $[Ca^{2+}]_i$ might reflect either an inhibition of the Ca^{2+} pumping mechanism(s) of the Sf9 cell or an increase in Ca^{2+} influx from the extracellular space. In order to clearly distinguish between these two possibilities we have employed Ba^{2+}. Ba^{2+} has been

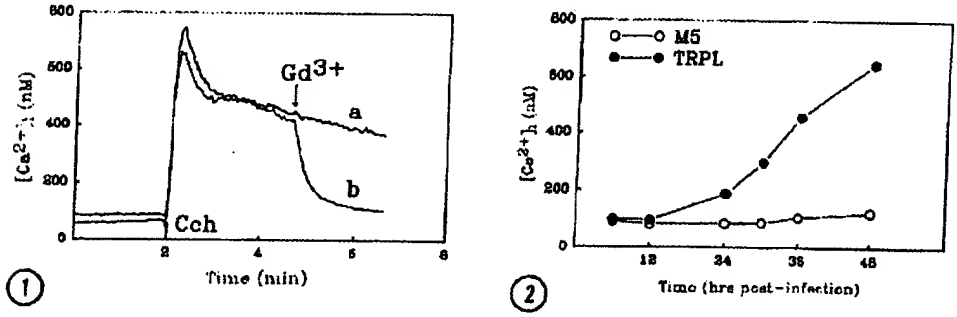

Fig. 1. Effect of carbachol on $[Ca^{2+}]_i$ in Sf9 cells infected with recombinant baculovirus containing the M_5 muscarinic receptor. Two traces are shown superimposed. Carbachol (Cch; 100 μM) was added to fura-2-loaded Sf9 cells (30-36 hrs post-infection) at the time indicated by the arrow in each trace. $GdCl_3$ (1 μM) was added to one trace during the sustained component of the Cch response (trace b).

Fig. 2. Effect of post-infection time on *trpl*-induced increase in basal $[Ca^{2+}]_i$. $[Ca^{2+}]_i$ was measured in fura-2-loaded Sf9 cells at various times following infection with either M_5 (O) or *trpl* (●) containing baculovirus. Representative results of two independent infections.

shown to carry current through all known Ca^{2+} channels (15), but is a poor substrate for known Ca^{2+} pumps and transporters (8,16,17). Ba^{2+} will however, bind to fura-2 and change fluorescence in a fashion analogous to Ca^{2+} (8). Addition of Ba^{2+} to M5 cells incubated in Ca^{2+}-free buffer had very little effect on cell fluorescence (Fig. 3A). In contrast, addition of Ba^{2+} to *trpl* cells produced a dramatic increase in fluorescence ratio indicative of Ba^{2+} influx. To confirm that the change in fluorescence following Ba^{2+} addition resulted from influx, Gd^{3+} was added before the addition of Ba^{2+} to *trpl* cells incubated in Ca^{2+}-free buffer (Fig. 3B). Gd^{3+} produced a concentration-dependent inhibition of Ba^{2+} influx in *trpl* cells with an apparent IC_{50} of approximately 200 μM. Basal Ba^{2+} influx was not observed at 6 or 12 hours post-infection,

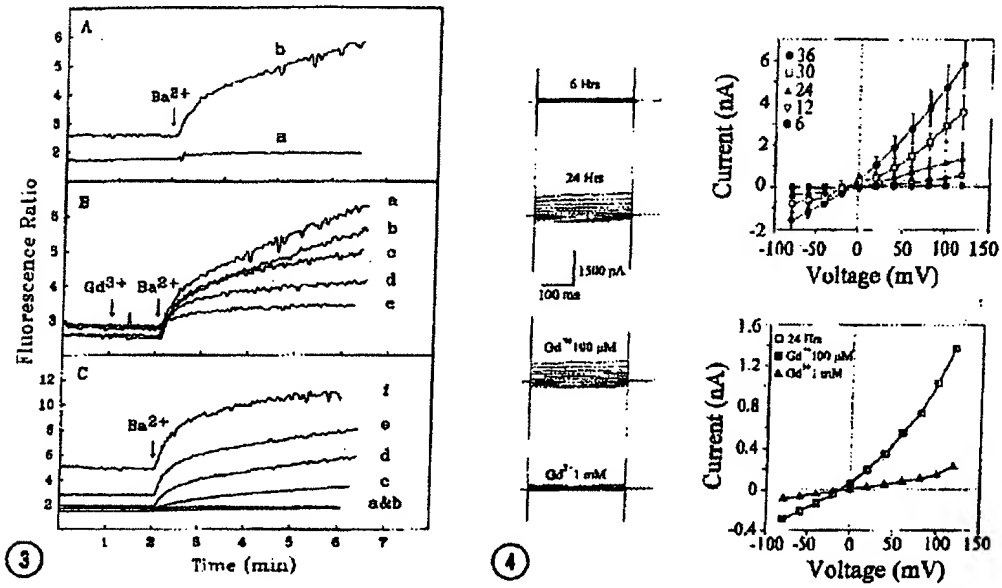

Fig. 3. Ba^{2+} influx in M_5 and *trpl* infected Sf9 cells. *Panel A:* Fluorescence ratio (for Ba^{2+} excitation wavelength alternated between 350 and 390 nm (8)) was measured in fura-2-loaded Sf9 cells suspended in Ca^{2+}-free MBS (30-36 hrs. post-infection). At the time indicated, $BaCl_2$ (10 mM) was added to either M_5 infected cells (trace a) or *trpl*-infected cells (trace b). *Panel B:* Five traces are superimposed. $BaCl_2$ (10 mM) was added at the time indicated to *trpl* infected Sf9 cells in the absence (trace a) or in the presence of 10, 100, 300, or 1000 μM $GdCl_3$ added at the arrow in traces b-e, respectively. *Panel C:* Cells were incubated in Ca^{2+}-free MBS. Six traces are shown superimposed. Ba^{2+} was added in each trace at the time indicated by the arrow. Traces a, b, c, d, e, and f show the response of the cells to added $BaCl_2$ (10 mM) at post-infection times of 6, 12, 24, 30, 36, and 48 hrs, respectively. Representative results of two independent infections.

Fig. 4. Whole cell current recording in *trpl*-infected Sf9 cells. Traces on the left show current records at different potentials obtained from Sf9 cells at 6 and 24 hours post-infection. The complete I-V is shown on the upper right at the indicated times post-infection. Each value represents the mean ± SD, n=10 cells. The lower two sets of traces were recorded at 24 hrs post-infection in the presence of 0.1 and 1 mM Gd^{3+} in the extracellular buffer. The complete I-V is shown on the lower right. Cell voltage was held at 0 mV and pulses were applied for 300 msec every 2 sec from -80 to +120 mV in 20 mV increments.

but increased in a time-dependent fashion from 24-48 hours (Fig. 3C) which correlates with the change in basal $[Ca^{2+}]_i$ seen in Fig. 2. These results suggest that expression of *trpl* is associated with an increased Ca^{2+} permeability of the Sf9 cell membrane which is, at least in part, responsible for the increased basal $[Ca^{2+}]_i$ observed in these cells.

To determine if expression of *trpl* is associated with the appearance of a novel cation channel, whole-cell membrane currents were recorded in non-infected Sf9 cells (control), and in M_5- and *trpl*-infected cells. As seen in Fig. 4, step changes in membrane potential from -80 to +120 mV produced large step changes in membrane current in *trpl* cells examined at 24 hours post-infection compared to 6 hours post-infection time. The current-voltage relationship at 6 hours was linear with a slope conductance of ~0.5 nS and a reversal potential near 0 mV. The current observed in *trpl* cells at 6 hours post-infection was not significantly different from control or M5-infected cells examined at 36 hours post-infection. However, current increased in *trpl* cells in a time-dependent fashion from 12 to 36 hours (Fig. 4) reaching a slope conductance of ~50 nS at 36 hours. The whole cell current was unaffected by 100 μM Gd^{3+}, but was reduced to control levels by 1 mM Gd^{3+}. Thus, the sensitivity of this current to Gd^{3+} and the time course of expression are similar to the results of the Ba^{2+} influx experiments.

The current observed in *trpl* cells reversed near zero mV suggesting that the current is cation selective since the equilibrium potential for Cl^- is -120 mV under these ionic conditions. Furthermore, replacing the cations in the extracellular solution with N-methyl-D-glucamine while maintaining Cl^- constant produced a shift in the reversal potential to -100 mV, as expected for a cation channel with low conductance to NMDG. In similar experiments, replacement of the bath solution with Ca^{2+}-gluconate (50 mM) produced little change in the reversal potential (n=5) indicating that the channel has similar permeability to both Na^+ and Ca^{2+}. These results demonstrate that expression of *trpl* is associated with the appearance of a non-selective cation current that also allows permeation of Ca^{2+} into the cell.

There are two possible mechanisms by which expression of the *trpl* protein can increase basal Ca^{2+} influx and membrane current. First, *trpl* may activate an endogenous non-selective cation channel. Or, second, *trpl* may itself form channels in the plasmalemma consistent with its proposed role in *Drosophila* phototransduction. It is clear that both non-infected Sf9 cells and M_5 cells exhibit little whole cell membrane current and there is no evidence for the presence of voltage-gated channel in these cells consistent with a previous report (18). Furthermore, the *trpl*-induced membrane current is large in magnitude, appears in a time-dependent fashion, and shows no evidence of saturation out to 36 hours. Thus, it seems unlikely that *trpl* is activating some endogenous channel pool. The results shown in Fig. 1 demonstrate however, that the Sf9 cell does possess a Ca^{2+} influx pathway that can be activated by heterologous receptor stimulation. The striking feature of this response is the potency of Gd^{3+} for inhibition of Ca^{2+} influx. Whereas 1 μM Gd^{3+} produced complete block of carbachol-induced Ca^{2+} influx, this concentration had essentially no effect on basal Ba^{2+} influx observed in *trpl* cells. Although these

results may reflect high expression of *trpl* protein, the >1000-fold difference in sensitivity to Gd^{3+} suggests independent pathways. Definitive proof that the *trpl* protein forms a channel will require functional expression and characterization of *trpl* mutants.

In conclusion, the results of the present study are consistent with the hypothesis that *trpl*, and perhaps *trp* proteins, form Ca^{2+} permeable, cation channels. Although of obvious importance for understanding the phototransduction pathway in *Drosophila*, these results may also provide general insight into agonist-induced Ca^{2+} signaling mechanisms in non-excitable cells of mammalian origin. The molecular mechanisms by which depletion of the Ins(1,4,5)P_3-sensitive internal Ca^{2+} store activates a surface membrane Ca^{2+} channel is currently an area of intense research. Although membrane current associated with Ca^{2+} store depletion, designated I_{CRAC}, has been measured in vascular endothelial cells (19), T lymphocytes (20), and in mast cells (21), the single channel events underlying this response have not been recorded. Noise analysis suggests that this current reflects the activity of Ca^{2+} channels of very low conductance (<<1 pS) (22). The protein responsible for this current in mammalian non-excitable cells, and in Sf9 cells, may be structurally homologous to *trp* and/or *trpl*. It will be important to begin screening mammalian cell and Sf9 cell cDNA libraries for these homologous sequences.

Acknowledgments: We thank Dr. Leonard E. Kelly for providing the *trpl* clone and Dr. Meera Pratap for help with preliminary patch clamp measurements. This study was performed during the tenure of an Established Investigatorship awarded to W.P. Schilling by the American Heart Association.

REFERENCES

1. Hardie, R.C. and Minke, B. (1993) Trends Neurosci.16, 371-376.
2. Minke, B. and Selinger, Z. (1991) In Progress in retinal research (N.N. Osborne and G.J. Chader, Eds.), pp. 99-124. Pergamon Press, Oxford.
3. Hardie, R.C. and Minke, B. (1992) Neuron 8, 643-651.
4. Cosens, D.J. and Manning, A. (1969) Nature 224, 285-287.
5. Phillips, A.M., Bull, A., and Kelly, L.E. (1992) Neuron 8, 631-642.
6. O'Reilly, D.R., Miller, L.K., and Luckow, V.A. (1992) Baculovirus expression vectors: A laboratory manual, W.H. Freeman and Co., New York.
7. Sambrook, J., Fritsch, E.F., and Maniatis, T. (1989) Molecular Cloning: A laboratory manual, Cold Spring Harbor Laboratory Press, Cold Spring Harbor.
8. Schilling, W.P., Rajan, L., and Strobl-Jager, E. (1989) J. Biol. Chem. 264, 12838-12848.
9. Tian, P., Hu, Y., Schilling, W.P., Lindsay, D.A., Eiden, J., and Estes, M.K. (1994) J. Virology 68, 251-257.
10. Hu, Y., Rajan, L., and Schilling, W.P. (1994) Am. J. Physiol.(in press).
11. Grynkiewicz, G., Poenie, M., and Tsien, R.Y. (1985) J. Biol. Chem.260, 3440-3450.
12. Shuttleworth, T.J. and Thompson, J.L. (1991) J. Biol. Chem.266, 1410-1414.

13. Hamill, O.P., Marty, A., Neher, E., Sakmann, B., and Sigworth, F.J. (1981) Pflugers Arch.391, 85-100.
14. Luckow, V.A. and Summers, M.D. (1988) Biotechnology 6, 47-55.
15. Hagiwara, S. and Byerly, L. (1981) Annu. Rev. Neurosci.4, 69-125.
16. Vanderkooi, J.M. and Martonosi, A. (1971) Arch. Biochem. Biophys.144, 99-106.
17. Gill, D.L. and Chueh, S.-H. (1985) J. Biol. Chem.260, 9289-9297.
18. Klaiber, K., Williams, N., Roberts, T.M., Papazian, D.M., Jan, L.Y., and Miller, C. (1990) Neuron 5, 221-226.
19. Vaca, L. and Kunze, D.L. (1993) Am. J. Physiol. Heart Circ. Physiol.264, H1319-H1322.
20. Zweifach, A. and Lewis, R.S. (1993) Proc.Natl.Acad.Sci. 90, 6295-6299.
21. Hoth, M. and Penner, R. (1992) Nature 355, 353-356.
22. Hoth, M. and Penner, R. (1993) J. Physiol. (Lond.) 465, 359-386.

J. Physiol. (1987), **383**, *pp.* 601–614
With 8 text-figures
Printed in Great Britain

PASSIVE AND ACTIVE MEMBRANE PROPERTIES OF MUDPUPPY TASTE RECEPTOR CELLS

BY S. C. KINNAMON AND S. D. ROPER

From the Rocky Mountain Taste and Smell Center, University of Colorado Health Sciences Center, 4200 East 9th Avenue, Denver, CO 80262, and the Department of Anatomy, Colorado State University, Fort Collins, CO 80523, U.S.A.

(*Received 17 March 1986*)

SUMMARY

1. Intracellular recordings were obtained from taste receptor cells and surface epithelial cells of isolated mudpuppy lingual epithelium.

2. Surface epithelial cells had a mean resting potential of $-40{\cdot}2 \pm 8{\cdot}9$ mV, a mean input resistance of $40{\cdot}3 \pm 11{\cdot}3$ MΩ, and a linear current–voltage (I–V) relationship. Taste receptor cells had a mean resting potential of $-61{\cdot}7 \pm 15$ mV, a mean input resistance of $380{\cdot}3 \pm 177{\cdot}2$ MΩ, and the I–V relationship showed pronounced outward rectification; the outward rectification persisted in high-K^+ saline, but was abolished by tetraethylammonium bromide (TEA).

3. Surface epithelial cells responded to depolarizing current injection with only passive membrane potential changes. Taste receptor cells responded to brief pulses of depolarizing current injection with regenerative action potentials characterized by an abrupt rising phase, an inflexion on the falling phase, and a prolonged after-potential.

4. The abrupt rising phase of the action potential was blocked by tetrodotoxin (TTX), suggesting that voltage-gated Na^+ currents are responsible for the rising phase.

5. Long-duration action potentials were elicited from cells treated with TEA to block outward K^+ currents and with TTX to block Na^+ currents, and from cells bathed in isotonic $CaCl_2$. These results suggest that the active membrane response contains a significant Ca^{2+} component.

6. The after-potential was blocked or greatly reduced by the addition of Ca^{2+} channel blockers to the bathing medium. In contrast, addition of TEA to the bathing medium greatly enhanced the after-potential. These data suggest that a significant portion of the after-potential is Ca^{2+} mediated.

7. The mean reversal potential for the after-potential ($-76{\cdot}8 \pm 6{\cdot}0$ mV) was significantly different from the mean reversal potential for the undershoot of the action potential ($-86 \pm 5{\cdot}6$ mV). Superfusion with TEA reduced the reversal potential of the after-potential to $-42{\cdot}3 \pm 8{\cdot}2$ mV and abolished the undershoot. These results suggest that the after-potential results from at least two conductances, one which is blocked by TEA and the other which is Ca^{2+} dependent and involves ions other than, or in addition to K^+.

8. Our data suggest that taste receptor cells, unlike surface epithelial cells, possess voltage-gated Na^+, Ca^{2+}, and K^+ channels, as well as Ca^{2+}-mediated channels. The role of the Ca^{2+} channels may be in part to regulate release of transmitter onto nerve terminals. The role of the other conductances in taste transduction is unknown.

INTRODUCTION

Intracellular recordings from individual sensory receptors have provided important information concerning mechanisms of sensory transduction. In many sensory cells it has been possible to record generator currents, receptor potentials and membrane conductance changes during sensory stimulation. From a number of studies in a variety of tissues it is becoming clear that many sensory receptors have voltage-gated and Ca^{2+}-activated conductances, and can generate action potentials under appropriate conditions (Lewis & Hudspeth, 1983; Corey, Dubinsky & Schwartz, 1984; Ohmori, 1984; Fuchs & Mann, 1986). In addition, there is evidence that these conductances play roles in sensory transduction. For example, pharmacological studies of rod photoreceptor cells have revealed that voltage-sensitive Ca^{2+} and K^+ channels, as well as Ca^{2+}-activated K^+ and Cl^- channels may be important in modulating the light-evoked receptor potential (Bader, Bertrand & Schwartz, 1982). Similar studies of isolated cochlear hair cells suggest that voltage-sensitive Ca^{2+} channels and Ca^{2+}-activated K^+ channels are involved in the electrical tuning mechanism of the hair cell membrane (Lewis & Hudspeth, 1983).

Much less is known about the ionic mechanisms underlying taste transduction. The lack of information concerning taste receptor cells is due in part to the difficulty in recording from the small taste cells of most species. Although intracellular recordings have been made from taste receptor cells in catfish (Teeter & Kare, 1974), frogs (Sato & Beidler, 1975; Akaike, Noma & Sato, 1976; Kashiwayanagi, Miyake & Kurihara, 1983; Sato, Sugimoto, Okada & Miyamoto, 1984), mudpuppies (West & Bernard, 1978), rats (Ozeki, 1971; Ozeki & Sato, 1972) and mice (Tonosaki & Funakoshi, 1984), what has been reported to date is that taste receptor cells generally have low resting potentials (less than -40 mV), low input resistances (17–80 MΩ), linear current–voltage (I–V) relationships and strictly passive membrane properties (however, cf. Roper, 1983; Kashiwayanagi *et al.* 1983). Taste receptor cells respond to a variety of chemical stimuli with depolarizing or hyperpolarizing membrane potential changes, but the ionic conductances underlying these receptor potentials are unknown (Sato, 1980).

We have re-examined the properties of taste receptor cells, using the large taste bud cells of *Necturus maculosus*. By stabilizing the isolated lingual epithelium in a vibration-free chamber and impaling single taste receptor cells under direct visual control, we have obtained data which differ significantly from the results of previous investigators. We report here that taste receptor cells have high resting potentials, high input resistances, non-linear I–V relationships, and most importantly that they produce regenerative action potentials when electrically excited. A preliminary report of these findings has been published (Roper, 1983).

METHODS

Mudpuppies (*Necturus maculosus*) were obtained from commercial suppliers and maintained at 4–10 °C in fresh water aquaria. They were fed minnows or earthworms bi-weekly.

Dissecting and recording procedures were those described by Roper (1983). To recapitulate, animals were rapidly decapitated and the upper jaw removed to expose the tongue. The lingual epithelium was gently freed from the dorsal anterior portion of the tongue by blunt dissection, and then stretched flat in a shallow chamber which had a glass bottom. The chamber was attached to the stage of a fixed-stage microscope equipped with a 40 × water immersion objective and Nomarski differential interference contrast optics. When viewed in this manner (400 ×), entire taste buds, individual taste cells, and even apical processes of single taste cells could be observed. Taste cells were clearly distinguishable from the surrounding epithelial cells by the following criteria: (1) taste cells were long and cylindrical, whereas epithelial cells were cuboidal in shape and (2) taste cells were always contained within the confines of the taste bud, which was clearly visible at 400 ×. Several taste cells have been filled with the dye Lucifer Yellow; dye-filled cells were always within the confines of the taste bud (Yang & Roper, 1986).

The preparation was perfused with an amphibian physiological saline (APS) solution (112 mM-NaCl, 2 mM-KCl, 8 mM-$CaCl_2$, 5 mM-HEPES (*N*-2-hydroxyethylpiperazine-*N'*-ethanesulphonic acid) buffered to pH 7·2 with NaOH) unless otherwise indicated. The elevated Ca^{2+} concentration facilitated stable intracellular impalements. Preparations remained viable for several hours under these conditions, and for up to two days if stored at 4 °C. Tetrodotoxin (TTX) was obtained from Sigma Chemical Corporation; apamin was obtained from Serva Biochemicals; charybdotoxin was a generous gift from Dr Christopher Miller, Brandeis University. All experiments were performed at room temperature (approximately 20 °C).

Micropipettes for intracellular recording had resistances of 50–150 MΩ (filled with 2·5 M-KCl). An agar–APS bridge connected to a AgCl pellet served as a reference electrode. Micro-electrodes were manipulated under visual control at 400 × and inserted into taste receptor cells (through the taste pore) or into surface epithelial cells. Stable impalements could be maintained for several minutes during constant perfusion of the bathing medium (approximately 1 ml/min).

Current was passed through the micro-electrode after carefully balancing the bridge circuit (WPI M4A electrometer with bridge) to obtain *I–V* relationships and to stimulate taste cells. Amplifier leakage currents were frequently checked and nulled to avoid artifacts during membrane potential measurements. Resting potentials were measured at the end of the impalement when the micro-electrode was abruptly and cleanly withdrawn from the cell.

RESULTS

Taste receptor cells (taste cells) of the mudpuppy are found within taste buds located on papillae which are usually spaced 2–3 mm apart on the anterior portion of the tongue. Non-gustatory epithelial cells comprise the remaining lingual epithelium. Since taste cells comprise a renewing neuroepithelial tissue which is derived from the surrounding lingual epithelium, it was of interest to compare membrane properties of taste cells with membrane properties of non-gustatory epithelial cells.

Passive membrane properties

Epithelial cells

Resting potentials obtained from micro-electrode impalements of surface epithelial cells varied from −22 to −60 mV, with a mean value of $-40{\cdot}2 \pm 8{\cdot}9$ mV ($n = 11$). The *I–V* relationship of a typical epithelial cell, obtained by passing a series of hyperpolarizing and depolarizing current pulses through the recording micro-electrode, is shown in Fig. 1*A*. In all cells examined, the *I–V* relationship was linear

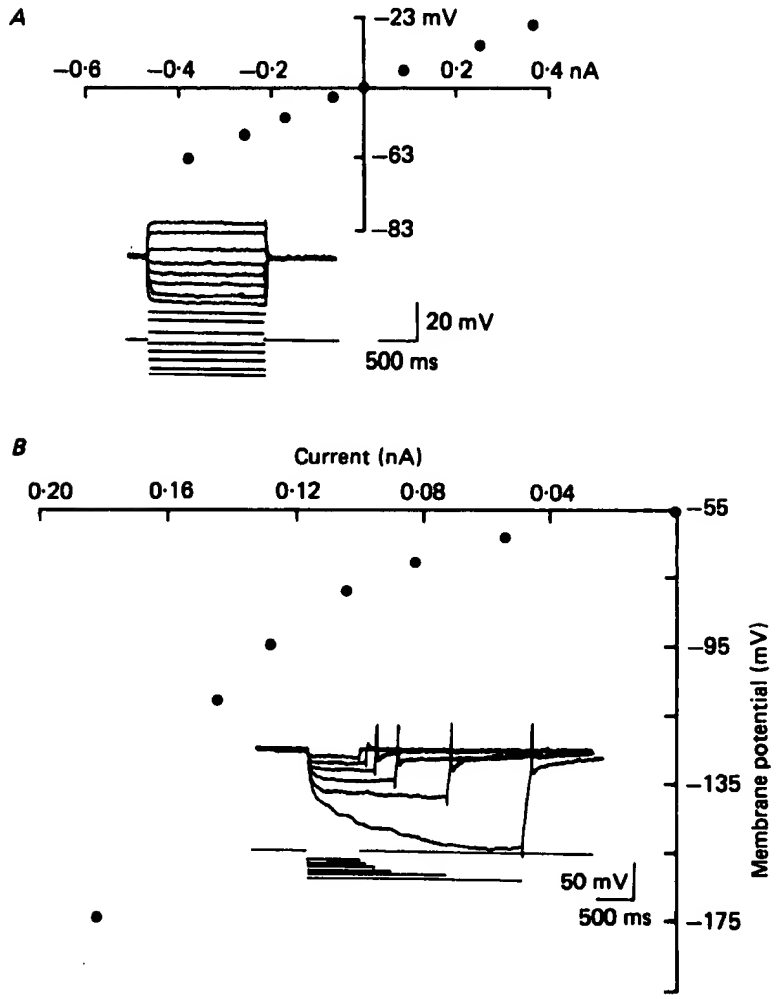

Fig. 1. Typical $I-V$ relationships of: A, a surface epithelial cell and B, a taste cell, obtained by passing current through the micro-electrode. Abscissa, current. Ordinate, membrane potential. Insets: top traces, membrane potential; bottom traces, current monitor. Note that the $I-V$ relationship for the epithelial cell is linear, whereas the $I-V$ relationship for the taste cell shows outward rectification. In a few experiments, measurements were made with depolarizing currents as well as hyperpolarizing currents. Such cells showed linear $I-V$ relationships with depolarizing current pulses until threshold was reached.

at all membrane potentials. The mean input resistance, calculated from the slopes of the individual $I-V$ relationships was $40{\cdot}3 \pm 11{\cdot}3$ MΩ ($n = 9$). With an average cell radius of $13{\cdot}7 \times 10^{-4} \pm 7{\cdot}2 \times 10^{-4}$ cm ($n = 15$) (measured from enzymatically dissociated epithelial cells which become spherical after isolation: S. C. Kinnamon, T. Cummings & S. D. Roper, in preparation), the specific membrane resistance was calculated to be 926 Ω cm². The average membrane time constant was $1{\cdot}68 \pm 0{\cdot}66$ ms ($n = 5$) which yields a specific capacitance for the epithelial cell membrane of $1{\cdot}8 \times 10^{-6}$ F/cm².

Taste cells

In contrast to epithelial cells, taste cells had high resting potentials: values varied from −41 to −110 mV. In one series where resting potentials were carefully measured after a brief impalement, we obtained a mean value of $-61{\cdot}7 \pm 15{\cdot}0$ mV ($n = 21$). We attribute the large variability in resting potentials to unavoidable damage accompanying impalement of these long, spindle-shaped cells. The input resistances (measured from the linear portion of the *I–V* relationship) were unexpectedly high, with a mean value of $380{\cdot}3 \pm 177{\cdot}2$ MΩ ($n = 8$). From a measured cell radius of $12{\cdot}6 \times 10^{-4} \pm 1{\cdot}3 \times 10^{-4}$ cm (taste cells, like epithelial cells, become spherical when enzymatically dissociated: S. C. Kinnamon, T. Cummings & S. D. Roper, in preparation) and a measured membrane time constant (measured from the linear portion of the *I–V* relationship) of $61{\cdot}7 \pm 31{\cdot}2$ ms ($n = 8$), we calculated a mean specific membrane resistance of 7600 Ω cm² and a mean specific membrane capacitance of $8{\cdot}3 \times 10^{-6}$ F/cm² for taste cells. The large value obtained for specific membrane capacitance of taste cells could reflect an underestimate of membrane area of individual taste cells, such as microvillar membrane or membrane folds that would not be detected in the light microscope. Alternatively, it could reflect electrotonic coupling between taste cells *in situ* (West & Bernard, 1978; Yang & Roper, 1986).

The *I–V* relationship of taste cells, unlike epithelial cells, showed a pronounced non-linearity with increasing hyperpolarization (Fig. 1*B*); in particular, the non-linearity appeared when the membrane was hyperpolarized in excess of −60 mV. Since rectification can occur simply because of unequal concentrations of permeant ions, especially K^+, across the membrane (Jack, Noble & Tsien, 1975), we repeated experiments in APS containing 60 mM-KCl (NaCl was replaced with KCl) so that K^+ concentrations would be similar across the membrane. Under these conditions, the membrane potential depolarized to approximately −20 mV and the *I–V* relationship became even more non-linear (Fig. 2*A*). Superfusion with the K^+ channel blocker tetraethylammonium bromide (TEA; 5 mM) increased the input resistance of taste cells and caused the *I–V* relationship to become linear (Fig. 2*B*). In addition, when taste cells were exposed to TEA in normal APS (2 mM-KCl), there was a 20–30 mV depolarization of the resting membrane potential and a concomitant increase in input resistance. These results indicate that taste receptor cells have a voltage-sensitive, non-inactivating resting K^+ conductance that closes with hyperpolarization.

Active membrane properties

Surface epithelial cells responded to depolarizing current pulses with only passive potential changes. In sharp contrast, *taste receptor cells* produced regenerative action potentials when depolarized with brief current pulses (Fig. 3*A*; cf. Roper, 1983). These impulses had several characteristic features: First, there was a distinct threshold for regenerative excitability. This threshold varied with the quality of micro-electrode impalement (i.e. the resting potential and the input resistance), but was usually 10–30 mV positive to the resting potential. Secondly, the falling phase of the impulse often had a noticeable inflexion or plateau, suggestive of a Ca^{2+} component to the underlying currents (Fig. 3*A*, arrow). Thirdly, only a single action potential was elicited even when the depolarizing current was maintained for several

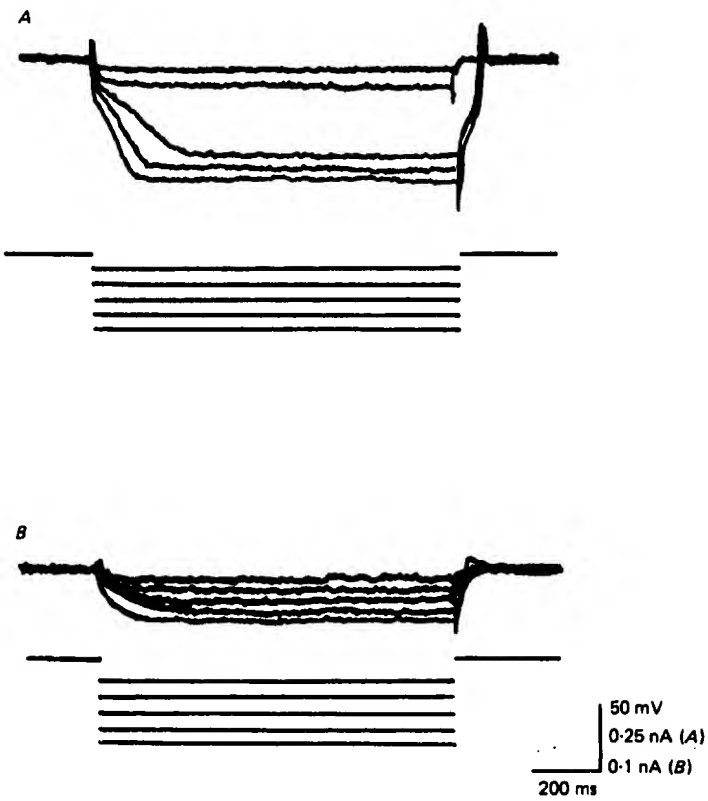

Fig. 2 Effect of elevated external K^+ and of TEA on the I–V relationship in taste cells. *A*, during exposure of taste cell to 60 mM-K^+; resting potential was −20 mV. Note that the non-linearity was enhanced by the elevated K^+. *B*, during exposure of taste cell to 60 mM-K^+ plus 5 mM-TEA. Note that TEA completely blocked the non-linearity and increased the input resistance of the cell.

seconds (Fig. 3*B*). Finally, most action potentials were followed by a prolonged after-potential. A hyperpolarizing after-potential occurred when an impulse was elicited at resting potential (−60 mV; Fig. 4*A*) and a depolarizing after-potential occurred when an impulse was elicited from a cell hyperpolarized approximately 40 mV by direct current injection (Fig. 4*B*). Although most cells were capable of generating action potentials, there was a large variability in the *duration* of impulses and after-potentials in cells within a taste bud.

Ionic basis of the rising phase of impulses

We superfused the preparation with TTX while recording from a single taste cell to determine if Na^+ currents are involved in impulses of taste cells. Action potentials were reversibly blocked in 1 μM-TTX (Fig. 5); lower doses of TTX were ineffective. These data suggest that the rising phase of the impulse in taste cells is produced by voltage-gated Na^+ channels and that the channels are somewhat less sensitive than Na^+ channels in nerve and intact muscle cells to the blocking action of TTX, as are Na^+ channels of denervated skeletal muscle (Pappone, 1980).

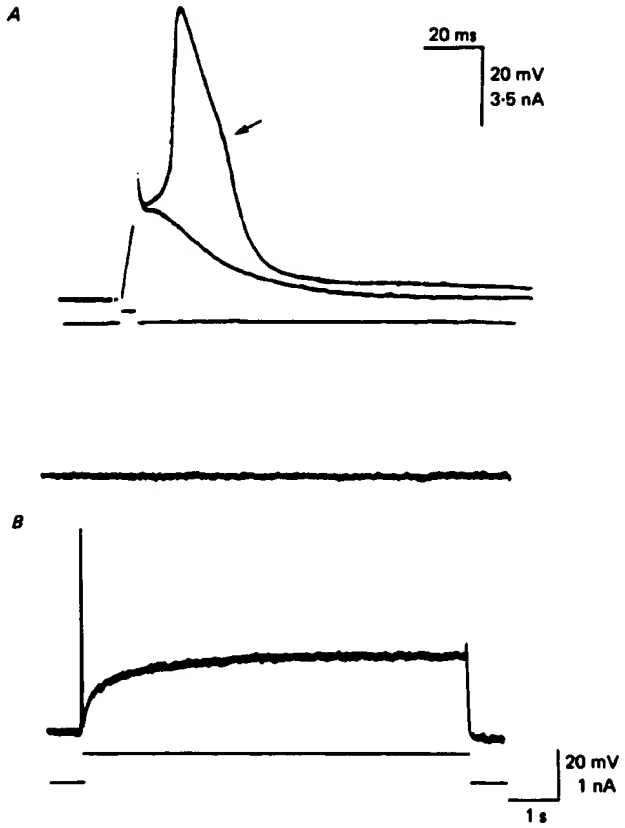

Fig. 3. Action potential elicited by depolarizing current injection in taste cells. *A*, sub- and suprathreshold responses to brief pulses of depolarizing current. Upper trace, membrane potential (resting potential = −58 mV); bottom trace, current through the micro-electrode. The arrow represents an inflexion on the falling phase of the impulse. *B*, response of a taste cell to prolonged current injection: top trace, zero potential; middle trace, intracellular membrane potential; bottom trace, current through the micro-electrode. Note that only a single action potential was elicited by prolonged electrical stimulation.

Ionic basis of the inflexion and falling phase of impulses

The inflexion on the falling phase of the impulse in taste cells suggests the presence of Ca^{2+} currents. To determine if Ca^{2+} currents are involved in taste cell action potentials, we blocked Na^+ currents with TTX and outward K^+ currents with TEA. Fig. 6*A* illustrates that taste cells were excitable under these conditions, and that impulses had a longer duration and a higher threshold than normal. Furthermore, impulses could be evoked even in the absence of Na^+; Fig. 6*B* illustrates an impulse elicited in the presence of 85 mM-$CaCl_2$. We conclude from these experiments that the regenerative membrane response contains a significant Ca^{2+} component in addition to the aforementioned Na^+ current.

TEA also blocked the undershoot of the action potential (Fig. 6*A*). TEA has been found to block a variety of voltage- and Ca^{2+}-dependent K^+ conductances in different cell types, including the delayed rectifier, Ca^{2+}-mediated K^+ conductance, and the sarcoplasmic reticulum K^+ channel (Latorre & Miller, 1983). Although our data

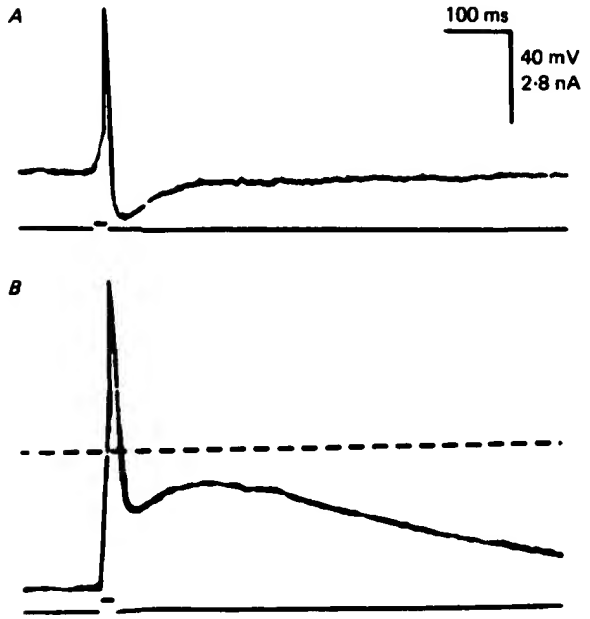

Fig. 4. After-potentials following an impulse in a taste cell. *A*, at the resting potential (−77 mV) and *B*, when the cell was hyperpolarized approximately 40 mV by passing current through the micro-electrode. The dashed line in *B* represents the resting potential of the cell. Note that the after-potential was hyperpolarizing at the resting potential and depolarizing when the cell was hyperpolarized.

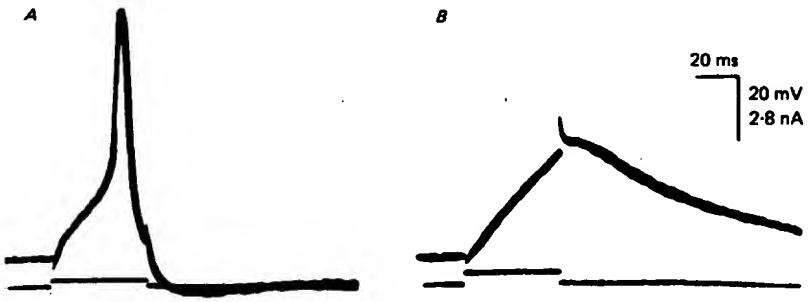

Fig. 5. Response of a taste cell to depolarizing current injection before (*A*) and after (*B*) superfusion with 1 μM-TTX. Note that most of the active membrane response was blocked by the TTX.

indicate that outward K^+ currents are important in repolarizing the membrane following an action potential, we do not know which type(s) of K^+ channel(s) is involved. It is possible that the voltage-sensitive K^+ conductance which is open at the resting potential (Figs. 1*B* and 2*A*, *B*) is the main conductance responsible for action potential repolarization.

Ionic basis of the after-potential

The after-potentials following impulses, an example of which is shown in Fig. 4*B*, sometimes lasted for several seconds. Since such after-potentials in many neurones are produced by Ca^{2+}-dependent conductances, and also because action potentials in

taste cells have a Ca^{2+} component, we examined the Ca^{2+} dependence of taste cell after-potentials by replacing Ca^{2+} with either 5 mM-$CdCl_2$, 8 mM-$CoCl_2$ or 8 mM-$MnCl_2$, which block Ca^{2+} channels in other tissues. After-potentials were either completely blocked or reduced in amplitude and duration by replacement of Ca^{2+} with these

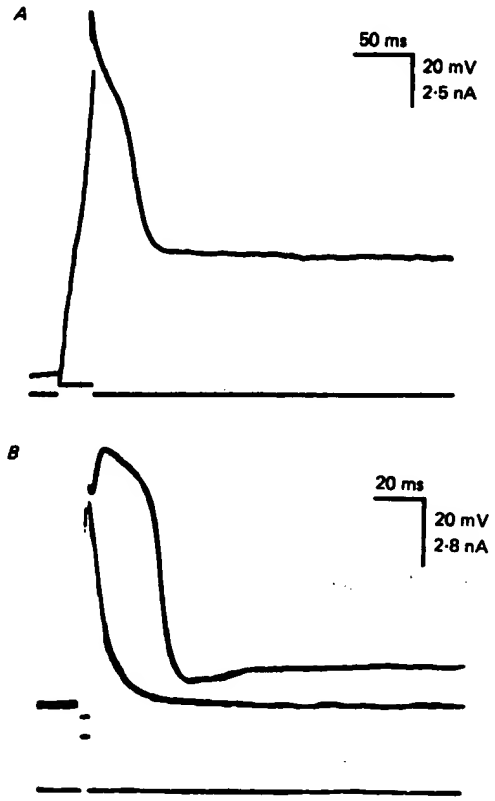

Fig. 6. Ca^{2+} action potentials in taste cells. *A*, action potential recorded from a taste cell superfused with 1 μM-TTX to block Na^+ currents and 5 mM-TEA to block outward K^+ currents; resting potential = −90 mV. *B*, action potential recorded from a taste cell bathed in isotonic (85 mM) $CaCl_2$; resting potential = −85 mV.

compounds (Fig. 7). In some experiments the effect of Ca^{2+} replacement could be reversed; however, reversal usually took several minutes and during this time the recording often deteriorated. In contrast, TEA greatly enhanced the amplitude and duration of the after-potential (Fig. 6*A*), presumably by prolonging the duration of Ca^{2+} influx during an action potential. These data suggest that a significant portion of the after-potential is Ca^{2+} mediated, either directly by a prolonged increase in Ca^{2+} conductance or indirectly by Ca^{2+}-activated permeability increases to other ions.

We measured the reversal potential of the after-potential to determine what ions are responsible for the after-potential. Fig. 8 illustrates impulses recorded at different membrane potential levels which had been established by injecting constant current through the micro-electrode. The after-potential reversed polarity at −76 mV in this example, which was similar to the mean value obtained from ten cells (−76·8 ± 6 mV). This value is much more negative than the Ca^{2+} equilibrium potential; therefore, the

after-potential is likely produced by a Ca^{2+}-mediated conductance rather than a prolonged increase in the conductance to Ca^{2+}. Superfusion with TEA (5 mM) shifted the reversal potential of the after-potential from -76 ± 6 to $-42{\cdot}3 \pm 8{\cdot}2$ mV.

The reversal potential of the after-potential differed significantly from the reversal

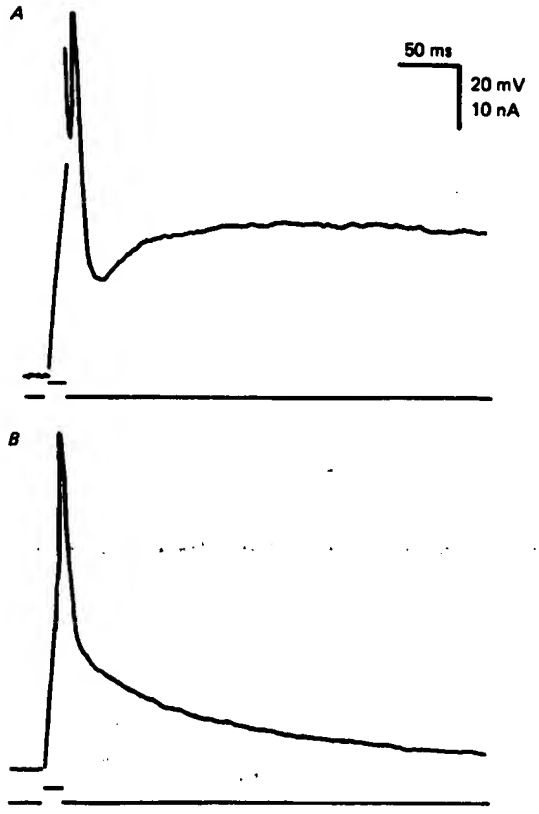

Fig. 7. Action potentials elicited from a taste cell before (*A*) and after (*B*) replacing $CaCl_2$ with 5 mM-$CdCl_2$. The cell was hyperpolarized by steady current injection to -100 mV to enhance the depolarizing after-potential. Note that the after-potential was greatly reduced, but not completely abolished by $CdCl_2$.

potential for the impulse undershoot (mean = $-86{\cdot}5 \pm 5{\cdot}6$ mV), which presumably reflects the K^+ equilibrium potential. The difference between the reversal potentials for the undershoot and the after-potential suggests a portion of the after-potential is mediated by ions other than K^+. Ca^{2+}-dependent Cl^- (Mayer, 1985) as well as Ca^{2+}-dependent non-specific cation conductances (Yellen, 1982; Petersen & Maruyama, 1984) have been found in a variety of tissues, and it is possible that these ions are involved in taste cell after-potentials.

The effect of TEA on the reversal potential suggests that either a voltage-dependent K^+ leak (Fig. 2) contributes significantly to the reversal potential of the after-potential, or that there is a Ca^{2+}-mediated K^+ conductance that is blocked by TEA, or that the delayed rectifier K^+ conductance is still active, as is true for hair cells (Lewis & Hudspeth, 1983). To determine if taste cells have a Ca^{2+}-dependent K^+ conductance, we examined the effects of toxins which have been shown to block

Ca^{2+}-dependent K^+ conductances in a variety of other tissues, namely apamin (Romey & Lazdunski, 1984) and charybdotoxin (Miller, Moczydlowski, Latorre & Phillips, 1985). Neither apamin (5 mM) nor charybdotoxin (100 nM) had any measurable effect on taste cell after-potentials.

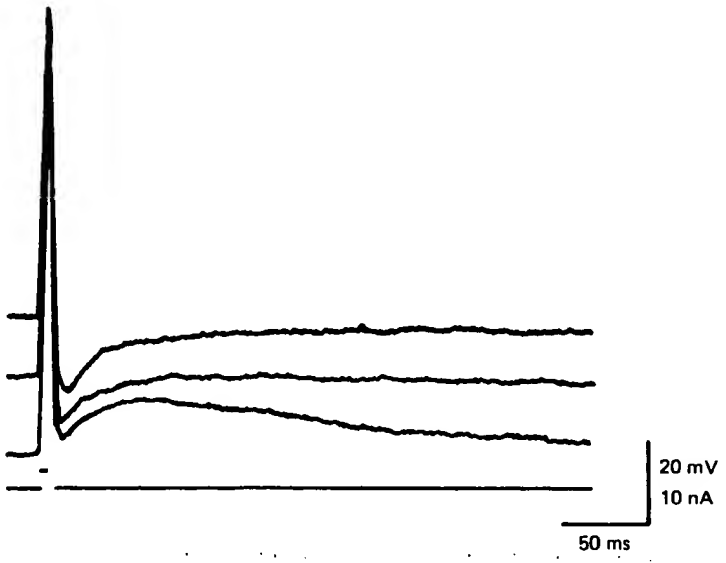

Fig. 8. Reversal potential for the after-potential. Action potentials were elicited at three different holding potentials which were established by passing steady current through the micro-electrode: top trace, resting potential (−60 mV); middle trace, holding potential = −76 mV; bottom trace, holding potential = −100 mV. Note that the after-potential reversed polarity at −76 mV.

In summary, the data suggest that the after-potential is produced by at least two conductances, one that is blocked by TEA and the other which is Ca^{2+} mediated and involves ions other than, or in addition to K^+.

DISCUSSION

The data presented here show that the membrane properties of taste receptor cells differ quite strikingly from surrounding epithelial cells. Most notably, taste cells in the mudpuppy are electrically excitable and possess voltage-gated Na^+, Ca^{2+}, and K^+ channels, as well as Ca^{2+}-mediated channels. Our findings were unexpected, since with the exception of one other investigation (Kashiwayanagi *et al.* 1983), these data are unprecedented. We attribute our findings to the improved recording conditions, namely a vibration-free environment for intracellular micro-electrode impalement. In addition, the large size of mudpuppy taste cells facilitates stable micro-electrode impalement. Although we cannot rule out the possibility that taste cells in the mudpuppy are fundamentally different from those of other species, we believe this is unlikely. Taste cells in the mudpuppy respond to the same basic stimuli as do taste cells of other species, with the exception that the mudpuppy lacks a response to sweet taste (McPheeters & Roper, 1985). Furthermore, we were able to replicate very closely

many of the findings from previous investigations in other species: when there were clear signs of cell damage during micro-electrode impalement, we obtained passive membrane properties identical to those reported by others and the taste cells were unexcitable. Voltage-gated channels similar to those in taste cells have been found recently in other non-neuronal cells, including Schwann cells (Gray & Ritchie, 1985), lymphocytes (Yellen, 1984), pancreatic islet of Langerhans cells (Ashcroft, Harrison & Ashcroft, 1984), cochlear hair cells (Lewis & Hudspeth, 1983; Ohmori, 1984; Fuchs & Mann, 1986), and photoreceptor cells (Corey *et al.* 1984).

The resting properties of taste cells are unusual, in that the so-called leak (resting) K^+ conductance appears to be voltage-sensitive. Voltage-dependent K^+ channels that can be open at the resting potential include Ca^{2+}-dependent K^+ channels (for review, Latorre & Miller, 1983) and the K^+ channels which mediate the M-current in amphibian sympathetic neurones (Adams, Brown & Constanti, 1982).

In this report we have emphasized properties of taste cells which were common to the majority of taste cells impaled. Nevertheless, there were large deviations from the mean values for several of the parameters measured. There are two possibilities for the variability in measured values. First, although taste cells in *Necturus* are large compared to taste cells of other species, they are still small relative to many excitable cells which have been studied with micro-electrodes. Thus, it is probable that we damaged the membrane of some taste cells during micro-electrode impalement. A second more intriguing possibility is that the different classes of taste cells have different properties (see West & Bernard, 1978). For example, there are at least four morphological classes of taste cells which are believed to represent different stages in the growth of taste receptor cells (Kinnamon, Taylor, Delay & Roper, 1985; Delay, Kinnamon & Roper, 1986). Thus, it is possible that membrane properties of taste cells vary with age of the cell, as has been found for muscle cells and several types of neurones (for review see Spitzer, 1979). Such a variability in basic membrane properties could influence the response of the taste cell to chemosensory stimulation.

A critical question is: what role do the passive and active membrane properties play in chemosensory transduction? In this paper we have not addressed the observations that chemosensory stimulation can also produce action potentials in taste cells (Kinnamon, McPheeters & Roper, 1985). It is possible that the Ca^{2+} influx associated with action potentials potentiates transmitter release from taste cells onto gustatory terminals (Kashiwayanagi *et al.* 1983). However, it is unlikely that action potentials would be *required* for transmitter release, since the length constant of the taste cell membrane is sufficient to allow subthreshold potentials to spread from the apical region to the basal region of the cell with little decrement (S. D. Roper, unpublished observation). It is also unlikely that action potentials serve to code stimulus intensity under normal conditions, since we rarely see repetitive impulses to either a sustained electrical depolarization (Fig. 3*B*) or a sustained chemical stimulation (S. C. Kinnamon & S. D. Roper, in preparation). One possibility is that voltage-gated channels are modulated by an electrogenic Na^+ pump. Electrogenic Na^+ pumps are commonly found in many transporting epithelia (Petersen, 1980). The presence of low concentrations of NaCl might be expected to hyperpolarize the basolateral membrane of taste cells by activating an electrogenic Na^+ pump. This hyperpolarization would in turn affect voltage-sensitive membrane channels and influence the receptivity to other substances.

An intriguing possibility is that the voltage-gated and Ca^{2+}-mediated channels are modulated by the taste stimulus and therefore directly cause chemosensory transduction. Modulation of ion channels could occur by direct interaction of the taste stimulus with ion channels on the apical membrane, or by indirect action on ion channels throughout the cell through the release of intracellular second messengers. Ionic channels in other systems have been found to be modulated by neurotransmitters acting through second messengers. For example, serotonin closes K^+ channels in sensory neurones of *Aplysia* (Siegelbaum, Camardo & Kandel, 1982), and noradrenaline increases the mean open time of cardiac Ca^{2+} channels (Reuter, Stevens, Tsien & Yellen, 1982). In addition, and of greater relevance to taste transduction, K^+ channels of pancreatic cells are closed in response to glucose (Ashcroft *et al.* 1984), and K^+ channels derived from sarcoplasmic reticulum of muscle are closed in response to protons (Bell, 1985). The precise role of the membrane conductances described in this report to taste transduction awaits more detailed investigations of the response of taste cells to chemical stimuli.

We thank Dr Paul Fuchs for a critical reading of the manuscript and Dr William Betz for the use of his digitizer and computer. This study was supported by N.I.H. grants NS20382, PO1NS20486-02, and AG03340 to S.D.R.

REFERENCES

ADAMS, P. R., BROWN, D. A. & CONSTANTI, A. (1982). M-currents and other potassium currents in bull-frog sympathetic neurones. *Journal of Physiology* **330**, 537–572.

AKAIKE, N., NOMA, A. & SATO, M. (1976). Electrical responses of frog taste cells to chemical stimuli. *Journal of Physiology* **254**, 87–107.

ASHCROFT, F. M., HARRISON, D. E. & ASHCROFT, S. J. H. (1984). Glucose induces closure of single potassium channels in isolated rat pancreatic b-cells. *Nature* **312**, 446–448.

BADER, C. R., BERTRAND, D. & SCHWARTZ, E. A. (1982). Voltage-activated and calcium-activated currents studied in solitary rod inner segments from the salamander retina. *Journal of Physiology* **331**, 253–284.

BELL, J. (1985). Protons decrease the single channel conductance of the sarcoplasmic reticulum K^+ channel in neutral and negatively charged bilayers. *Biophysical Journal* **48**, 349–353.

COREY, D. P., DUBINSKY, J. M. & SCHWARTZ, E. A. (1984). The calcium current in inner segments of rods from the salamander *Ambystoma tigrinum* retina. *Journal of Physiology* **354**, 557–575.

DELAY, R. J., KINNAMON, J. C. & ROPER, S. D. (1986). Ultrastructure of mouse vallate taste buds: II. Cell types and cell lineage. *Journal of Comparative Neurology* (in the Press).

FUCHS, P. A. & MANN, A. C. (1986). Voltage oscillations and ionic currents in hair cells isolated from the apex of the chick's cochlea. *Journal of Physiology* **371**, 31*P*.

GRAY, P. T. A. & RITCHIE, J. M. (1985). Ion channels in Schwann and glial cells. *Trends in Neurosciences* **87**, 411–415.

JACK, J. J. B., NOBLE, D. & TSIEN, R. W. (1975). *Electric Current Flow in Excitable Cells*, p. 235. Oxford: Oxford University Press.

KASHIWAYANAGI, M., MIYAKE, M. & KURIHARA, K. (1983). Voltage-dependent Ca^{2+} channel and Na^+ channel in frog taste cells. *American Journal of Physiology* **244**, C82–88.

KINNAMON, J. C., TAYLOR, B. J., DELAY, R. J. & ROPER, S. D. (1985). Ultrastructure of mouse vallate taste buds I. Taste cells and their associated synapses. *Journal of Comparative Neurology* **235**, 48–60.

KINNAMON, S. C., MCPHEETERS, M. & ROPER, S. (1985). Electrophysiology of isolated taste cells from the mudpuppy. *Neuroscience Abstracts* **11**, 1131.

LATORRE, R. & MILLER, C. (1983). Conduction and selectivity in potassium channels. *Journal of Membrane Biology* **71**, 11–30.

LEWIS, R. S. & HUDSPETH, A. J. (1983). Voltage- and ion-dependent conductances in solitary vertebrate hair cells. *Nature* **304**, 538–541.

MAYER, M. L. (1985). A calcium-activated chloride current generates the after-depolarization of rat sensory neurones in culture. *Journal of Physiology* **364**, 217–239.

MILLER, C. MOCZYDLOWSKI, E., LATORRE, R. & PHILLIPS, M. (1985). Charybdotoxin, a protein inhibitor of single Ca^{2+}-activated K^+ channels from mammalian skeletal muscle. *Nature* **313**, 316–318.

MCPHEETERS, M. & ROPER, S. D. (1985). Amiloride does not block taste transduction in the mudpuppy, *Necturus maculosus*. *Chemical Senses* **10**, 341–352.

OHMORI, H. (1984). Studies of ionic currents in the isolated vestibular hair cell of the chick. *Journal of Physiology* **350**, 561–581.

OZEKI, M. (1971). Conductance change associated with receptor potentials of gustatory cells in rat. *Journal of General Physiology* **58**, 688–699.

OZEKI, M. & SATO, M. (1972). Responses of gustatory cells in the tongue of rat to stimuli representing four taste qualities. *Comparative Biochemistry and Physiology* **41A**, 391–407.

PAPPONE, P. A. (1980). Voltage-clamp experiments in normal and denervated mammalian skeletal muscle fibres. *Journal of Physiology* **306**, 377–410.

PETERSEN, O. H. (1980). *The Electrophysiology of Gland Cells*. London: Academic Press.

PETERSEN, O. H. & MARUYAMA, Y. (1984). Calcium-activated potassium channels and their role in secretion. *Nature* **307**, 693–696.

REUTER, H., STEVENS, C. F., TSIEN, R. W. & YELLEN, G. (1982). Properties of single calcium channels in cardiac cell culture. *Nature* **297**, 501–504.

ROMEY, G. & LAZDUNSKI, M. (1984). The coexistence in rat muscle cells of two distinct classes of Ca^{2+}-dependent K^+ channels with different pharmacological properties and different physiological functions. *Biochemical and Biophysical Research Communications* **118**, 669–674.

ROPER, S. (1983). Regenerative impulses in taste cells. *Science* **220**, 1311–1312.

SATO, T. (1980). Recent advances in the physiology of taste cells. *Progress in Neurobiology* **14**, 25–67.

SATO, T. & BEIDLER, L. M. (1975). Membrane resistance change of the frog taste cells in response to water and NaCl. *Journal of General Physiology* **66**, 735–763.

SATO. T., SUGIMOTO, K., OKADA, Y. & MIYAMOTO, T. (1984). Ionic basis of the resting membrane potential in frog taste cells. *Japanese Journal of Physiology* **34**, 973–983.

SIEGELBAUM, S. A., CAMARDO, J. S. & KANDEL, E. R. (1982). Serotonin and cyclic AMP close single K^+ channels in *Aplysia* sensory neurones. *Nature* **299**, 413–417.

SPITZER, N. C. (1979). Ion channels in development. *Annual Review of Neuroscience* **2**, 363–397.

TEETER, J. & KARE, M. R. (1974). Passive electrical properties and responses to chemical stimulation of cutaneous taste bud cells. *Federation Proceedings* **33**, 416.

TONOSAKI, K. & FUNAKOSHI, M. (1984). Intracellular taste cell responses of mouse. *Comparative Biochemistry and Physiology* **78A**, 651–656.

WEST, C. H. K. & BERNARD, R. A. (1978). Intracellular characteristics and responses of taste bud and lingual cells of the mudpuppy. *Journal of General Physiology* **72**, 305–326.

YANG, J. & ROPER, S. D. (1986). Dye-coupling in the lingual epithelium in the mudpuppy, *Necturus maculosus*. *Chemical Senses* (in the Press).

YELLEN, G. (1982). Single Ca^{2+}-activated nonselective cation channels in neuroblastoma. *Nature* **296**, 357–359.

YELLEN, G. (1984). The immune system uses ion channels, too. *Trends in Neurosciences* **7**, 179–181.

Orchestration of Neuronal Migration by Activity of Ion Channels, Neurotransmitter Receptors, and Intracellular Ca^{2+} Fluctuations

Hitoshi Komuro, Pasko Rakic

Section of Neurobiology, Yale University School of Medicine, 333 Cedar St., New Haven, Connecticut 06510

Accepted 26 May 1998

ABSTRACT: **The real-time observation of cell movement in acute cerebellar slices reveals that granule cells alter their shape concomitantly with changes in the mode and rate of migration as they traverse different cortical layers. Although the origin of local environmental cues responsible for these position-specific changes in migratory behavior remains unclear, several signaling mechanisms involved in controlling granule cell movement have emerged. The onset of one such mechanism is marked by the expression of voltage-gated ion channels and neurotransmitter receptors in postmitotic cells prior to the initiation of their migration. Granule cells start their radial migration after the expression of N-type Ca^{2+} channels and the *N*-methyl-D-aspartate subtype of glutamate receptors on the plasmalemmal surface. Blockade of the channel or receptor activity significantly decreases the rate of cell movement, indicating that the activation of these membrane constituents provides an essential signal for the translocation of granule cells. Another signal that controls the rate of cell migration is embedded in the combined amplitude and frequency components of Ca^{2+} fluctuations in the somata of migrating granule cells. Interestingly, each phase of Ca^{2+} fluctuation controls a separate phase of saltatory movement in the granule cells: The cells move forward during the phase of transient Ca^{2+} elevation and remain stationary during the troughs. Consequently, the changes in the amplitude and frequency components of Ca^{2+} fluctuations directly affect granule cell movement: Reducing the amplitude or frequency of Ca^{2+} fluctuations slows down the speed of cell movement, while the enhancement of these components accelerates migration. These findings suggest that signaling molecules present in the local cellular milieu encountered on the migratory route control the shape and motility of granule cells by modifying Ca^{2+} fluctuations in the soma through the activation of specific ion channels and neurotransmitter receptors.** J Neurobiol 37: 110–130, 1998

Keywords: **granule cell migration; N-type Ca^{2+} channel; NMDA receptor; intracellular Ca^{2+} fluctuation; rate of cell movement**

The migration of postmitotic neurons from their sites of origin to their final destinations, where they make synaptic connections, is a fundamental cellular event essential for building large neuronal assemblies (Rakic, 1990, 1997). Although cellular and molecular mechanisms involved in neuronal migration have been studied for more than 100 years, the role of voltage-gated ion channels and neurotransmitter receptors in the translocation of immature neurons was not suggested until 1992 (Komuro and Rakic, 1992). It had been widely assumed that the activity of ion channels and neurotransmitter receptors was associated only with late developmental stages, after neurons had established their synaptic contacts and neurotransmitter receptors had become engaged in the usual form of chemical signaling (Goodman and Shatz, 1993). However, in 1992, Komuro and Rakic found that N-type calcium channels, which have been predominantly associated with neurotransmitter release in adult brain,

Correspondence to: H. Komuro
 CCC 0022-3034/97/010110-21

also play a transient but important role in the directed migration of immature neurons, before they attain their final position and establish synaptic circuits. This finding was followed by evidence that the activity of a variety of ion channels and neurotransmitter receptors are important in neuronal migration (Komuro and Rakic, 1992, 1993, 1996; Rossi and Slater, 1993; Farrant et al., 1994; Patil et al., 1995; Rakic and Komuro, 1995; Liao et al., 1996; Behar et al., 1996; Fueshko et al., 1998).

Cerebellar granule cells provide an exceptional opportunity to study the cellular and molecular mechanisms underlying neuronal cell migration because the movement and morphogenetic transformation of granule cells have been well described (Ramon y Cajal, 1911; Uzman, 1960; Miale and Sidman, 1961; Mugnaini and Forstronen, 1967; Rakic, 1971; Quesada and Genis-Galvez, 1983; O'Donoghue et al., 1987; Ono et al., 1997). Precursors of granule cells actively proliferate at the upper strata of the external granular layer (EGL) in the developing cerebellum. After the final mitotic division, granule cells become transiently located in the lower strata of the EGL (Fujita, 1967; Altman, 1972). Shortly thereafter, they become bipolar and extend two horizontal processes before developing a third vertical process through which each cell subsequently moves its soma across the molecular layer (ML). Electron microscopic analysis revealed that migrating granule cells are closely associated with Bergmann glial fibers that traverse the developing ML, suggesting that their movement may be guided by surface-mediated interactions with the Bergmann glial fibers (Rakic, 1971, 1981, 1985a,b). This interpretation inspired a large number of experiments that examined the role of Bergmann glial cells in granule cell migration (Rakic and Sidman, 1973a,b; Rakic, 1976, 1981; Trenkner and Sidman, 1977; Hatten et al., 1984, 1986; Edmondson and Hatten, 1987; Gregory et al., 1988; Hatten and Mason, 1990; Rakic, 1990). Several cell adhesion molecules involved in the attachment of granule cells to the surface of Bergmann glial processes were isolated, and the functional role of these molecules in granule cell migration has been examined in an *in vitro* assay system (Antonicek et al., 1987; Edmondson et al., 1987; Fishell and Hatten, 1991; Fishman and Hatten, 1993; Cameron and Rakic, 1994; Rakic et al., 1994; Anton et al., 1996; Cameron et al., 1997).

During the past 3 decades, studies of granule cell migration have been confined to determining the cellular and molecular mechanisms of cell movement along the glial processes within the ML, while little is known about granule cell translocation across the Purkinje cell layer (PCL) and the extent of their movement within the internal granular layer (IGL). Since granule cells lose contact with the surface of Bergmann glial fibers after leaving the ML, it remains unclear if the further movement of these cells is due to a passive displacement or an active process reminiscent of their earlier glial cell–associated migration. To address this issue, acute brain slice culture systems were developed (Komuro and Rakic, 1992, 1993, 1995, 1998a,b; Rakic and Komuro, 1995). The use of brain slices in conjunction with confocal microscopy and fluorescent lipophilic carbocyanine dyes allows the direct observation of granule cell movement within their natural cellular milieu in a real-time manner. This approach revealed how granule cells migrate through the different cortical layers—the ML, the PCL, and the IGL—of the developing cerebellum, and determined how an identified granule cell attains its final destination within the IGL (Komuro and Rakic, 1995, 1998a).

Although the role of cell adhesion and extracellular molecules in granule cell migration has been well established (Edelman, 1984; Pollerberg et al., 1987; Gloor et al., 1990; Liesi, 1992; Anton et al., 1996; Cameron et al., 1997; Lom and Hockberger, 1997), other signaling mechanisms involved in its movement have emerged during the past several years (Komuro and Rakic, 1992, 1993, 1996; Rossi and Slater, 1993; Patil et al., 1995; Rakic and Komuro, 1995; Liesi and Wright, 1996; Miyata et al., 1996; Silverman et al., 1996; Ackerman et al., 1997; Rio et al., 1997; Soriano et al., 1997; Bix and Clark, 1998). Physiological and pharmacological approaches revealed that the activity of voltage-gated ion channels and neurotransmitter receptors is crucial for normal granule cell migration (Komuro and Rakic, 1992, 1993; Slater and Rossi, 1996). For example, the potentiation of the activity of N-type Ca^{2+} channels and/or the *N*-methyl-D-aspartate (NMDA) subtype of glutamate receptors increases the rate of granule cell movement, while reduction of their activity decreases cell movement (Komuro and Rakic, 1992, 1993). These findings led to studies that examined the question of whether changes in intracellular Ca^{2+} levels may affect cell migration, since activation of N-type Ca^{2+} channels and/or the NMDA receptors could induce substantial Ca^{2+} influxes into the migrating granule cells. Real-time recording of intracellular Ca^{2+} levels ($[Ca^{2+}]_i$) revealed that migrating granule cells exhibit spontaneous elevations in $[Ca^{2+}]_i$ in the cell soma (Komuro and Rakic, 1996). Most impor-

tantly, the combination of the amplitude and frequency components of Ca^{2+} elevations in the cell soma, caused mainly by Ca^{2+} influxes through N-type Ca^{2+} channels and NMDA receptors, provide an intracellular signal controlling the rate of granule cell migration (Komuro and Rakic, 1996).

In this article, we first review recent studies on position-specific changes in granule cell shape and migrating behavior through different migratory terrains of the developing cerebellar cortex. We then present possible roles for the coordinated activity of ion channels, neurotransmitter receptors, and intracellular Ca^{2+} fluctuations in controlling granule cell movement.

PHASES OF GRANULE CELL MIGRATION

To understand the signaling role of intracellular calcium and its fluctuations controlled by channels and receptors, it is essential to first describe the major cellular events and phases of granule cell migration in the developing cerebellum.

Bergmann Glia-Guided Granule Cell Migration through the ML

In his studies of Golgi-stained material, Ramon y Cajal (1911) described migrating granule cells in the ML that have a vertically elongated cell body, a thin trailing process, and a more voluminous leading process. Use of electron microscopy revealed that the granule cell soma, trailing process, and leading process are closely apposed to the surface of Bergmann glial fibers, and suggested that the granule cell moves along Bergmann glial fibers during the entire translocation of its soma across the ML (Rakic, 1971). The recent development of methods for real-time monitoring of granule cell movement in living slice preparations revealed several temporal and cytological aspects of the dynamic movement of granule cells that had not been observed using either *in vivo* or *in vitro* systems (Komuro and Rakic, 1995). For example, comparing the speed of cell movement in slices from different postnatal cerebella demonstrated that rates of granule cell movement in the ML depend critically on the age of the cerebellum. Although there was considerable variation in the speed of individual cells, the average rate of granule cell migration in the ML increased systematically from 9.6 μm/h in cerebella from 7-day-old mice to 18.0 μm/h in cerebella from 13-day-old mice (Komuro and Rakic, 1995). Consequently, granule cells traversed the developing ML within a relatively constant time period despite the doubling in width of the ML during the second week of postnatal life. Furthermore, granule cell movement in the ML was characterized by alternations of short stationary phases with movement in a forward or backward direction (Komuro and Rakic, 1995). The net displacement of a cell depended on the duration and frequency of these phases as well as on the speed of movement. Moreover, studies of the topographical flow of the plasma membrane of granule cells indicated that new membrane material is incorporated primarily at the leading process, while a large portion of the existing plasma membrane moves in register with the nucleus and surrounding cytoplasm during migration (Komuro and Rakic, 1995).

Changes in Cell Shape and Migratory Behavior in the PCL

A major problem in understanding granule cell migration is the question of whether they complete their movement after losing contact with Bergmann glial cells in the PCL. Recently, real-time monitoring of the behavior of identified granule cells revealed dynamic changes in the shape and movement of their leading processes after they detach from the surface of Bergmann glia (Komuro and Rakic, 1998a). At the bottom of the ML, the elongated bipolar soma of granule cells moved toward the PCL, while the length of their leading process gradually decreased. The shortening of the leading process is due to the advance of the granule cell soma within the leading process rather than to its active retraction. Furthermore, the distal portion of the leading process positioned in the PCL began to extend large motile lamellipodia and filopodia. This is not characteristic of the leading process of migrating granule cells in the ML, which is invariably associated with Bergmann glial fibers and usually tapers without motile lamellipodia (Rakic, 1985).

Once the granule cell soma entered the PCL, its shape abruptly transformed from a vertically elongated spindle to a sphere (Komuro and Rakic, 1988a) (Fig. 1). These rounded somata significantly slowed their movement, which stopped completely in the PCL. The rounded somata remained stationary in the PCL for an average of 115 min, with times ranging from 30 to 220 min (Komuro and Rakic, 1998a). However, highly motile lamellipodia developed at the distal portion of the leading process, which penetrates the IGL, although the leading process did not exhibit a net extension in

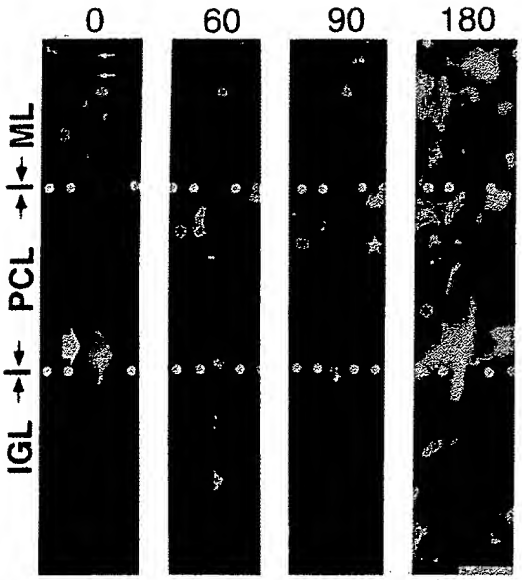

Figure 1 Time-lapse series showing an example of changes in granule cell shape and speed of movement in the PCL. Migrating granule cells in a slice preparation obtained from postnatal 10-day-old mouse cerebellum were labeled fluorescently with a lipophilic carbocyanine dye, DiI, and their movement was tracked using a laser scanning confocal microscope. After a granule cell soma (asterisks) crossed the ML–PCL border, it transformed from a vertically elongated spindle to spherical shape (white star). The granule cell slowed down significantly and then stopped completely in the PCL. One can argue that the rounding up of the soma and slowing of movement could be due to physiological deterioration after a prolonged period of observation. However, we consider this unlikely, since the cells appeared healthy, and 1.5 h after the soma became round, they resumed a spindle shape as they entered the deep strata of the PCL at 180 min. A wide arrow indicates a motile lamellipodia at the tip of the leading process, while small arrows indicate the trailing process of the migrating granule cell. The time interval (in minutes) is indicated on top of each photograph. Bar = 10 μm.

length. The tips of the leading processes exhibited alternative changes that ranged in form from tapered to broad, suggesting that the tips of leading processes actively search for potential guidance cues.

The loss of attachment to Bergmann glial surfaces in the PCL may directly lead to the observed dynamic changes in the shape and behavior of granule cells. Previous *in vitro* studies demonstrate that both the cytology and migratory behavior of granule cells are highly responsive to the adjacent substrates (Fishell and Hatten, 1991; Fishman and Hatten, 1993; Rivas and Hatten, 1995). For example, dissociated granule cells display an elongated bipolar migrating shape when they are plated onto astroglial plasma membranes, laminin, or fibronectin, while cells are rounded when plated on collagen (Fishell and Hatten, 1991).

Resumption of Radial Migration in the IGL

The question of how stationary granule cells in the PCL could attain their final position in the IGL was recently addressed using slice preparations (Komuro and Rakic, 1998a). We found that after a prolonged stationary period, granule cells in the PCL begin to reextend their somata and leading processes (Fig. 2). Furthermore, during this transformation, granule cells gradually accelerated the rate of their migration and crossed the PCL–IGL border (Komuro and Rakic, 1998a). Thus, granule cells do not complete their migration in the PCL as commonly assumed, but, rather, initiate a new phase of migration within the IGL, independent of Bergmann glial fibers.

Monitoring their migratory behavior revealed that the spindle-shaped granule cells migrate toward

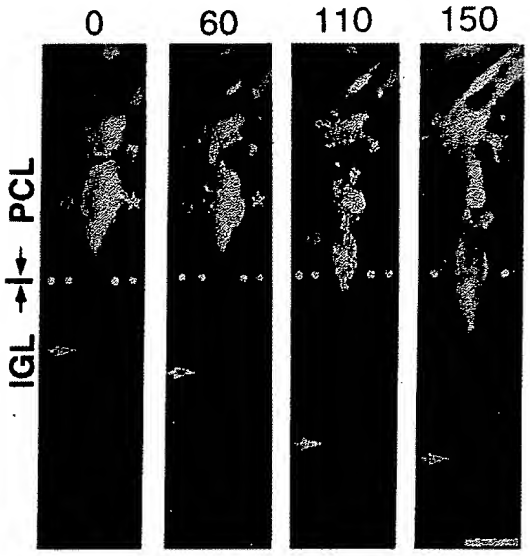

Figure 2 Time-lapse series showing the secondary transformation of a rounded granule cell at the PCL–IGL border. During the observation period, a rounded granule cell (white stars) began to reextend its soma and leading process. It gradually accelerated the rate of its migration and crossed the PCL–IGL border. Arrows indicate a broad tip at the leading process. The time interval (in minutes) is indicated on top of each photograph. Bar = 10 μm.

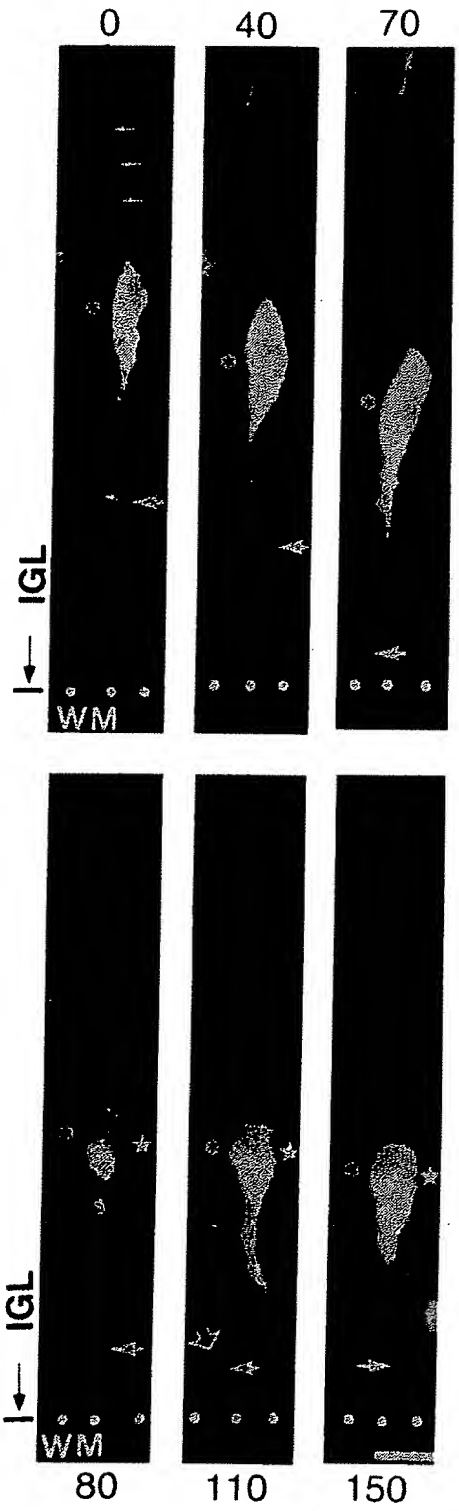

Figure 3 Time-lapse series showing an example of the completion of granule cell migration in the deep strata of the IGL. During the observation period, the spindle-shaped soma (asterisks), initially located in the middle of the IGL, migrated vertically toward the IGL–WM border at a rate of 14.7 μm/h. After 70 min of recording, the active tip of its leading process approached the IGL–WM border and the cell soma became rounded (white stars). The granule cell gradually slowed its migration and stopped near the IGL–WM border. Although the soma of the granule cell ceased movement in the deep strata of the IGL, its leading process exhibited dynamic changes in shape. White arrows indicate the tip of the leading process. An open arrow indicates a horizontally extended tip of the leading process, while small arrows indicate the trailing process of the migrating granule cell. The time interval (in minutes) is indicated on the top or bottom of each photograph. Bar = 10 μm.

the bottom of the IGL at a rate comparable to that recorded for granule cells migrating along Bergmann glial fibers within the ML (Komuro and Rakic, 1995, 1998a). The long axis of the granule cell soma remained oriented perpendicular to the PCL–IGL boundary line during this radial migration. These observations reveal that granule cells migrate rapidly, radially, and unidirectionally toward the deep strata of the IGL in the absence of guidance cues provided by Bergmann glial cells (Komuro and Rakic, 1998a). Although the cellular and signaling mechanisms involved in granule cell movement in the IGL remain to be elucidated, there are several candidate molecules that may be responsible for the resumption of their movement. These candidates include a variety of extracellular matrix molecules that are expressed in distinct distributions in the PCL and the IGL (Choung et al., 1987; Choung, 1990; Liesi, 1992; Fishman and Hatten, 1993). Alternatively, later-generated granule cells could migrate along the ascending axons of earlier-generated granule cells that are already present in the IGL. *In vivo* as well as in microexplant cultures, granule cells move along the neurites of more differentiated granule cells (Rakic, 1971; Nagata and Nakatsuji, 1990; Komuro and Rakic, 1996). Therefore, the vertically oriented axons of postmigratory granule cells might also support the inward migration of later-generated granule cells as they transit the PCL and the IGL. However, since Bergmann glial cells extend short vertical processes into the upper strata of the IGL during the period of granule cell migration (shown in Fig. 6 in Rakic, 1971; Muller et al., 1994), we can not exclude the possibility that glial cells continue to play a role in granule cell migration, particularly within the upper strata of the IGL. After granule cell migration is

completed, Bergmann glial cells withdraw these short vertical processes (Rakic, 1971; Muller et al., 1994), suggesting that granule cells that settle in the upper strata of the IGL may migrate along them in a similar way as in the ML.

Completion of Migration at the Bottom of the IGL

Real-time observation of cell behavior revealed the final stage of granule cell migration at the bottom of the IGL (Komuro and Rakic, 1998a). Once the tip of a leading process approaches the IGL–white matter (WM) border, the granule cell soma becomes rounded (Fig. 3). The granule cells then slow their migration and stop their movement near the IGL–WM border (Fig. 3). In the postnatal 10-day-old mouse cerebellum, a majority of granule cells complete their migration at the bottom stratum of the IGL, while <20% of the granule cells settle in the middle or top strata (Komuro and Rakic, 1998a). The average distance between the PCL–IGL border and the final position of granule cells in the IGL of the postnatal 10-day-old mouse cerebellum was approximately 113 μm. Therefore, after entering the IGL, most granule cells migrate radially more than 100 μm (a distance comparable to that observed in the ML) toward the IGL–WM border, suggesting that, as in the cerebral cortex (Rakic, 1972, 1997), late-generated granule cells pass through the strata of early-generated granule cells (Komuro and Rakic, 1998a). This observation suggests that granule cells may stop their movement in response to putative cues residing in the deep strata of the IGL; but at present, it is unknown which cells or candidate molecules are involved in this process. The molecular mechanisms and signals for stopping cell movement are not known.

Length and Duration of Granule Cell Transit across the Cortical Layers

Although there are large differences in the total migrating distance of granule cells between different species and between different ages in a given species, granule cells in the postnatal 10-day-old mouse cerebellum migrate radially about 250 μm to attain their final position in the IGL (Komuro and Rakic, 1998a). Of this distance, granule cells move an average of 110 μm to cross the ML, about 27 μm to traverse the PCL, and an additional 113 μm in the IGL toward the IGL–WM border. We found that the average rate of granule cell movement in the postnatal 10-day-old mouse cerebellum was 11.2

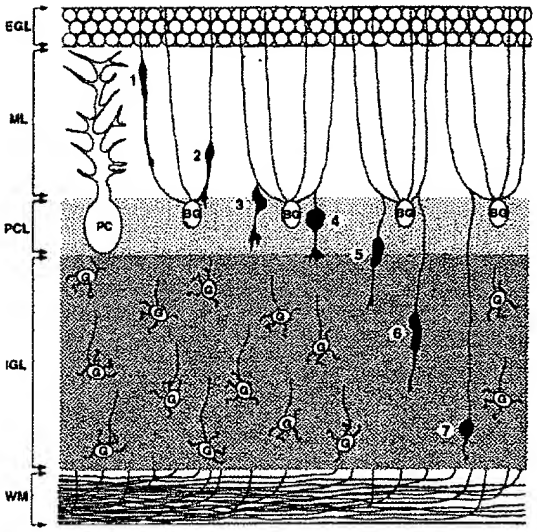

Figure 4 The morphogenetic transformation of granule cells as they migrate across the various cellular compartments of the developing cerebellar cortex. BG = Bergmann glial cell; G = postmigratory granule cell; PC = Purkinje cell. (From Komuro and Rakic, *J. Neurosci.* **18**:1478–1490, © 1998 Society for Neuroscience, reprinted with permission.)

μm/h in the ML, 5.2 μm/h in the PCL, and 10.2 μm/h in the IGL. Therefore, the average transit time of granule cells was 9.8 h in the ML, 5.2 h in the PCL, and 11.1 h to attain their final position in the IGL. These results suggest that in the postnatal 10-day-old mouse, cerebellar granule cells move from the premigratory zone of the EGL through the ML and the PCL to their final position in the bottom of the IGL within about 1 day (average 26 h) after the initiation of their radial migration (Komuro and Rakic, 1998a).

It may be important to emphasize that we found a direct and consistent relationship between granule cell shape (expressed as the ratio between the width and length of cell soma), the length of the leading process, and the rate of cell movement (Komuro and Rakic, 1998a). Changes in local environmental cues, including various cell adhesion and extracellular matrix molecules combined with signaling from different cellular compartments in the migrating pathway, may induce granule cells to alter their shape and the rate of their movement (Rakic, et al., 1994) (Fig. 4). However, intrinsic signals might also participate in the dynamic changes in cell shape and migratory behavior seen in different domains of the cerebellar cortex. It has been shown that migrating granule cells express specific genes at given

points along their pathway and that some of these genes encode receptors that are activated by cell adhesion molecules (Kuhar et al., 1993; Rocamora et al., 1993; Friedman and Seeds, 1995; Hatten and Heintz, 1995; Zheng et al., 1996; Hatten et al., 1997). Although the role of these genes in the developing cerebellum has not been determined, it has been shown that mutated cell adhesion molecule-related kinase genes can transform fibroblasts from a typical polar migratory shape to a more rounded one and dramatically reduce their mobility compared with wildtype (Ilic et al., 1995). Furthermore, laminar and cytoarchitectonic abnormalities of cerebral and cerebellar cortices may be caused by the mutation of specific genes that are involved in the completion of migration (Howell et al., 1997; Sheldon et al., 1997; Ware et al., 1997). Therefore, changes in gene expression during the translocation of granule cells from the EGL to the IGL may function to modulate changes in their shape and behavior, as well as in their allocation to the final position. The use of slice preparations in conjunction with confocal microscopy allows the examination of the role of various genes, adhesive molecules, ion channels, and receptors in cell migration through the heterogeneous terrain of the developing mammalian brain.

ACTIVITY OF N-TYPE CALCIUM CHANNELS AND GRANULE CELL MIGRATION

It is well established that immature neurons in the developing central and peripheral nervous system express voltage-gated ion channels before reaching their final destinations (LoTurco et al., 1991; Spitzer, 1994; Navarro et al., 1996). Activity of ion channels also modulates growth cone motility and the rate of neurite extension (Lankford and Letourneau, 1989; Kater and Mills, 1991; Spitzer, 1994; Gu and Spitzer, 1995). However, the role of these channels in neuronal migration is less well known. Recently, the combined use of acute slice preparations and pharmacological tools revealed the role of voltage-gated Ca^{2+} channels, the especially N-type Ca^{2+} channel, in granule cell migration (Komuro and Rakic, 1992). Blockade of N-type Ca^{2+} channel activity by a specific antagonist, ω-conotoxin GVIA, curtailed granule cell migration in the ML (Komuro and Rakic, 1992). This effect was dose dependent in the range of 30–3000 n*M*. The smallest statistically significant decrease in the rate of granule cell movement ($p < .05$) was detected at a concentration of 30 n*M* ω-conotoxin GVIA (24%), and the decrease in the rate of movement became gradually more pronounced ($p < .01$) as the concentration of toxin increased: at 300 n*M* (50%), at 1000 n*M* (65%), and at 3000 n*M* (>78%). However, blocking other types of voltage-gated Ca^{2+} channels, such as L- or T-type Ca^{2+} channels, by adding nifedipine or Ni^{2+}, respectively, had no significant effect. Likewise, the blockade of the voltage-sensitive Na^+ channels by tetrodotoxin and K^+ channels by tetraethylammonium chloride or 4-aminopyridine failed to alter substantially the rate of granule cell migration. These results demonstrate that the activity of N-type Ca^{2+} channels plays a critical role in controlling the rate of granule cell movement in the ML (Komuro and Rakic, 1992).

When do immature granule cells begin to express N-type Ca^{2+} channels on their plasmalemmal surface? Although electrophysiological analysis has shown that differentiated granule cells express functional N-type Ca^{2+} channels on their plasmalemmal surface (Randall and Tsien, 1995; Blair and Marshall, 1997), the time of onset of N-type Ca^{2+} channel expression in immature granule cells has not been examined. To determine the time of onset of expression and distribution of N-type Ca^{2+} channels on the plasmalemmal surface, brain slices from postnatal 10-day-old mouse cerebella were labeled with tetramethylrhodamine-conjugated ω-conotoxin (Komuro and Rakic, 1992). The outer and inner halves of the EGL were distinctly marked by a sharp difference in labeling. The outer half of the EGL, which contains mainly proliferating cells, was devoid of fluorescence. However, the inner half, which is composed mainly of postmitotic cells in their premigratory phase, was fluorescent. The intensity of fluorescence increased as the granule cells passed through the ML and attained its maximum level when the cells migrated into the IGL. These results demonstrated that postmitotic granule cells at the bottom of the EGL start to express N-type Ca^{2+} channels prior to the initiation of their radial migration towards the ML. Furthermore, the number of N-type Ca^{2+} channels on the plasmalemmal surface of granule cells rapidly increases during the translocation of the cell soma from the EGL to the IGL.

How does the activity of the N-type Ca^{2+} channels control the rate of granule cell movement? One possible scenario is that the activation of N-type Ca^{2+} channels induces substantial Ca^{2+} influxes through the plasma membrane, thereby regulating the rate of granule cell migration. This hypothesis is supported by the following evidence. Lowering

extracellular Ca^{2+} concentrations (0.1–1.0 m*M*) resulted in a graded significant decrease in the rate of granule cell migration in the ML (Komuro and Rakic, 1992). In contrast, increasing extracellular Ca^{2+} concentrations to 5.0 m*M* slightly enhanced the rate of migration. These results indicate that the rate of granule cell migration in the ML is highly sensitive to changes in the extracellular Ca^{2+} concentration, suggesting that blocking the N-type Ca^{2+} channel activity may affect the migration by reducing Ca^{2+} entry into the cell.

These findings indicate that the activity of N-type Ca^{2+} channels is crucial to granule cell migration. In contrast, the activity of Na^+, K^+, and L- and T-type Ca^{2+} channels seems to be far less or not significant for migration. This result was unexpected, because the N-type Ca^{2+} channels have been mainly implicated in the release of neurotransmitters (reviewed in Hess, 1990), while growth cone movement and neurite extension appear to be regulated, for the most part, by the activity of L-type Ca^{2+} channels (Robson and Burgoyne, 1989; Silver et al., 1990). It should, however, be kept in mind that N-type Ca^{2+} channels are a highly heterogeneous group of molecules (Westenbroek et al. 1992). Furthermore, the ratio of N-type to L-type Ca^{2+} channels varies between *in vitro* and *in vivo* situations, between cell classes, and, most importantly, between immature and adult neurons (Wagner et al., 1988; Martin-Moutot et al., 1990; Vigers and Pfenninger, 1991; Rossi et al., 1994). Use of [^{125}]ω-conotoxin GVIA to study the distribution of N-type calcium channels in the developing brain showed their transient expression in several regions where they may be involved in early developmental events (Fillaux et al., 1994). It is therefore likely that during their migration phase, immature granule cells express different subtypes and ratios of N-type of Ca^{2+} channels than they do after their arrival in the IGL.

ACTIVITY OF THE NMDA RECEPTOR AND THE RATE OF GRANULE CELL MOVEMENT

The discovery that Ca^{2+} influxes through N-type Ca^{2+} channels are involved in cell migration led to the question of whether neurotransmitter receptors also play a role in granule cell movement, since activation of NMDA, non-NMDA, $GABA_A$, and $GABA_B$ receptors of immature granule cells can alter Ca^{2+} influx into their soma (Connor et al., 1987; Zhu and Chuang, 1987; Burgoyne et al., 1988; Howe et al., 1991; Laurie et al., 1992). Indeed, several lines of evidence have demonstrated that spontaneous activation of the NMDA subtype of glutamate receptors modulates the rate of granule cell migration (Komuro and Rakic, 1993; Rossi and Slater, 1993; Farrant et al., 1994; Rakic et al., 1994; Rakic and Komuro, 1995; Slater and Rossi, 1996). First, blocking NMDA receptor activity with its antagonists, D-2-amino-5-phosphonopentanoic acid (D-AP5) or (+)-5-methyl-10,11-dihydro-5H-dibenzo[a,d]-cyclohepten-5,10-imine hydrogen maleate (MK-801), significantly decreases the rate of granule cell movement (Komuro and Rakic, 1993). The effect of D-AP5 and MK-801 is dose dependent. For example, the addition of 1–10 μM of D-AP5 to the medium does not significantly affect the rate of granule cell movement. However, 50 μM D-AP5 reduces the rate to 48%, and 100 μM D-AP5 to 38% of normal cell movement. In contrast, the rate of cell migration is not substantially altered by blocking the activity of non-NMDA receptors (i.e., kainate and AMPA receptors) with 6-cyano-7-nitroquinoxaline-2,3-dione (CNQX), $GABA_A$ receptors with bicuculline, and $GABA_B$ receptors with phaclofen (Komuro and Rakic, 1993).

The role of the NMDA receptor in granule cell migration was further supported by evidence that changes in Mg^{2+} or glycine concentration affect the rate of cell movement (Komuro and Rakic, 1993). Because extracellular Mg^{2+} blocks NMDA receptor activity in a voltage-dependent manner (Nowak et al., 1984) and application of glycine potentates the NMDA receptor activity (Johnson and Ascher, 1987), it is expected that they both would influence cell migration. Indeed, the removal of Mg^{2+} from the medium significantly increases the rate of granule cell movement in the ML (Komuro and Rakic, 1993). In contrast, the rate of cell movement was reduced in a high-Mg^{2+} medium. Likewise, the application of 10 μM glycine significantly increases the rate of cell movement in the ML. These results demonstrate that granule cell mobility is highly sensitive to small fluctuations in extracellular Mg^{2+} and glycine levels, suggesting that the activity of NMDA receptors modulates the rate of granule cell movement (Komuro and Rakic, 1993).

The presence of spontaneously active NMDA receptors on the surface of migrating granule cells in cerebellar slices has been confirmed by patch-clamp analysis (Rossi and Slater, 1993). Interestingly, the frequency of the spontaneous NMDA receptor-coupled channel activity was low in the premigratory zone of the EGL, with large increases recorded in

migrating neurons of the ML. Furthermore, single-channel recordings revealed developmentally related changes in the biophysical properties of the NMDA receptors during the course of granule cell differentiation, suggesting that migrating granule cells express one or more specific receptor subunits that are distinct from those comprising the receptors present in mature granule cells (Farrant et al., 1994). In particular, it seems that migrating granule cells coexpress the NR1 and NR2A or NR2B subunits, whereas postmigratory cells in the IGL express the NR1 and NR2C types (Farrant et al., 1994; Monyer et al., 1994). This progressive alteration in subunit composition could account for a change in NMDA receptor function during development (Farrant et al., 1994; Moyner et al., 1994; Sheng et al., 1994; Feldmeyer and Cull-Candy, 1996). Moreover, there is evidence that the sensitivity of the NMDA receptors on granule cells in the EGL to glutamate increases in the course of cerebellar development (Rossi and Slater, 1993). This increase can at least partly account for the acceleration of neuronal cell migration during the late stages of cerebellar development (Komuro and Rakic, 1995).

The question of how NMDA receptors expressed by migrating granule cells could be activated is intriguing, because migrating granule cells do not form synapses before the completion of their translocation in the IGL (Rakic and Sidman, 1973a). One possibility is that endogenous extracellular glutamate may activate the immature form of the NMDA receptor by nonsynaptic means. Interestingly, the elevation of extracellular glutamate concentrations by inhibiting glutamate uptake by astrocytes increased the frequency of spontaneous NMDA receptor-coupled channel activity (Rossi and Slater, 1993) and significantly accelerated the rate of granule cell movement in the ML (Komuro and Rakic, 1993). These results suggest that endogenous glutamate may be an important signal for the activation of NMDA receptors and that the increase of extracellular glutamate could enhance the rate of cell migration until the concentration reaches a toxic level (Marret et al., 1996).

Although the source of extracellular glutamate in the ML has not been established, several possible sources alone or in combination could be sufficient to activate NMDA receptors in migrating neurons. First, astrocytes are known to influence directly neighboring neurons by releasing neuroactive substances (Parpura et al., 1994). For example, glutamate released from cultured astrocytes in response to local signals causes an NMDA receptor–mediated increase in intracellular calcium levels in

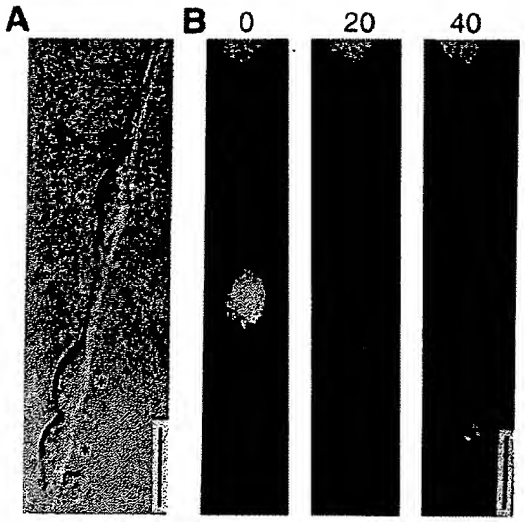

Figure 5 Granule cell migration in cerebellar microexplant cultures. (A) Typical migrating granule cells from a microexplant culture of postnatal 2-day-old mouse cerebella. Migrating neurons (asterisks) in this assay display characteristic leading and trailing processes. (B) A migrating granule cell loaded with the cell-permeant, acetoxymethyl ester form of 1 μM Fluo-3 shows changes in fluorescence intensity over the time indicated in minutes at the top of each photograph. Bars = 10 μm.

neighboring neurons (Parpura et al., 1994; Pon and Robinson, 1994). Therefore, it is possible that Bergmann glial cells, which belong to the astrocyte cell class, release glutamate in response to local signals and influence the rate of granule cell movement by regulating the activity of NMDA receptors. The intimate association and large mutually shared surface area that exists between Bergmann glial fibers and adjacent migrating neurons could considerably facilitate this process. However, parallel fibers belonging to granule cells that have attained their final positions below the PCL are the most obvious source of extracellular glutamate in the ML (Levi et al., 1991). Although parallel fibers eventually form synapses with Purkinje cell dendrites in this territory, migrating cells do not (Rakic and Sidman, 1973a). Therefore, any glutamate released by parallel fibers must activate the NMDA receptor of migrating granule cells in a paracrine manner. Spontaneous, nonsynaptic activation of the NMDA receptor by extracellular glutamate has been observed in immature cortical neurons before they form synapses (Blanton and Kriegstein, 1992). Furthermore, the possibility that NMDA receptors mediate paracrine signals during the migration of postmitotic neurons has received support from other studies. For

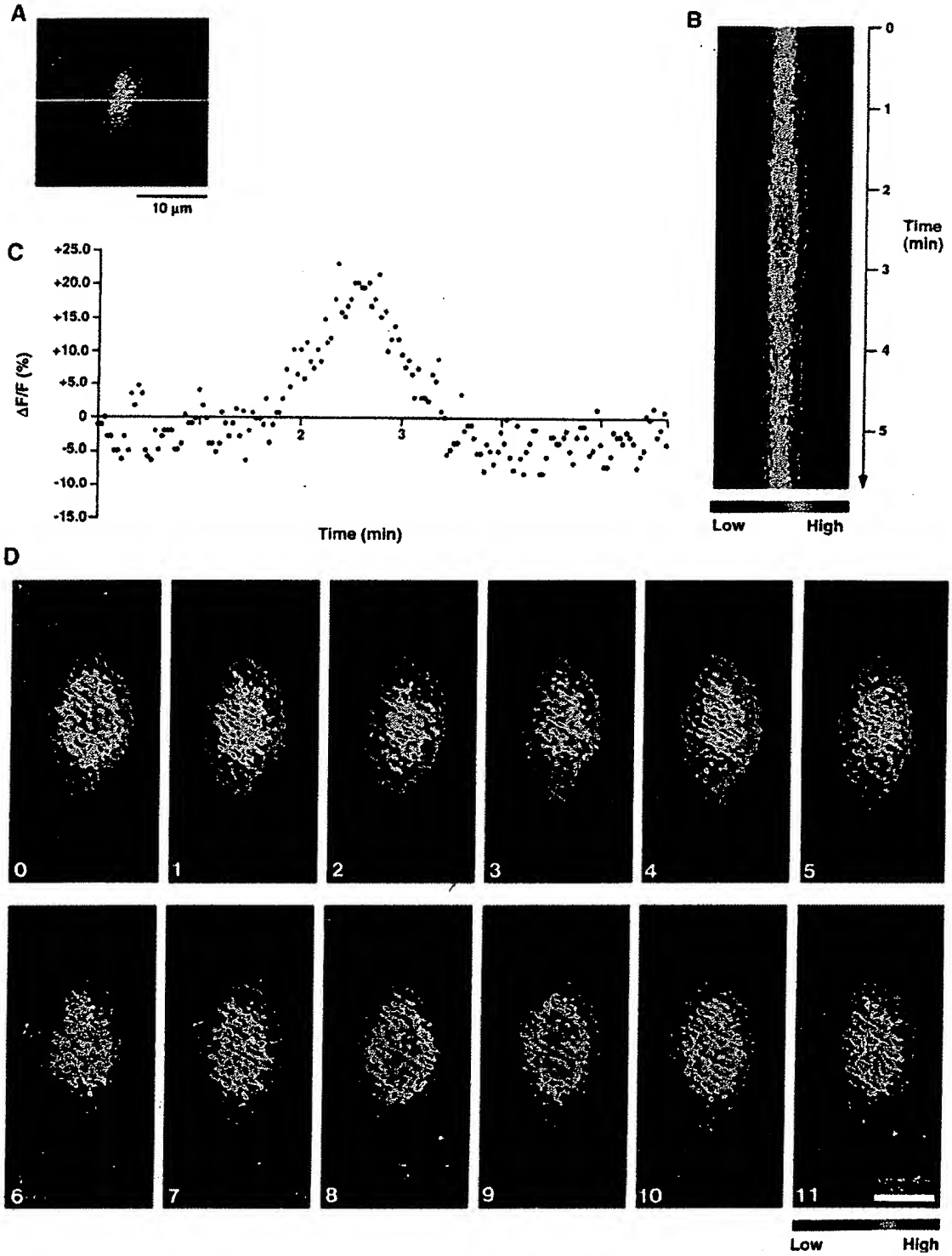

Figure 6 Spontaneous intracellular Ca^{2+} elevations in migrating granule cells. (A) Pseudocolor frame image of $[Ca^{2+}]_i$ in a migrating cell loaded with 1 μM Fluo-3. The yellow line indicates the equator of the cell soma. (B) Pseudocolor line scan image of $[Ca^{2+}]_i$ obtained

example, the NMDA antagonist MK-801 applied to the developing rodent cerebrum *in vivo* produces a migration defect in the hippocampal formation (Gould et al., 1994), suggesting that cell motility in diverse regions of the mammalian brain may use a similar mechanism.

Since activation of N-type Ca^{2+} channels and NMDA receptors induces substantial Ca^{2+} influxes into migrating granule cells (Rakic and Komuro, 1995; Slater and Rossi, 1996), it is expected that elevations in $[Ca^{2+}]_i$ would affect granule cell migration. Therefore, the logical next step is to examine the intracellular Ca^{2+} dynamics of granule cells during their migration.

CORRELATION OF CELL MOVEMENT AND INTRACELLULAR CALCIUM FLUCTUATIONS

Monitoring $[Ca^{2+}]_i$ using Ca^{2+} indicator dyes demonstrated fluctuations in $[Ca^{2+}]_i$ in migrating granule cells (Fig. 5). For example, continuous single-line scanning across the equator of a migrating cell soma loaded with Ca^{2+} indicator dye, Fluo-3, revealed a spontaneous elevation of $[Ca^{2+}]_i$ with slopes rising and falling symmetrically [Fig. 6(A–C)]. The average amplitude of $[Ca^{2+}]_i$ elevations was 14% of the baseline intensity, and the average duration was 1.3 min (Komuro and Rakic, 1996). In addition, whole-cell frame images of $[Ca^{2+}]_i$ also showed that $[Ca^{2+}]_i$ elevations in the cell soma were frequent and irregular during movement of the cell body [Fig. 6(D)]. Transient elevations of $[Ca^{2+}]_i$ in migrating granule cells occurred 4–24 times/h, with average frequencies of 13/hr. Although these results suggest that migrating cells exhibit spontaneous and transient elevations of $[Ca^{2+}]_i$, there is a possible alternative explanation for changes in Fluo-3 intensity. For example, transient increases in Fluo-3 intensity may be related to small changes in the thickness of migrating cells. However, a series of ratiometric measurements of $[Ca^{2+}]_i$ excluded this possibility (Komuro and Rakic, 1996). Migrating granule cells were loaded with a mixture of two Ca^{2+} indicator dyes, Fluo-3 and Fura-Red. When excited at 514 nm upon Ca^{2+} binding, Fluo-3 exhibits an increase in the fluorescence intensity at 540 nm, while Fura-Red shows a decrease in the fluorescence intensity at 600 nm (Lipp and Niggli, 1993a,b; Schild et al., 1994; Floto et al., 1995). Therefore, the ratio of Fluo-3 to Fura-Red intensity accurately reflects changes in $[Ca^{2+}]_i$. In contrast, uniform changes in the fluorescence intensity of both dyes would implicate artificial signals, including a change in cell thickness. Simultaneous dual-emission images revealed that Fluo-3 and Fura-Red were colocalized within the soma of the migrating cell. Most importantly, the periodicity and time course as well as the shape of $[Ca^{2+}]_i$ fluctuations obtained with the Fluo-3/Fura-Red ratio were identical to those obtained with the Fluo-3 alone [Fig. 7(A,B)]. These results confirmed that granule cells exhibit dynamic changes in $[Ca^{2+}]_i$ during movement of the cell body.

Do the spontaneous fluctuations of $[Ca^{2+}]_i$ play a role in granule cell migration? If so, how are changes in $[Ca^{2+}]_i$ involved in the saltatory movement of granule cells? Simultaneous measurements of $[Ca^{2+}]_i$ and cell movement revealed a temporal relationship between the direction and distance traversed by the cell body and the time course of intracellular Ca^{2+} changes (Komuro and Rakic, 1996). During a recording period of 45 min, a migrating cell typically exhibited eight cycles of saltatory movement and a corresponding number of transient $[Ca^{2+}]_i$ elevations (Fig. 8). Interestingly, each phase of the saltatory movement of the migrating cell correlated temporally with each phase of spontaneous Ca^{2+} fluctuations. For example, the cell exhibited forward movement during the phase of transient elevations of $[Ca^{2+}]_i$. In particular, at the peak

by scanning the beam at the relative position indicated by the yellow horizontal line through the cell soma in (A). To measure changes in $[Ca^{2+}]_i$ over time at the same relative position in somata of migrating cells, a single line was scanned at a fixed point every 2 s, for a period of 6 min. Sequential intensities of the fluorescence signal are displayed from top to bottom. (C) Time course of $[Ca^{2+}]_i$ change in the cell illustrated in (B). Upward deflections represent elevations in $[Ca^{2+}]_i$ and downward deflections indicate decreases in $[Ca^{2+}]_i$. (D) Pseudocolor frame images of a migrating cell exhibiting spontaneous elevations in $[Ca^{2+}]_i$. The migrating cell exhibited spontaneous multiple elevations in $[Ca^{2+}]_i$ during somal translocation, although their frequency and amplitude were irregular. Numerals at the bottom of each photograph indicate time in minutes. Bar = 5 μm. (From Komuro and Rakic, Neuron 17:275–285 © 1996 Cell Press, reprinted with permission.)

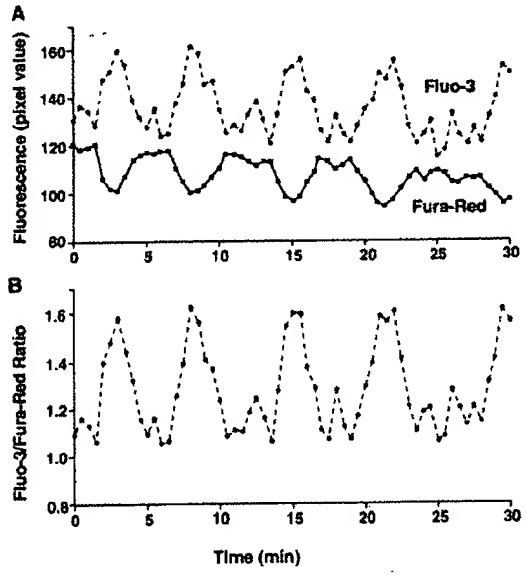

Figure 7 Ratiometric measurements of spontaneous intracellular Ca^{2+} fluctuations in migrating cells. Granule cells were coloaded with 3 μM Fluo-3 and 4 μM Fura-Red. The 514-nm line of the argon laser was used to excite both fluorophores, while fluorescence emission was detected simultaneously at 540 ± 15 nm (Fluo-3) and >600 nm (Fura-Red) by the dual-emission mode of a laser-scanning confocal microscope. (A) Changes in the fluorescence intensity of Fluo-3 and Fura-Red taken from the soma of a migrating granule cell. Upward deflections in Fluo-3 signals (dotted line) represent elevations in $[Ca^{2+}]_i$, and downward deflections represent decreases in $[Ca^{2+}]_i$. In contrast, upward deflections in Fura-Red signals (solid line) represent decreases in $[Ca^{2+}]_i$, and downward deflections represent elevations in $[Ca^{2+}]_i$. (B) Time course of changes in Fluo-3/Fura-Red ratio signal. Upward deflections in Fluo-3/Fura-Red ratio signals represent elevations in $[Ca^{2+}]_i$, and downward deflections indicate decreases in $[Ca^{2+}]_i$. Fluo-3/Fura-Red ratio signals were calculated by dividing pixel values of Fluo-3 fluorescence intensity by pixel values of Fura-Red fluorescence intensity.

of each Ca^{2+} elevation, the distance traversed by the cell body was the largest. In contrast, at each trough of Ca^{2+} fluctuation, the cell remained stationary or exhibited a small backward movement. These results suggest that individual fluctuations in $[Ca^{2+}]_i$ in migrating neurons may control different phases of their saltatory movement.

If $[Ca^{2+}]_i$ fluctuations are involved in regulating cell movement, fast- and slow-moving cells might exhibit different sizes and/or cycles of Ca^{2+} fluctuations. To test this possibility, the amplitude and frequency of Ca^{2+} elevations were analyzed as a function of the rate of single cell movement (Komuro and Rakic, 1996). Despite considerable variations in $[Ca^{2+}]_i$ elevations in individual cells, there was a clear positive correlation between the rate of cell movement and both the amplitude and frequency components of Ca^{2+} fluctuations (Fig. 9). The correlation coefficient between the rate of cell movement and the amplitude of Ca^{2+} fluctuations was 0.74, and that of the rate of cell movement and the frequency of Ca^{2+} fluctuations was 0.83. For example, fast-moving cells exhibited a larger amplitude and higher frequency of Ca^{2+} fluctuations than slow-moving cells. Furthermore, cells that displayed a higher amplitude of Ca^{2+} fluctuations demonstrated more frequent changes in $[Ca^{2+}]_i$ than cells that displayed lower amplitudes. Taken together, these results suggest that both the amplitude and frequency components of Ca^{2+} fluctuations may be one of the intracellular signals controlling the rate of cell movement.

Previous studies showed that transient elevations of $[Ca^{2+}]_i$ are essential for initiating and maintaining the movement of cells ranging in type from fibroblasts to immature glial cells (Newgreen and Gooday, 1985; Sawyer et al., 1985; Jaconi et al., 1991; Moran, 1991; Brundage et al., 1993; Anton et al., 1995). For example, an increase in the rate of Schwann cell migration induced by the application of antibodies to the cell surface glycoprotein, CD9, was correlated with a rise in $[Ca^{2+}]_i$ (Anton et al., 1995). Likewise, migrating human neutrophils exhibit multiple increases and decreases in $[Ca^{2+}]_i$ (Marks and Maxfield, 1990). Buffering of $[Ca^{2+}]_i$ by the addition of the cell-permeant calcium ion chelator BAPTA-AM or removal of extracellular Ca^{2+} blocks transient increases in $[Ca^{2+}]_i$ in neutrophils, and thus reduces or inhibits cell migration (Marks and Maxfield, 1990).

COMBINATION OF AMPLITUDE AND FREQUENCY OF INTRACELLULAR CALCIUM FLUCTUATIONS CONTROLS RATE OF CELL MOVEMENT

It is well known that the average $[Ca^{2+}]_i$ affects the motility of growth cones and the rate of neurite extension (Kater and Mills, 1991; al-Mohanna et al., 1992). Does the average $[Ca^{2+}]_i$, independent of Ca^{2+} fluctuations, affect the movement of granule cells? To test this possibility, the average $[Ca^{2+}]_i$ was changed without a corresponding change in the amplitude and frequency of Ca^{2+} fluctuations (Komuro and Rakic, 1996). Addition of a Ca^{2+} iono-

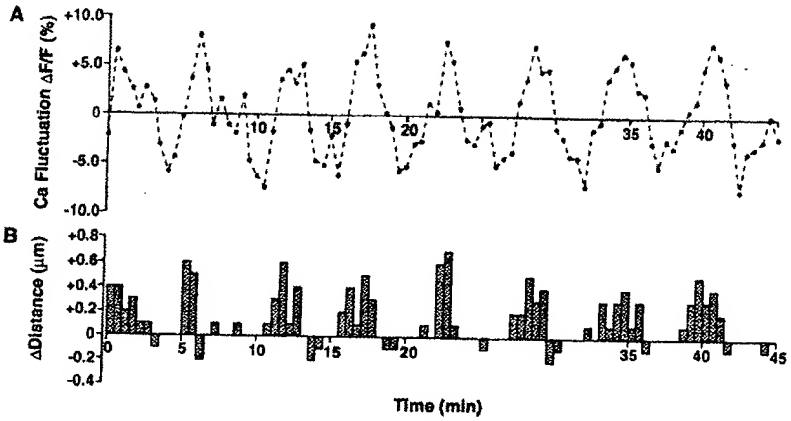

Figure 8 Temporal correlation between individual Ca^{2+} fluctuations and individual cell movement during migration. (A) Example of the time course of intracellular Ca^{2+} changes in a migrating cell. Upward deflections represent elevations in $[Ca^{2+}]_i$, and downward deflections indicate decreases in $[Ca^{2+}]_i$. (B) The direction and distance traversed by the same cell during each minute of the testing period. Positive values represent forward movement of the cell body, while negative values represent backward movement. Frame images of migrating cells loaded with 1 μM Fluo-3 were recorded every 30 s for 45 min. (From Komuro and Rakic, Neuron 17:275–285, © 1996 Cell Press, reprinted with permission.)

phore, 100 nM ionomycin, to the medium increased the average intracellular Ca^{2+} level ($F_{1/2}$) (which was calculated as the Ca^{2+} level midway between peak and trough of Ca^{2+} fluctuations, from 92 nM to 250 nM), but did not affect significantly the amplitude and frequency of Ca^{2+} fluctuations [Fig. 10(A–C)]. Interestingly, the ionomycin-induced elevations of average $[Ca^{2+}]_i$ failed to substantially affect the rate of cell movement [Fig. 10(D)].

To further examine the relationship between the average $[Ca^{2+}]_i$ and cell movement, Ca^{2+} fluctuations in migrating cells that showed elevated $[Ca^{2+}]_i$ were blocked (Komuro and Rakic, 1996). The addition of 1 μM ω-conotoxin GVIA, 100 μM D-AP5, 1 μM thapsigargin, and 50 nM ionomycin to the medium increased the average $[Ca^{2+}]_i$ from 101 nM to 154 nM [Fig. 10(E)]. The size of these tonic elevations of average $[Ca^{2+}]_i$ was approximately similar to the elevations of Ca^{2+} levels seen during spontaneous Ca^{2+} fluctuations. However, the application of these compounds decreased both the amplitude (to 16% of control value) and frequency (to 36% of control value) of Ca^{2+} fluctuations [Figs. 10(F,G)]. Importantly, blocking Ca^{2+} fluctuations with concomitant tonic elevations of average $[Ca^{2+}]_i$ in the migrating cells resulted in a significant decrease in the rate of cell movement, to 18% of the control value [Fig. 10(H)]. Taken together, these results demonstrate that the rate of granule cell migration does not depend on the average $[Ca^{2+}]_i$.

If the amplitude and frequency components of Ca^{2+} fluctuations control the migratory behavior of granule cells, experimentally induced changes in these components would affect their movement. To address this issue, Ca^{2+} fluctuations in migrating cells were altered either by changing Ca^{2+} influx through the plasma membrane or by decreasing Ca^{2+} release from intracellular Ca^{2+} stores (Komuro and Rakic, 1996). Reduction of Ca^{2+} influx by lowering extracellular Ca^{2+} concentrations from 1.8 mM to 0.1 mM resulted in a 68% decrease in the amplitude of spontaneous Ca^{2+} elevations [Fig. 11(A)]. Moreover, blocking N-type Ca^{2+} channels with 1 μM ω-conotoxin GVIA or NMDA receptors with 100 μM D-AP5 resulted in a decrease in the amplitude of spontaneous Ca^{2+} elevations to 45% and 49% of control values, respectively [Fig. 11(A)]. The reduced Ca^{2+} concentrations and the blockade of N-type Ca^{2+} channels or NMDA receptors also reduced the frequency of Ca^{2+} fluctuations to 62%, 85%, and 74% of the control value, respectively [Fig. 11(B)]. Most importantly, this reduction was linearly related to the rate of cell movement [Fig. 11(A,B)]. Furthermore, reduction of Ca^{2+} release from intracellular Ca^{2+} stores by 1 μM thapsigargin decreased the amplitude of Ca^{2+} elevations to 90% of the control value and slowed cell movement to 78% of the control value without significant effects on the frequency of Ca^{2+} elevations (Komuro and Rakic, 1996). These results demonstrated that the rate of granule cell movement is highly

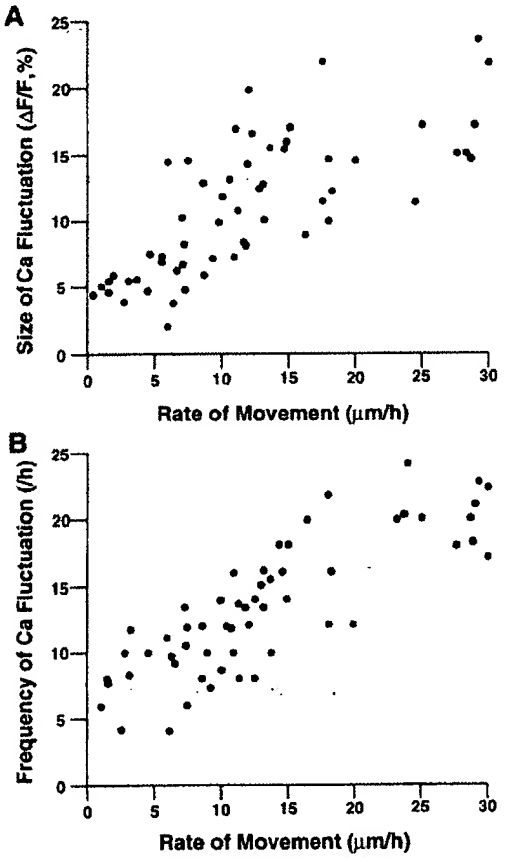

Figure 9 Positive correlation between the amplitude component of Ca^{2+} fluctuations and the rate of cell movement (A), and between the frequency component of Ca^{2+} fluctuations and the rate of cell movement (B). Each point displays either the size or frequency of Ca^{2+} fluctuations in relation to the rate of cell movement of a single neuron. (From Komuro and Rakic, Neuron 17:275–285, © 1996 Cell Press, reprinted with permission.)

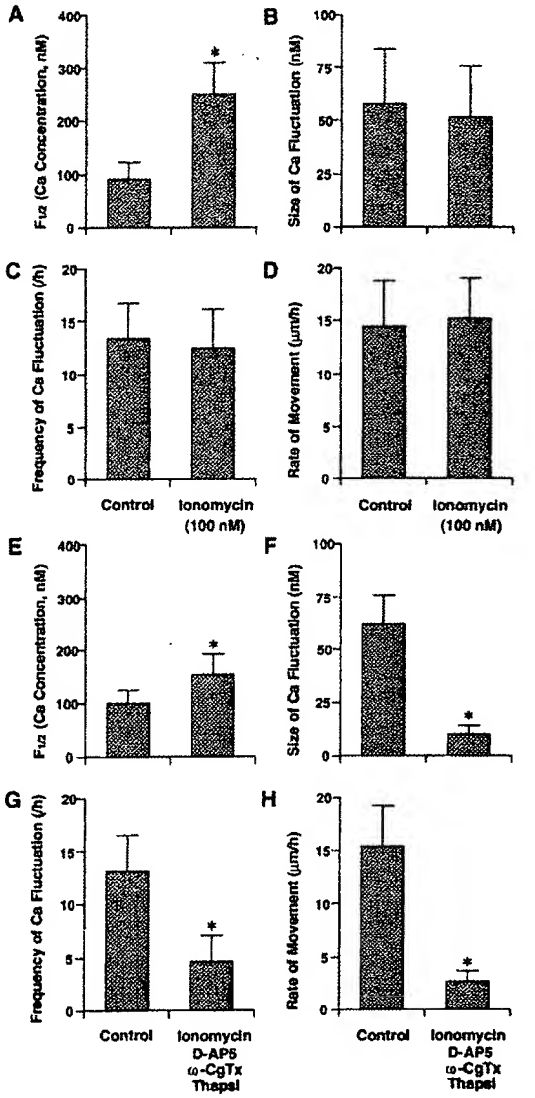

Figure 10 Average intracellular Ca^{2+} levels do not affect the rate of cell movement. (A–D) Effect of applying 100 n*M* ionomycin, a Ca^{2+} ionophore, on (A) the average $[Ca^{2+}]_i$ level ($F_{1/2}$), (B) the size of Ca^{2+} fluctuations, (C) the frequency of Ca^{2+} fluctuations, and (D) the rate of cell movement in migrating cells. (E–H) Effect of applying 1 μM ω-conotoxin-GVIA (ω-CgTx), 100 μM D-AP5, 1 μM thapsigargin, and 50 n*M* ionomycin on (E) the average $[Ca^{2+}]_i$ level ($F_{1/2}$), (F) the size of Ca^{2+} fluctuations, (G) the frequency of Ca^{2+} fluctuations, and (H) the rate of cell movement. Frame images of migrating cells loaded with 1 μM Fluo-3 were recorded every minute for a total of 60 min, including the period before and after the addition of these compounds. Each column represents the average obtained from 28 migrating cells (A–D) and 10 migrating cells (E–H). Asterisks indicate statistical significance ($p < .01$). Bar = S.D. (From Komuro and Rakic, Neuron 17:275–285, © 1996 Cell Press, reprinted with permission.)

sensitive to changes in the amplitude and frequency of Ca^{2+} fluctuations.

The role of the amplitude and frequency of Ca^{2+} fluctuations in controlling cell migration was confirmed by the demonstration that the accelerated forward movement of granule cells can be induced by large elevations in $[Ca^{2+}]_i$ (Komuro and Rakic, 1996). Intracellular Ca^{2+} levels of migrating granule cells were repeatedly elevated by 3-min pulses of depolarizing levels of KCl delivered every 14 min. Each application of 30 m*M* KCl resulted in large elevations in $[Ca^{2+}]_i$ and concomitant increases in the forward movement of migrating cells (Fig. 12). Furthermore, the application of KCl significantly increased the distance traveled by the cell

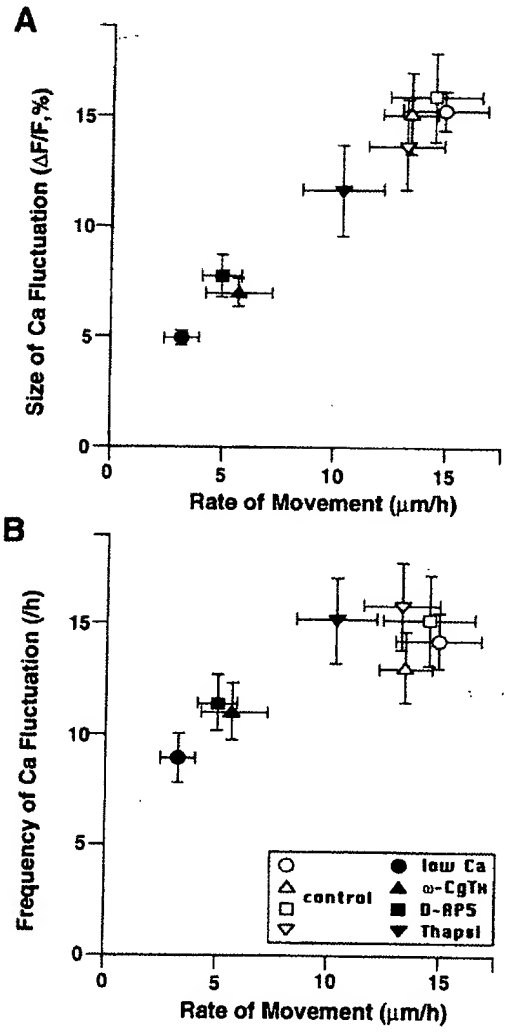

Figure 11 Experimentally induced reductions in Ca^{2+} fluctuations affect the rate of cell movement. To alter the amplitude components (A) and/or the frequency components (B) of the Ca^{2+} fluctuations in migrating granule cells, Ca^{2+} influxes were reduced by lowering extracellular Ca^{2+} concentrations from 1.8 m*M* to 0.1 m*M*, or by adding 1 μM ω-conotoxin-GVIA (ω-CgTx) or 100 μM D-AP5. Furthermore, the Ca^{2+} fluctuations were also modified by an application of 1 μM thapsigargin (thapsi), which decreases Ca^{2+} release from intracellular Ca^{2+} stores. Importantly, reduction of the amplitude components (A) or the frequency components (B) of the Ca^{2+} fluctuations was linearly related to the rate of granule cell movement. Each agent was added to culture medium in separate experiments. Images were recorded every minute for a total of 60 min, including the period before and after the addition of each agent. Each experimental group (indicated by filled symbols) should be compared with the appropriate control (indicated by open symbols). Each value is the average obtained from 10 migrating cells. Bar = S.D. (From Komuro and Rakic, Neuron 17:275–285, © 1996 Cell Press, reprinted with permission.)

during the accelerated forward movement (Fig. 12). For example, the average distance traveled by the cell during each 30 s of forward movement was 0.3 μm at control levels, while the distance during the application of KCl increased to 0.6 μm. Taken together, these results indicated that the combination of amplitude and frequency components of intracellular Ca^{2+} fluctuations provide an intracellular signal controlling the granule cell migration.

The cellular mechanisms underlying the generation of Ca^{2+} fluctuations observed in migrating neurons are similar to those of growth cones, but there are also noticeable differences (Kater and Mills, 1991; Gu and Spitzer, 1993, 1995; Gu et al., 1994). For example, the rate of cell migration is positively correlated with the amplitude and frequency components of Ca^{2+} fluctuations. In contrast, spontaneous and/or experimentally induced Ca^{2+} spikes in growth cone slow neurite migration (Gomez et al., 1995). Neurite outgrowth is significantly reduced immediately and transiently following Ca^{2+} spikes (Gomez et al., 1995). It is important to emphasize that transient elevations of $[Ca^{2+}]_i$ in growth cones do not synchronize with the elevation of $[Ca^{2+}]_i$ in the cell bodies of differentiating neurons (Gomez et al., 1995). Moreover, $[Ca^{2+}]_i$ in growth cones fluctuates more frequently and over a greater amplitude than does $[Ca^{2+}]_i$ in cell bodies in differentiating neurons (Gomez et al., 1995). However, the major difference between these two cellular events is the translocation of the cell nucleus and surrounding cytoplasm in migrating neurons. This translocation may depend on the assembly and disassembly of microtubules (Gregory et al., 1988; Rakic et al., 1996), whereas the motility of growth cones depends largely on the assembly and disassembly of actin filaments (Okabe and Hirokawa, 1991; Forscher et al., 1992). Such differences may explain, in part, the differences in the roles of Ca^{2+} fluctuations in neuronal cell migration and neurite outgrowth.

It is not well understood how transient elevations of $[Ca^{2+}]_i$ control cell motility. One possibility is that fluctuations of $[Ca^{2+}]_i$ regulate the dynamic assembly and disassembly of cytoskeletal elements required for the operation of a force-generating

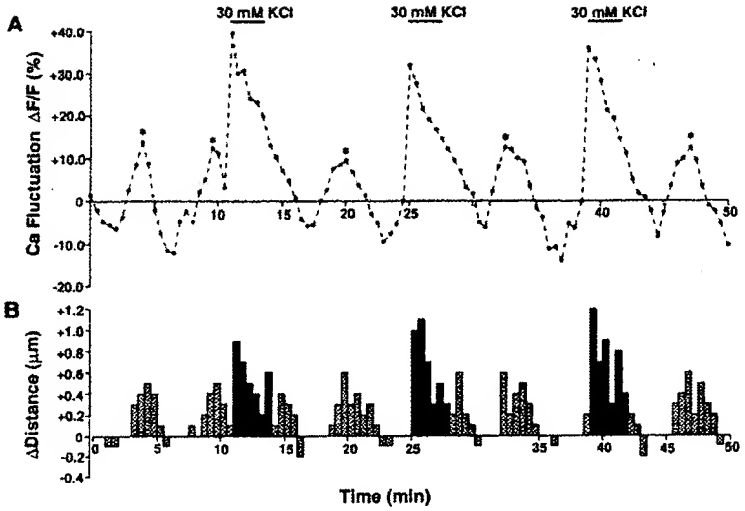

Figure 12 Experimentally induced transient elevations in intracellular Ca^{2+} levels accelerate forward movement of granule cells. (A) Example of the time course of intracellular Ca^{2+} changes in a migrating cell loaded with Fluo-3. Intracellular Ca^{2+} levels in the migrating cell were repeatedly elevated by the application of short (3-min) pulses of 30 m*M* KCl. Upward deflections represent elevations in $[Ca^{2+}]_i$, and downward deflections indicate decreases in $[Ca^{2+}]_i$. Each asterisk indicates the peak of spontaneous Ca^{2+} fluctuations. (B) The direction and distance traversed by the same cell during each 30-s interval of the testing period. Positive values represent forward movement of the cell body, while negative values represent backward movement. Filled columns represent the direction and distance traversed by the cell during the application of KCl, while stippled columns represent spontaneous movements of the same cell. (From Komuro and Rakic, Neuron **17**:275–285, © 1996 Cell Press, reprinted with permission.)

mechanism involved in cell movement (Rakic et al., 1996). Furthermore, elevation of $[Ca^{2+}]_i$ in neutrophils leads to the disruption of specific sites of attachment to an adhesive substratum (Marks and Maxfield, 1990). Changes in $[Ca^{2+}]_i$ in migrating neurons may modulate the repetitive formation and elimination of binding sites between migrating neurons and their migratory substrates. Intracellular calcium may control conformational changes of cell adhesion molecules, such as integrins, which are expressed on the plasma membrane of migrating neurons (Fishell and Hatten, 1991; Hynes, 1992; Clark and Brugge, 1995; Lawson and Maxfield, 1995).

CONCLUSION

The orchestrated activity of ion channels, neurotransmitter receptors, and intracellular Ca^{2+} fluctuations can, at least in part, explain position-specific changes in cell shape and migratory behavior of granule cells. Despite these new discoveries, the isolation of the responsible extracellular signaling molecules remains a continuing challenge. In particular, the question of which local environmental cues induce the completion of granule cell movement in the deep strata of the EGL remains to be elucidated.

REFERENCES

ACKERMAN, S. L., KOZAK, L. P., PRZYBORSKI, S. A., RUND, L. A., BOYER, B. B., and KNOWLES, B. B. (1997). The mouse rostral cerebellar malformation gene encodes an UNC-5-like protein. *Nature* **386**:838–842.

AL-MOHANNA, F. C., CAVE, J., and BOLSOVER, S. R. (1992). A narrow window of intracellular calcium concentration is optimal for neurite outgrowth in rat sensory neurons. *Dev. Brain Res.* **70**:287–290.

ALTMAN, J. (1972). Postnatal development of the cerebellar cortex in the rat. III. Maturation of the components of the granular layer. *J. Comp. Neurol.* **145**:465–514.

ANTON, E., CAMERON, R. S., and RAKIC, P. (1996). Role of neuron-glial junctional domain proteins in the maintenance and termination of neuronal migration across

the embryonic cerebral wall. *J. Neurosci.* **16**:2283–2293.

ANTON, E., HADJIARGYROU, M., PATTERSON, P. H., and MATTHEW, W. D. (1995). CD9 plays a role in Schwann cell migration in vitro. *J. Neurosci.* **15**:584–595.

ANTONICEK, H., PERSOHN, E., and SCHACHNER, M. (1987). Biochemical and functional characterization of a novel neuron-glia adhesion molecule that is involved in neuronal migration. *J. Cell Biol.* **104**:1587–1595.

BEHAR, T. N., LI, Y.-X., TRAN, H. T., MA, W., DUNLAP, V., SCOTT, C., and BAKER, J. L. (1996). GABA stimulates chemotaxis and chemokinesis of embryonic cortical neurons via calcium-dependent mechanisms. *J. Neurosci.* **16**:1808–1818.

BIX, G. J. and CLARK, G. D. (1998). Platelet-activating factor receptor stimulation disrupts neuronal migration in vitro. *J. Neurosci.* **18**:307–318.

BLAIR, L. A. C. and MARSHALL, J. (1997). IGF-1 modulates N and L calcium channels in a PI 3-kinase-dependent manner. *Neuron* **19**:421–429.

BLANTON, M. G. and KRIEGSTEIN, A. R. (1992). Properties of amino acid neurotransmitter receptors of embryonic cortical neurons when activated by exogenous and endogenous agonists. *J. Neurophysiol.* **67**:1185–1200.

BRUNDAGE, R. A., FOGARTY, K. E., TUFT, R. A., and FAY, F. S. (1993). Chemotaxis of newt eosinophils: calcium regulation of chemotactic response. *Am. J. Physiol.* **265**:C1527–C1543.

BURGOYNE, R. D., PEARCE, I. A., and CAMBRAY-DEAKIN, M. (1988). *N*-Methyl-D-aspartate raises cytosolic calcium concentration in rat cerebellar granule cells in culture. *Neurosci. Lett.* **91**:47–52.

CAMERON, R. S. and RAKIC, P. (1994). Polypeptides that comprise the plasmalemmal microdomain between migrating neuronal and glial cells. *J. Neurosci.* **14**:3139–3155.

CAMERON, R. S., RUFFIN, J., CHO, N. K., CAMERON, P. L., and RAKIC, P. (1997). Developmental expression, pattern of distribution, and effect on cell aggregation implicate a neuron-glial junctional domain protein in neuronal migration. *J. Comp. Neurol.* **387**:467–488.

CHOUNG, C.-M. (1990). Differential roles of multiple adhesion molecules in cell migration: granule cell migration in cerebellum. *Experientia* **46**:892–899.

CHOUNG, C.-M., CROSSIN, K. L., and EDELMAN, G. M. (1987). Sequential expression and differential function of multiple adhesion molecules during the formation of cerebellar cortical layers. *J. Cell Biol.* **104**:331–342.

CLARK, E. A. and BRUGGE, J. S. (1995). Integrins and signal transduction pathways: the road taken. *Science* **268**:233–239.

CONNOR, J. A., TSENG, H.-Y., and HOCKBERGER, P. E. (1987). Depolarization- and transmitter-induced changes in intracellular Ca^{2+} of rat cerebellar granule cells in explant cultures. *J. Neurosci.* **7**:1384–1400.

EDELMAN, G. M. (1984). Modulation of cell adhesion during induction, histogenesis and perinatal development of the nervous system. *Annu. Rev. Neurosci.* **7**:339–377.

EDMONDSON, J. C. and HATTEN, M. E. (1987). Glial-guided granule neuron migration in vitro: a high-resolution time-lapse video microscopic study. *J. Neurosci.* **7**:1928–1934.

EDMONDON, J. C., LIEM, R. K. H., KUSTER, J. C., and HATTEN, M. E. (1987). Astrotactin: a novel neuronal cell surface antigen that mediates neuron-astroglial interactions in cerebellar microcultures. *J. Cell Biol.* **106**:505–517.

FARRANT, M., FELDMEYER, D., TAKAHASHI, T., and CULL-CANDY, S. G. (1994). NMDA-receptor channel diversity in the developing cerebellum. *Nature* **368**:335–339.

FELDMEYER, D. and CULL-CANDY, S. (1996). Functional consequences of changes in NMDA receptor subunit expression during development. *J. Neurocytol.* **25**:857–867.

FILLAUX, F., SCHAPPER, A., NAISBITT, S. R., OLIVERA, B. M., and MCINTOSH, J. M. (1994). Complex patterns of [^{125}]ω-conotoxin GVIA binding site expression during postnatal rat brain development. *Dev. Brain Res.* **78**:131–136.

FISHELL, G. and HATTEN, M. E. (1991). Astrotactin provides a receptor system for CNS neuronal migration. *Development* **113**:755–765.

FISHMAN, R. B. and HATTEN, M. E. (1993). Multiple receptor systems promote CNS neuronal migration. *J. Neurosci.* **13**:3485–3495.

FLOTO, R. A., MAHAUT-SMITH, M. P., SOMASUNDARAM, B., and ALLEN, J. M. (1995). IgG-induced Ca^{2+} oscillation in differentiated U937 cells: a study using laser scanning confocal microscopy and co-loaded Fluo-3 and Fura-Red fluorescent probes. *Cell Calcium* **18**:377–389.

FORSCHER, P., LIN, C. H., and THOMPSON, C. (1992). Novel form of growth cone motility involving site-directed actin filament assembly. *Nature* **357**:515–518.

FRIEDMAN, G. C. and SEEDS, N. W. (1995). Tissue plasminogen activator mRNA expression in granule neurons coincides with their migration in the developing cerebellum. *J. Comp. Neurol.* **360**:658–670.

FUESHKO, S. M., KEY, S., and WRAY, S. (1998). GABA inhibits migration of luteinizing hormone-releasing hormone neurons in embryonic olfactory explants. *J. Neurosci.* **18**:2560–2569.

FUJITA, S. (1967). Quantitative analysis of cell proliferation and differentiation in the cortex of the postnatal mouse cerebellum. *J. Cell Biol.* **32**:277–287.

GLOOR, S., ANTONICEK, H., SWEADNER, K. J., PAGLIUSI, S., FRANCK, R., MOOS, M., and SCHACHNER, M. (1990). The adhesion molecule on glia (AMOG) is a homologue of the β subunit of the Na, K-ATPase. *J. Cell Biol.* **110**:165–174.

GOMEZ, T. M., SNOW, D. W., and LETOURNEAU, P. C. (1995). Characterization of spontaneous calcium tran-

sients in nerve growth cones and their effect on growth cone migration. *Neuron* **14**:1233–1246.

GOODMAN, C. S. and SHATZ, C. J. (1993). Developmental mechanisms that generate precise patterns of neuronal connectivity. *Cell* **72**:77–98.

GOULD, E., CAMERON, H. A., and MCEWEN, B. (1994). Blockade of NMDA receptors increases cell death and birth in developing rat dentate gyrus. *J. Comp. Neurol.* **340**:551–565.

GREGORY, W. A., EDMONDSON, J. C., HATTEN, M. E., and MASON, C. A. (1988). Cytology and neuron-glial apposition of migrating cerebellar granule cells in vitro. *J. Neurosci.* **8**:1728–1738.

GU, X., OLSON, E. C., and SPITZER, N. C. (1994). Spontaneous neuronal calcium spikes and waves during early differentiation. *J. Neurosci.* **14**:6325–6335.

GU, X. and SPITZER, N. C. (1993). Low-threshold Ca^{2+} current and its role in spontaneous elevations of intracellular Ca^{2+} in developing *Xenopus* neurons. *J. Neurosci.* **13**:4936–4948.

GU, X. and SPITZER, N. C. (1995). Distinct aspects of neuronal differentiation encoded by frequency of spontaneous Ca^{2+} transients. *Nature* **375**:784–787.

HATTEN, M. E., ALDER, J., ZIMMERMAN, K., and HEINNTZ, N. (1997). Genes involved in cerebellar cell specification and differentiation. *Curr. Opin. Neurobiol.* **7**:40–47.

HATTEN, M. E. and HEINTZ, N. (1995). Mechanisms of neural patterning and specification in the developing cerebellum. *Annu. Rev. Neurosci.* **18**:385–408.

HATTEN, M. E., LIEM, R. K. H., and MASON, C. A. (1984). Defects in specific associations between astroglia and neurons occur in microcultures of *weaver* mouse cerebellar cells. *J. Neurosci.* **4**:1163–1172.

HATTEN, M. E., LIEM, R. K. H., and MASON, C. A. (1986). Weaver mouse cerebellar granule neurons fail to migrate on wild-type astroglial process in vitro. *J. Neurosci.* **6**:2676–2683.

HATTEN, M. E. and MASON, C. A. (1990). Mechanisms of glial-guided neuronal migration in vitro and in vivo. *Experientia* **46**:907–916.

HESS, P. (1990). Calcium channels in vertebrate cells. *Annu. Rev. Neurosci.* **13**:1337–1356.

HOWE, J. R., CULL-CANDY, S. G., and COLQUHOUN, D. (1991). Currents through single glutamate receptor channels in outside-out patches from rat cerebellar granule cells. *J. Physiol. Lond.* **432**:143–202.

HOWELL, B. W., HAWKES, R., SORIANO, P., and COOPER, J. A. (1997). Neuronal position in the developing brain is regulated by *mouse disabled-1*. *Nature* **389**:733–737.

HYNES, R. O. (1992). Integrins: versatility, modulation, and signaling in cell adhesion. *Cell* **69**:11–25.

ILIC, D., FURUTA, Y., KANAZAWA, S., TAKEDA, N., SOBUE, K., NAKATSUJI, N., NOMURA, S., FUJIMOTO, J., OKADA, M., YAMAMOTO, T., and AIZAWA, S. (1995). Reduced cell motility and enhanced focal adhesion contact formation in cells from FAK-deficient mice. *Nature* **377**:539–544.

JACONI, M. E. E., THELER, J. M., SCHLEGEL, W., APPEL, R. D., WRIGHT, S. D., and LEW, P. D. (1991). Multiple elevation of cytosolic-free Ca^{2+} in human neutrophils: Initiation by adherence receptors of the integrin family. *J. Cell Biol.* **112**:1249–1257.

JOHNSON, J. W. and ASCHER, P. (1987). Glycine potentiates the NMDA response in cultured mouse brain neurons. *Nature* **325**:529–531.

KATER, S. B. and MILLS, L. R. (1991). Regulation of growth cone behavior by calcium. *J. Neurosci.* **11**:891–899.

KOMURO, H. and RAKIC, P. (1992). Specific role of N-type calcium channels in neuronal migration. *Science* **257**:806–809.

KOMURO, H. and RAKIC, P. (1993). Modulation of neuronal migration by NMDA receptors. *Science* **260**:95–97.

KOMURO, H. and RAKIC, P. (1995). Dynamics of granule cell migration: a confocal microscopic study in acute cerebellar slice preparations. *J. Neurosci.* **15**:1110–1120.

KOMURO, H. and RAKIC, P. (1996). Intracellular Ca^{2+} fluctuations modulate the rate of neuronal migration. *Neuron* **17**:275–285.

KOMURO, H. and RAKIC, P. (1998a). Distinct modes of neuronal migration in different domains of developing cerebellar cortex. *J. Neurosci.* **18**:1478–1490.

KOMURO, H. and RAKIC, P. (1998b). *In vitro* analysis of signal mechanisms involved in neuronal migration. In: *The Neuron in Tissue Culture*. L. W. Haynes, Ed. Wiley, New York (in press).

KUHAR, S. G., FENG, L., VIDAN, S., ROSS, M. E., HATTEN, M. E., and HEINTZ, N. (1993). Changing patterns of gene expression define four stages of cerebellar granule neuron differentiation. *Development* **117**:97–104.

LANKFORD, K. L. and LETOURNEAU, P. C. (1989). Evidence that calcium may control neurite outgrowth by regulating the stability of filaments. *J. Cell Biol.* **109**:1229–1243.

LAURIE, D. J., WISDEN, W., and SEEBURG, P. H. (1992). The distribution of thirteen $GABA_A$ receptor subunit mRNAs in the rat brain. III. Embryonic and postnatal development. *J. Neurosci.* **12**:4151–4172.

LAWSON, M. A. and MAXFIELD, F. R. (1995). Ca^{2+}- and calcineurin-dependent recycling of an integrin to the front of migrating neutrophils. *Nature* **377**:75–79.

LEVI, G., PATRIZIO, M., and GALLO, V. (1991). Release of endogenous and newly synthesized glutamate and of other amino acids induced by non-*N*-methyl-D-aspartate receptor activation in cerebellar granule cell cultures. *J. Neurochem.* **56**:199–206.

LIAO, Y. J., JAN, Y. N., and JAN, L. Y. (1996). Heteromultimerization of G-protein-gated inwardly rectifying K^+ channel protein GIRK1 and GIRK2 and their altered expression in *weaver* brain. *J. Neurosci.* **16**:7137–7150.

LIESI, P. (1992). Neuronal migration on laminin involves neuronal contact formation followed by nuclear movement inside a preformed process. *Exp. Neurol.* **117**:103–113.

LIESI, P. and WRIGHT, J. M. (1996). Weaver granule neurons are rescued by calcium channel antagonists and antibodies against a neurite outgrowth domain of the B2 chain of laminin. *J. Cell Biol.* **134**:477–486.

LIPP, P. and NIGGLI, E. (1993a). Microscopic spiral waves reveal positive feedback in subcellular calcium signaling. *Biophys. J.* **65**:2272–2276.

LIPP, P. and NIGGLI, E. (1993b). Ratiometric confocal Ca^{2+}-measurements with visible wavelength indicators in isolated cardiac myocytes. *Cell Calcium* **14**:359–372.

LOM, B. and HOCKBERGER, P. E. (1997). Is laminin-1 a guidance cue for cerebellar granule cell migration? *J. Neurobiol.* **33**:72–84.

LOTURCO, J. J., BLANTON, M. G., and KRIEGSTEIN, A. R. (1991). Initial expression and endogenous activation of NMDA channels in early neocortical development. *J. Neurosci.* **11**:792–799.

MARKS, P. W. and MAXFIELD, F. R. (1990). Transient increases in cytosolic calcium appear to be required for the migration of adherent human neutrophils. *J. Cell Biol.* **110**:43–52.

MARTIN-MOUTOT, N., SEAGAR, M., and COURAUD, F. (1990). Subtypes of voltage-sensitive calcium channels in cultured rat brain neurons. *Neurosci. Lett.* **115**:300–306.

MARRET, S., GRESSENS, P., and EVRARD, P. (1996). Arrest of neuronal migration by excitatory amino acid in hamster developing brain. *Proc. Natl. Acad. Sci. USA* **93**:15463–15468.

MIALE, L. L. and SIDMAN, R. L. (1961). An autoradiographic analysis of histogenesis in the mouse cerebellum. *Exp. Neurol.* **4**:277–296.

MIYATA, T., NAKAJIMA, J., ARUGA, J., TAKAHASHI, S., IKENAKA, K., MIKOSHIBA, K., and OGAWA, M. (1996). Distribution of a reeler gene-related antigen in the developing cerebellum: an immunohistochemical study with an allogeneic antibody CR-50 on normal and reeler mice. *J. Comp. Neurol.* **372**:215–228.

MONYER, H., BURNASHEV, N., LAURIA, D. J., SAKMAN, B., and SEEBURG, P. H. (1994). Development of regional expression in the rat brain and functional properties of four NMDA receptors. *Neuron* **12**:529–540.

MORAN, D. (1991). Voltage-dependent-L-type Ca^{2+} channels participate in regulating neural crest migration and differentiation. *Am. J. Anat.* **192**:14–22.

MUGNAINI, E. and FORSTRONEN, P. F. (1967). Ultrastructual studies on the cerebellar histogenesis. I. Differentiation of granule cells and development of glomeruli in the chick embryo. *Z. Zellforsch.* **77**:115–143.

MULLER, T., FRITSCHY, J. M., GROSCHE, J., PRATT, G. D., MOHLER, H., and KETTERMANN, H. (1994). Developmental regulation of voltage-gated K^+ channel and $GABA_A$ receptor expression in Bergmann glial cells. *J. Neurosci.* **14**:2503–2514.

NAGATA, I. and NAKATSUJI, N. (1990). Granule cell behavior on laminin in cerebellar microexplant cultures. *Dev. Brain Res.* **52**:63–73.

NAVARRO, B., KENNEDY, M. E., VELIMIROVIC, B., BHAT, D., PETERSON, A. S., and CLAPHAM, D. E. (1996). Nonselective and $G_{\beta\gamma}$-insensitive *weaver* K^+ channels. *Science* **272**:1950–1953.

NEWGREEN, D. F. and GOODAY, D. (1985). Control of the onset of migration of neural crest cells in avian embryos. *Cell Tissue Res.* **239**:329–336.

NOWARK, L., BREGESTOVSKI, P., ASCHER, P., HERBET, A., and PROCHIANTZ, A. (1984). Magnesium gates glutamate-activated channels in mouse central neurons. *Nature* **307**:462–465.

O'DONOGHUE, D. L., MARTIN, G. F., and KING, J. S. (1987). The timing of granule cell differentiation and mossy fiber morphogenesis in the opossum. *Anat. Embryol.* **175**:341–354.

OKABE, S. and HIROKAWA, N. (1991). Actin dynamics in growth cones. *J. Neurosci.* **11**:1918–1929.

ONO, K., SHOKUNBI, T., NAGATA, I., TOKUNAGA, A., YASUI, Y., and NAKATSUJI, N. (1997). Filopodia and growth cones in the vertically migrating granule cells of the postnatal mouse cerebellum. *Exp. Brain Res.* **117**:17–29.

PARPURA, V., BASARSKI, T. A., LIN, F., JEFTINIA, K., JEFTINIA, S., and HAYDON, P. G. (1994). Glutamate-mediated astrocyte-neuron signaling. *Nature* **369**:744–747.

PATIL, N., COX, D. R., BHAT, D., FAHAM, M., MYERS, R. M., and PETERSON. (1995). A potassium channel mutation in *weaver* mice implicates membrane excitability in granule cell differentiation. *Nat. Genet.* **11**:126–129.

POLLERBERG, G. E., BURRIDGE, K., KREBS, K., GOODMAN, S., and SCHACHNER, M. (1987). The 180 kD component of neural cell adhesion molecule is involved in cell–cell contacts and cytoskeleton–membrane interactions. *Cell Tissue Res.* **250**:227–238.

PON, D. V. and ROBINSON, S. R. (1994). Glutamate in some retinal neurons is derived solely from glia. *Neuroscience* **60**:355–366.

QUESADA, A. and GENIS-GALVEZ, J. M. (1983). Early development of the granule cell in the cerebellum of the chick embryo. *J. Morphol.* **178**:323–334.

RAKIC, P. (1971). Neuron–glia relationship during granule cell migration in developing cerebellar cortex: a Golgi and electronmicroscopic study in *Macacus rhesus*. *J. Comp. Neurol.* **141**:283–312.

RAKIC, P. (1972). Mode of cell migration to the superficial layers of fetal monkey neocortex. *J. Comp. Neurol.* **145**:61–84.

RAKIC, P. (1976). Synaptic specificity in the cerebellar cortex: study of anomalous circuits induced by single gene mutation in mice. *Cold Spring Harbor Symp. Quant. Biol.* **40**:333–346.

RAKIC, P. (1981). Neuronal–glial interaction during brain development. *Trends Neurosci.* **4**:184–187.

RAKIC, P. (1985a). Mechanisms of neuronal migration in developing cerebellar cortex. In: *Molecular Basis of Neural Development.* G. E. Edelman, W. M. Cowan, and E. Gall, Eds. Wiley, New York, pp. 139–160.

RAKIC, P. (1985b). Contact regulation of neuronal migration In: *The Cell in Contact: Adhesions and Junctions as Morphogenetic Determinants.* G. M. Edelman and J.-P. Thiery, Eds. Wiley, New York, pp. 67–91.

RAKIC, P. (1990). Principles of neuronal cell migration. *Experientia* **46**:882–891.

RAKIC, P. (1997). Intra- and extracellular control of neuronal migration: relevance to cortical malformations. In: *Normal and Abnormal Development of Cortex.* A. M. Galaburda and Y. Christen, Eds. Springer-Verlag, New York, pp. 81–98.

RAKIC, P., CAMERON, R. S., and KOMURO, H. (1994). Recognition, adhesion, transmembrane signaling and cell motility in guided neuronal migration. *Curr. Opin. Neurobiol.* **4**:63–69.

RAKIC, P., KNYIHAR-CSILLIK, E., and CSILLIK, B. (1996). Polarity of microtubule assemblies and during neuronal cell migration. *Proc. Natl. Acad. Sci. USA* **93**:9218–9222.

RAKIC, P. and KOMURO, H. (1995). The role of receptor/channel activity in neuronal cell migration. *J. Neurobiol.* **26**:299–315.

RAKIC, P. and SIDMAN, R. L. (1973a). Sequence of developmental abnormalities leading to granule cell deficit in cerebellar cortex of weaver mutant mice. *J. Comp. Neurol.* **152**:103–132.

RAKIC, P. and SIDMAN, R. L. (1973b). Weaver mutant mouse cerebellum: defective neuronal migration secondary to specific abnormality of Bergmann glia. *Proc. Natl. Acad. Sci. USA* **70**:240–244.

RAMON Y CAJAL, S. (1911). *Histologie du System Nerveux de l'Homme et des Vertebres,* Vol. 2. Malonine, Paris.

RANDALL, A. and TSIEN, R. W. (1995). Pharmacological dissection of multiple type of Ca^{2+} channel current in rat cerebellar granule neurons. *J. Neurosci.* **15**:2995–3012.

RIO, C., RIEFF, H. I., QI, P., and CORFAS, G. (1997). Neuregulin and erbB receptors play a critical role in neuronal migration. *Neuron* **19**:39–50.

RIVAS, R. J. and HATTEN, M. E. (1995). Motility and cytoskeletal organization of migrating cerebellar granule neurons. *J. Neurosci.* **15**:981–989.

ROBSON, S. J. and BURGOYNE, R. D. (1989). L-type calcium channels in the regulation of neurite outgrowth from rat dorsal root ganglion neurons in culture. *Neurosci. Lett.* **104**:110–114.

ROCAMORA, N., GARCIA-LADONA, F. J., PALACIOS, J. M., and MENGOD, G. (1993). Differential expression of brain-derived neurotrophic factor, neurotrophin-3, and low-affinity nerve growth factor receptor during the postnatal development of the rat cerebellar system. *Mol. Brain Res.* **17**:1–8.

ROSSI, D. and SLATER, T. N. (1993). The developmental onset of NMDA receptor channel activity during neuronal migration. *Neuropharmacology* **32**:1239–1248.

ROSSI, P., D'ANGELO, E., MAGISTRETTI, J., TOSELLI, M., and TAGLIETTI, V. (1994). Age-dependent expression of high-voltage activated calcium currents during cerebellar granule cell development in situ. *Pflugers Arch.* **429**:107–116.

SAWYER, D. W., SULLIVAN, J. A., and MANDELL, G. L. (1985). Intracellular free calcium localization in neutrophils during phagocytosis. *Science* **230**:663–666.

SCHILD, D., JUNG, A., and SCHULTENS, H. A. (1994). Localization of calcium entry through calcium channels in olfactory receptor neurons using a laser scanning microscope and the calcium indicator dyes Fluo-3 and Fura-Red. *Cell Calcium* **15**:341–348.

SHELDON, M., RICE, D. S., D'ARCANGELO, G., YONESHIMA, H., NAKAJIMA, K., MIKOSHIBA, K., HOWELL, B. W., COOPER, J. A., GOLDOWITZ, D., and CURRAN, T. (1997). *Scrambler* and *yotari* disrupt the *disabled* gene and produce a *reeler*-like phenotype in mice. *Nature* **389**:730–733.

SHENG, M., CUMMINGS, J., ROLDAN, L. A., NUNG, Y., and JAN, L. Y. (1994). Changing subunit composition of heteromeric NMDA receptors during development of rat cortex. *Nature* **368**:144–146.

SILVER, R. A., LAMB, A. G., and BOLSOVER, S. R. (1990). Calcium hotspots caused by L-type channel clustering promote morphological changes in neuronal growth cones. *Nature* **343**:751–754.

SILVERMAN, S. K., KOFUJI, P., DOUGHERTY, D. A., DAVIDSON, N., and LESTER, H. A. (1996). A regenerative link in the ionic fluxes through the *weaver* potassium channel underlies the pathophysiology of the mutation. *Proc. Natl. Acad. Sci. USA* **93**:15429–15434.

SLATER, N. T. and ROSSI, D. J. (1996). Functional expression of NMDA receptors in developing neurons. In: *Excitatory Amino Acid and the Cerebral Cortex.* F. Conti and T. P. Hicks, Eds. MIT Press, Cambridge, pp. 215–226.

SORIANO, E., ALVARADO-MALLART, R. M., DUMESNIL, N., DEL RIO, J. A., and SOTELO, C. (1997). Cajal-Retzius cells regulate the radial glia phenotype in the adult and developing cerebellum and alter granule cell migration. *Neuron* **18**:563–577.

SPITZER, N. C. (1994). Spontaneous Ca^{2+} spikes and waves in embryonic neurons: signaling systems for differentiation. *Trends Neurosci.* **17**:115–118.

TRENKNER, E. and SIDMAN, R. L. (1977). Histogenesis of mouse cerebellum in microwell cultures. *J. Cell Biol.* **75**:915–940.

UZMAN, L. L. (1960). The histogenesis of the mouse cerebellum as studied by its tritiated thymidine uptake. *J. Comp. Neurol.* **114**:137–159.

VIGERS, A. J. and PFENNINGER, K. H. (1991). N-type and L-type calcium channels are present in nerve growth

cones: numbers increase on synaptogenesis. *Dev. Brain Res.* **60**:197–203.

WAGNER, J. A., SNOWMAN, A. M., BISWAS, A., OLIVERA, B. M., and SNYDER, S. H. (1988). ω-Conotoxin GVIA binding to a high-affinity receptor in brain: characterization, calcium sensitivity, and solubilization. *J. Neurosci.* **8**:3354–3359.

WARE, M. L., FOX, J. W., GONZALEZ, J. L., DAVIS, N. M., LAMBERT DE ROUVROIT, C., RUSSO, C. J., CHUA, S. C., JR., GOFFINET, A. M., and WALSH, C. A. (1997). Aberrant splicing of a mouse *disabled* homolog, *mdab1*, in the *scrambler* mouse. *Neuron* **19**:239–249.

WESTENBROEK, R. E., HELL, J. W., WARNER, C., DUBEL, S. J., SNUTCH, T. P., and CATTERALL, W. A. (1992). Biochemical properties and subcellular distribution of an N-type calcium channel α1 subunit. *Neuron* **9**:1099–1115.

ZHENG, C., HEINTZ, N., and HATTEN, M. E. (1996). CNS gene encoding astrotactin, which supports neuronal migration along glial fibers. *Science* **272**:417–419.

ZHU, X.-Z. and CHUANG, D.-M. (1987). Modulation of calcium uptake and D-aspartate release by $GABA_B$ receptors in cultured cerebellar granule cells. *Eur. J. Pharmacol.* **141**:401–408.